The Role of Subsidence during the Development of North American Polar/Subtropical Jet Superpositions

Andrew C. Winters

University of Colorado Boulder

Daniel Keyser and Lance F. Bosart

University at Albany, SUNY

This work was funded by an NSF-PRF (AGS-1624316)

19th Cyclone Workshop

Seeon, Bavaria, Germany

30 September 2019

Jet Superposition Conceptual Model

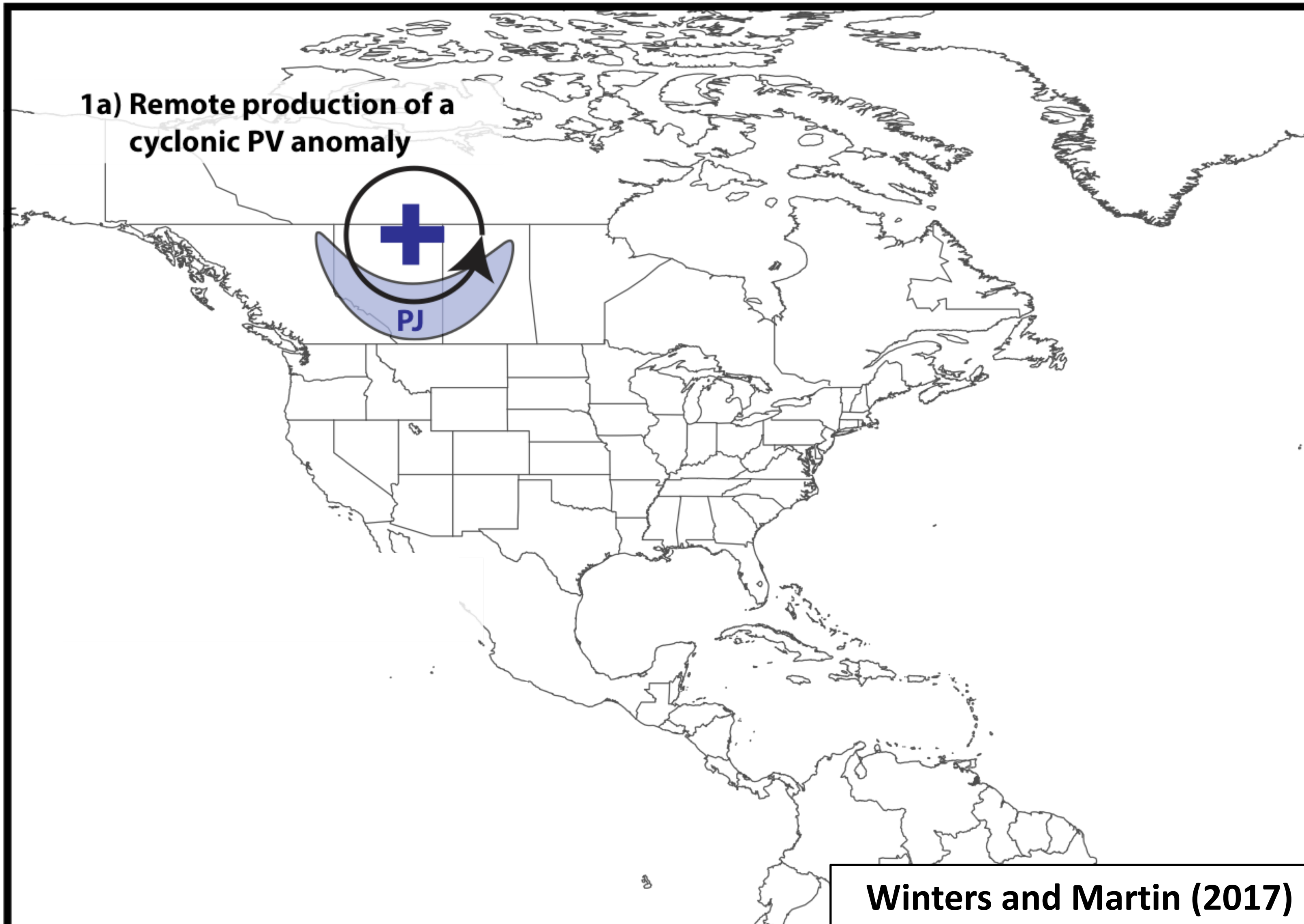

Jet Superposition Conceptual Model

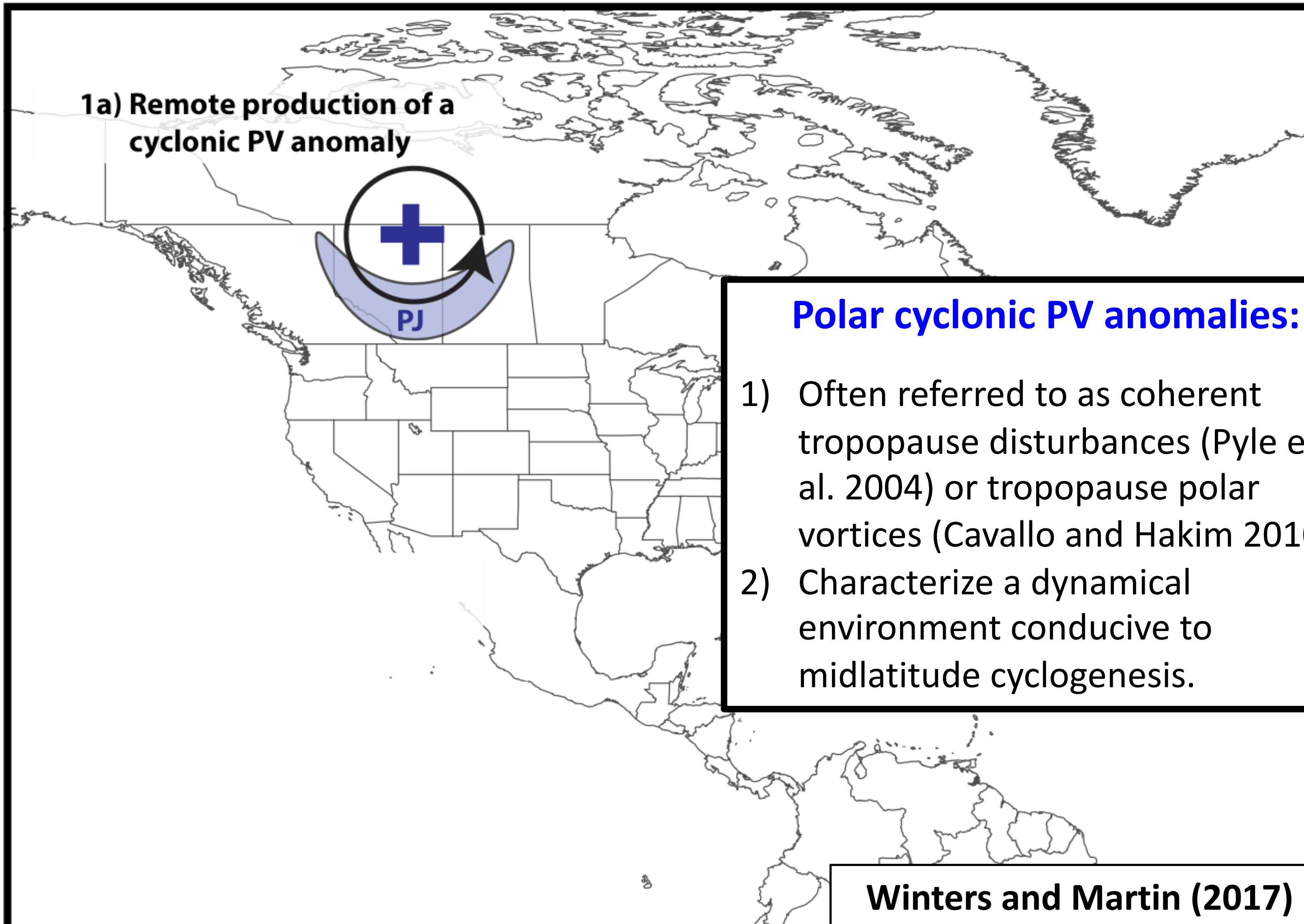

Polar cyclonic PV anomalies:

1) Often referred to as coherent tropopause disturbances (Pyle et al. 2004) or tropopause polar vortices (Cavallo and Hakim 2010).
2) Characterize a dynamical environment conducive to midlatitude cyclogenesis.

Jet Superposition Conceptual Model

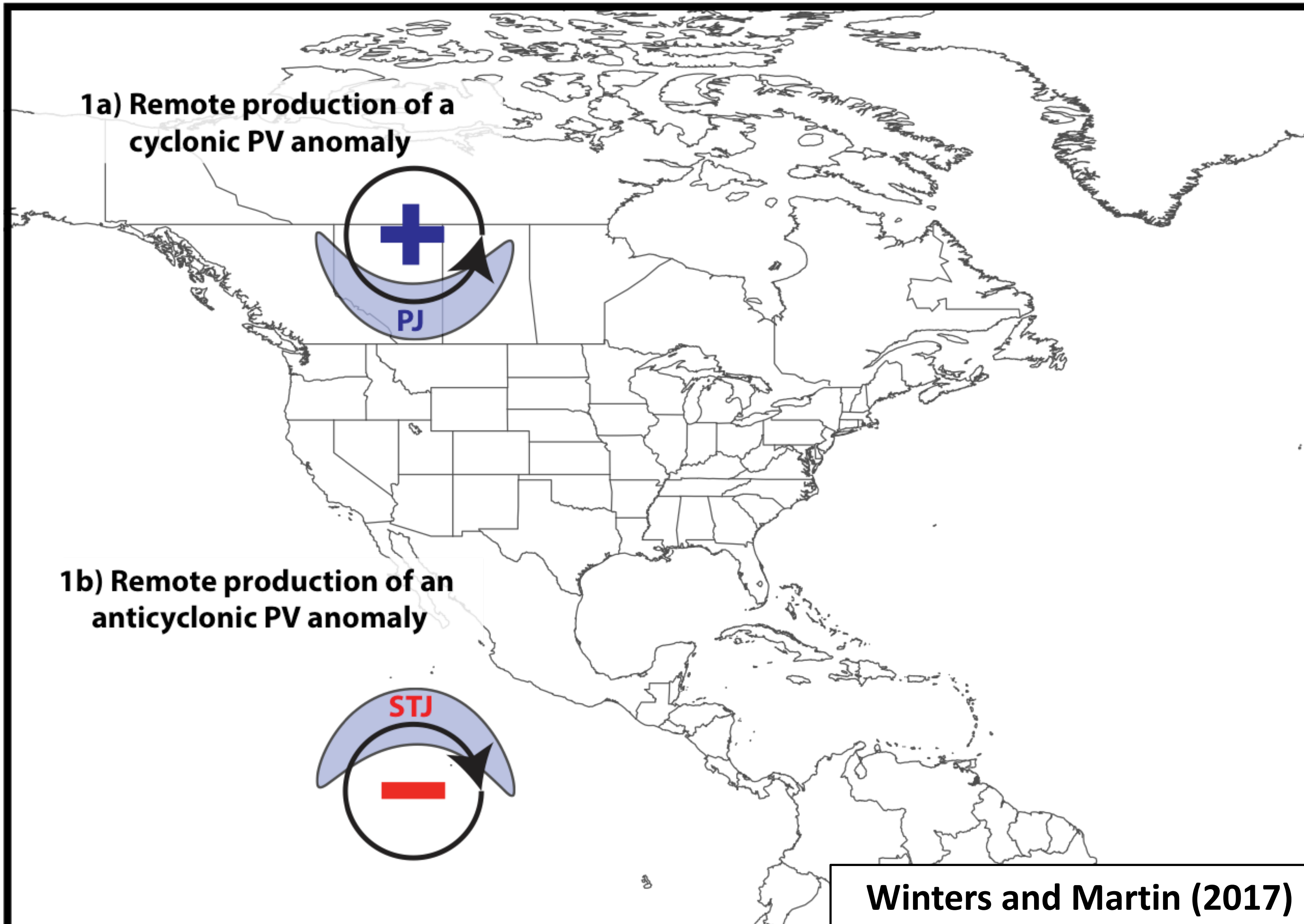

Jet Superposition Conceptual Model

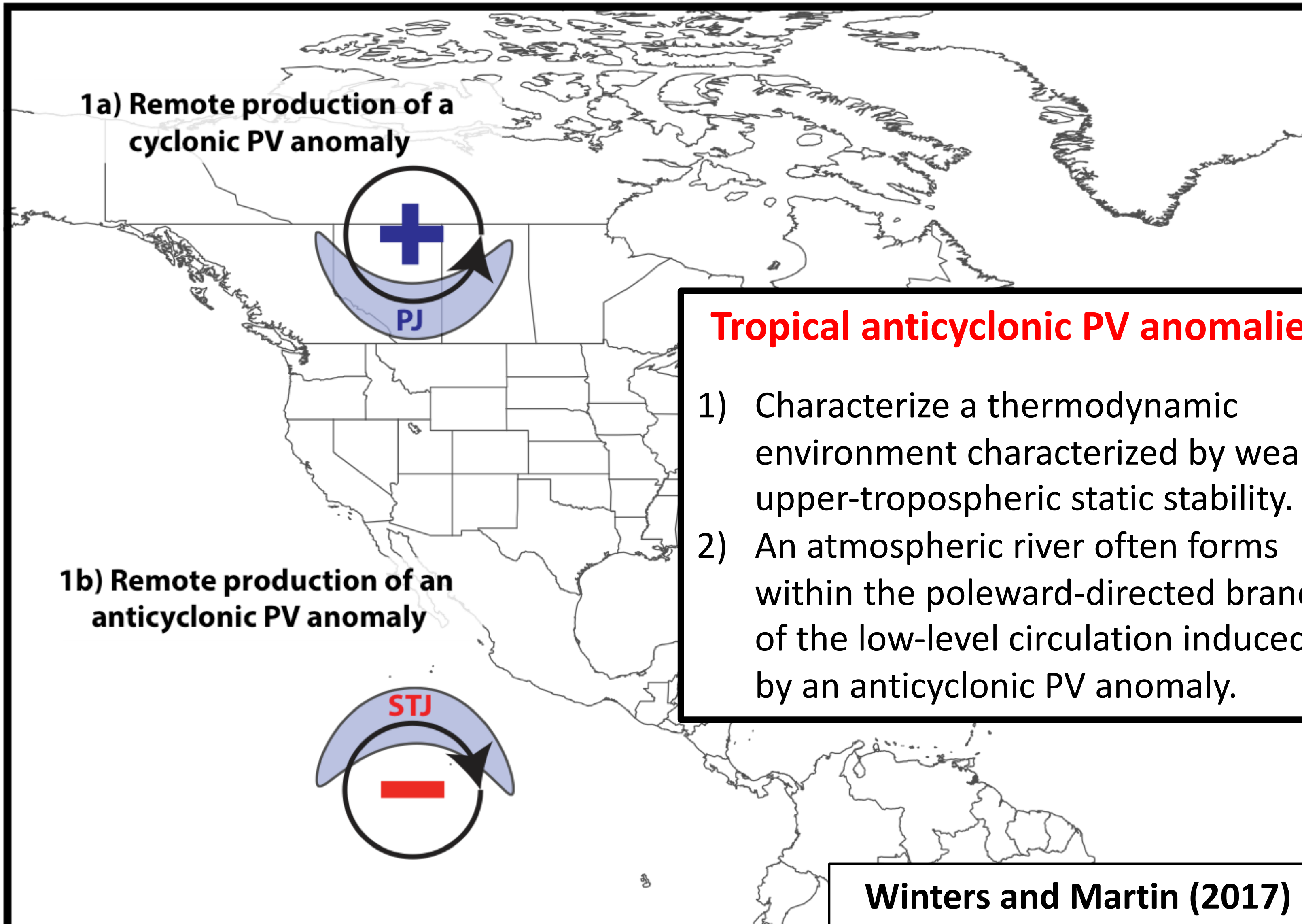

Tropical anticyclonic PV anomalies:

1) Characterize a thermodynamic environment characterized by weak upper-tropospheric static stability.
2) An atmospheric river often forms within the poleward-directed branch of the low-level circulation induced by an anticyclonic PV anomaly.

Jet Superposition Conceptual Model

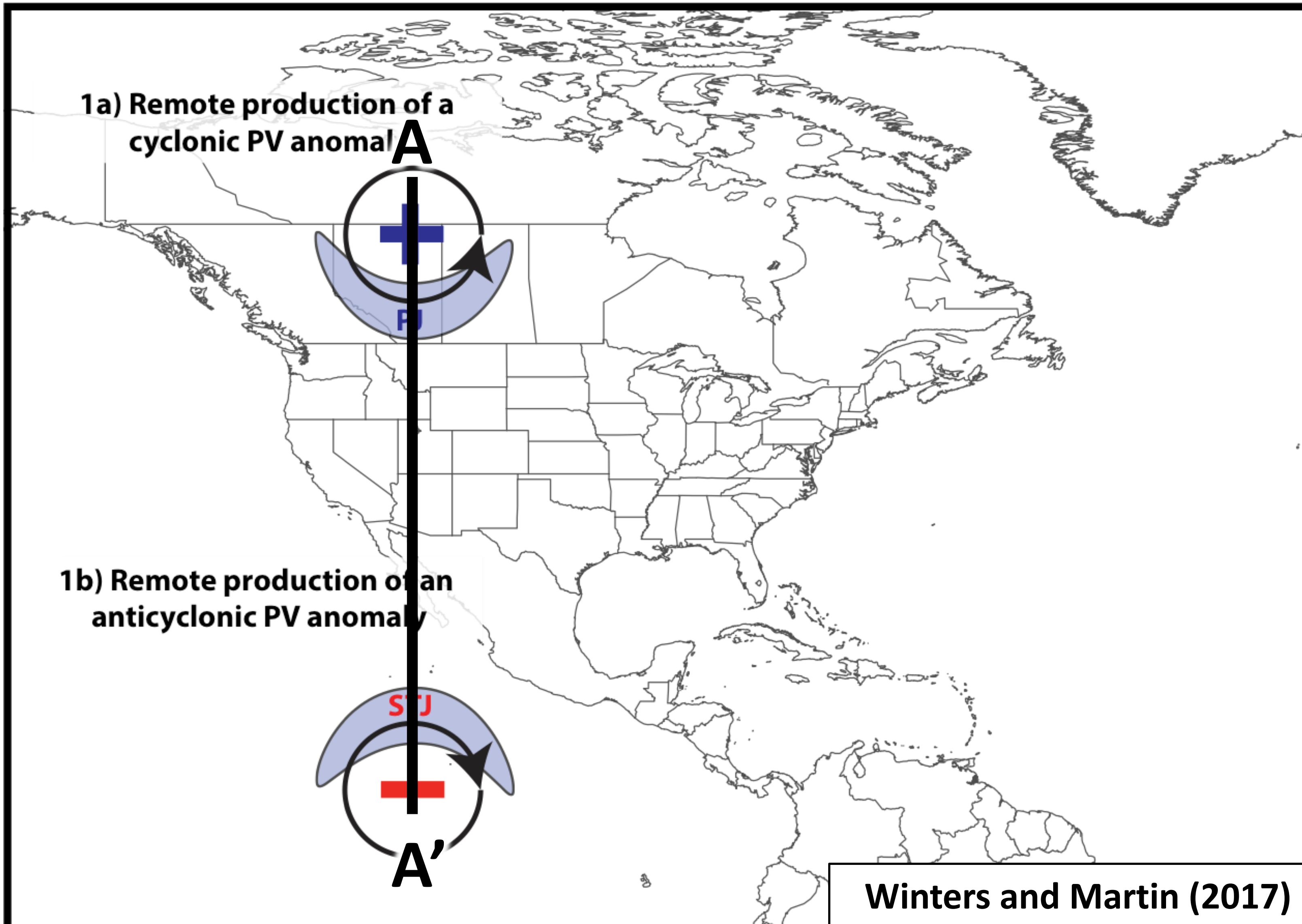

Winters and Martin (2017)

Jet Superposition Conceptual Model

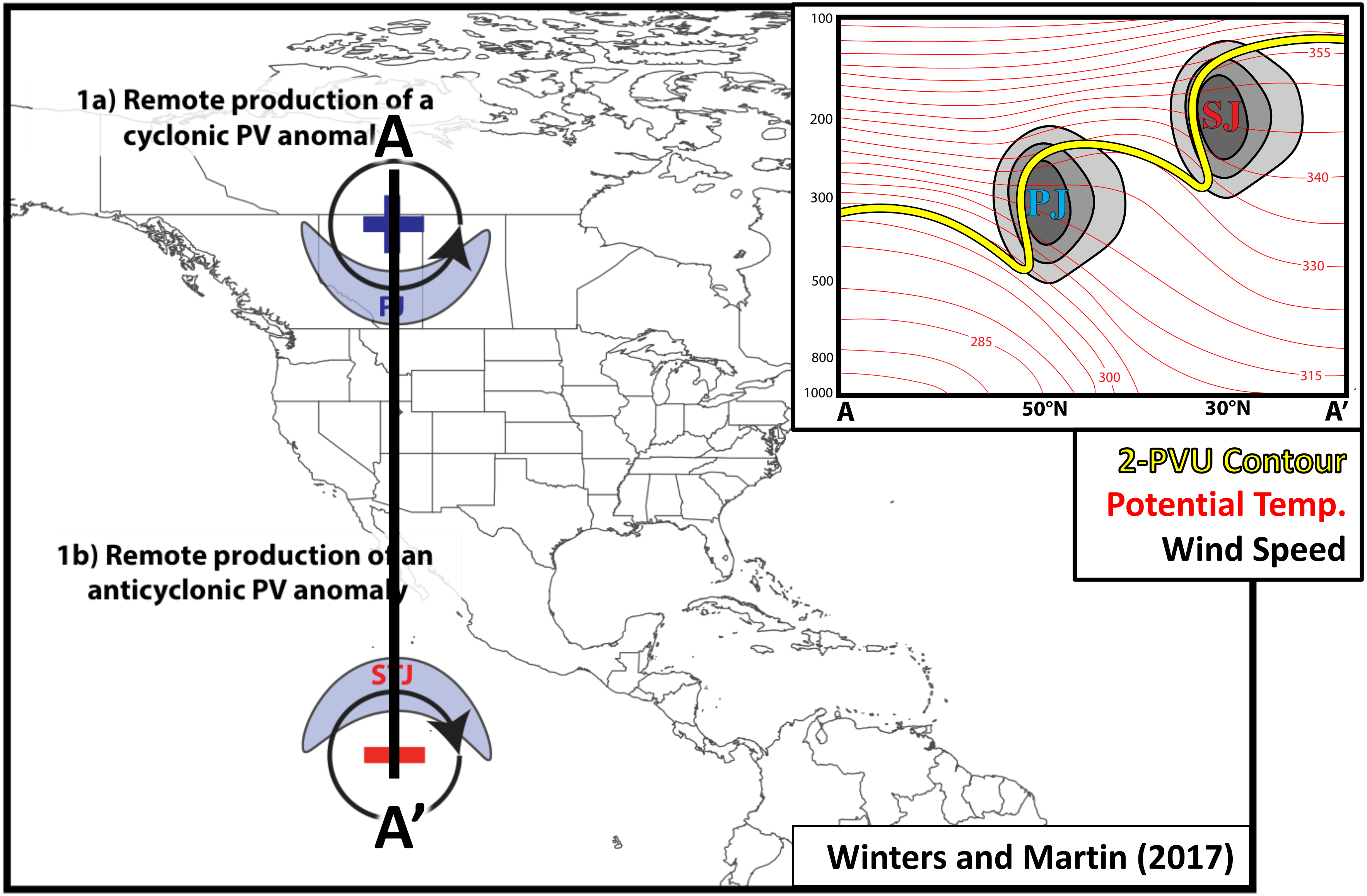

Jet Superposition Conceptual Model

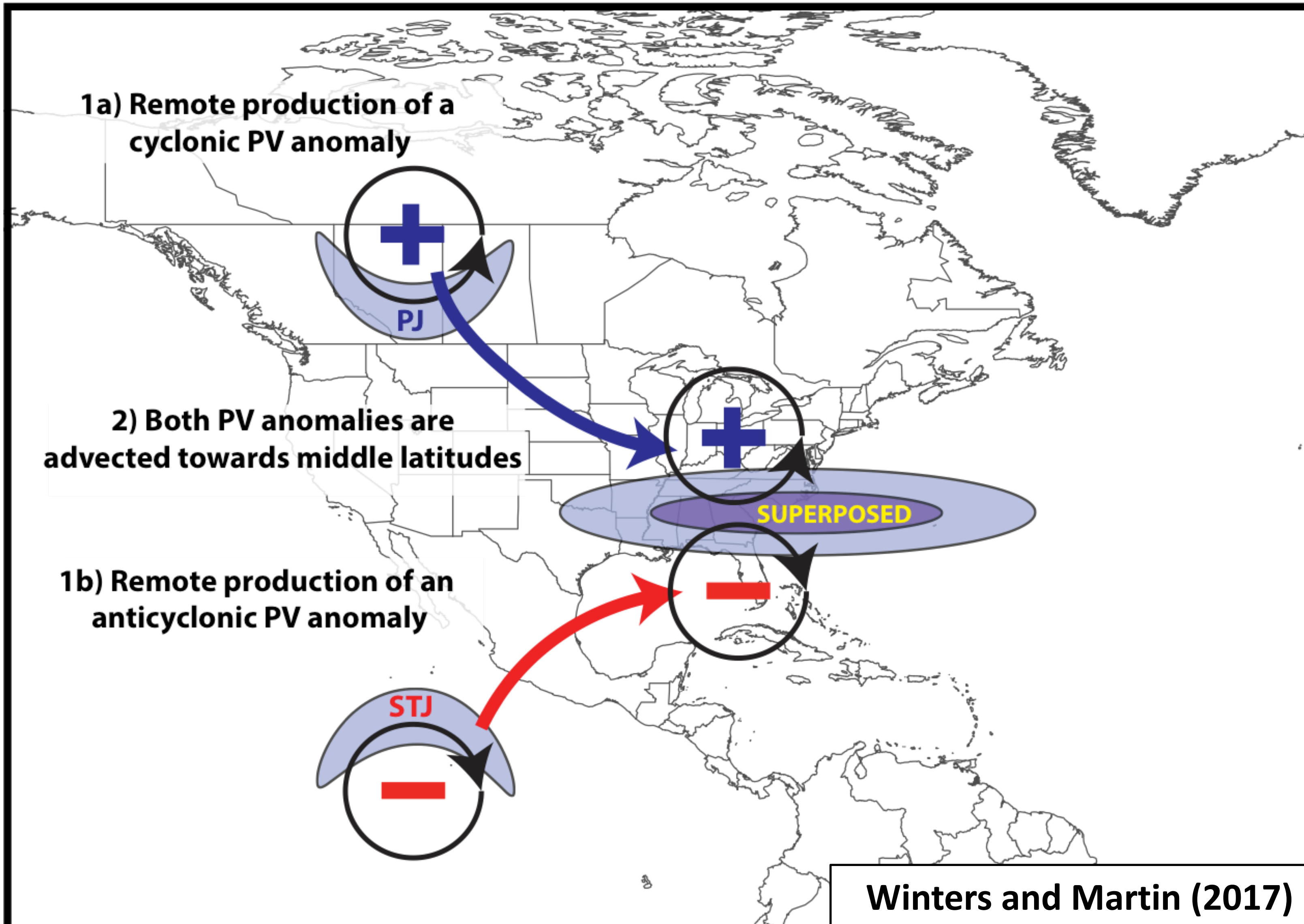

Jet Superposition Conceptual Model

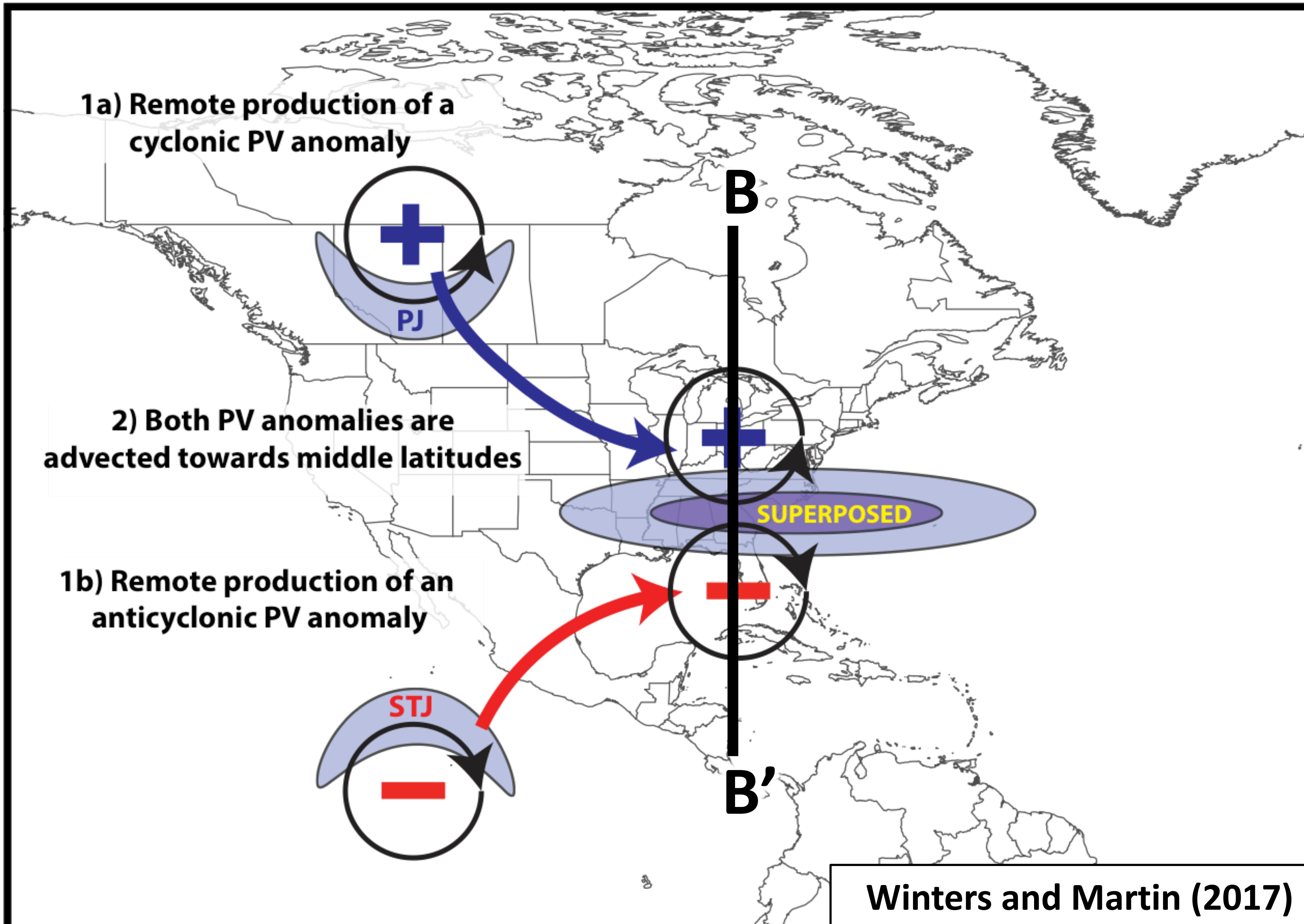

Jet Superposition Conceptual Model

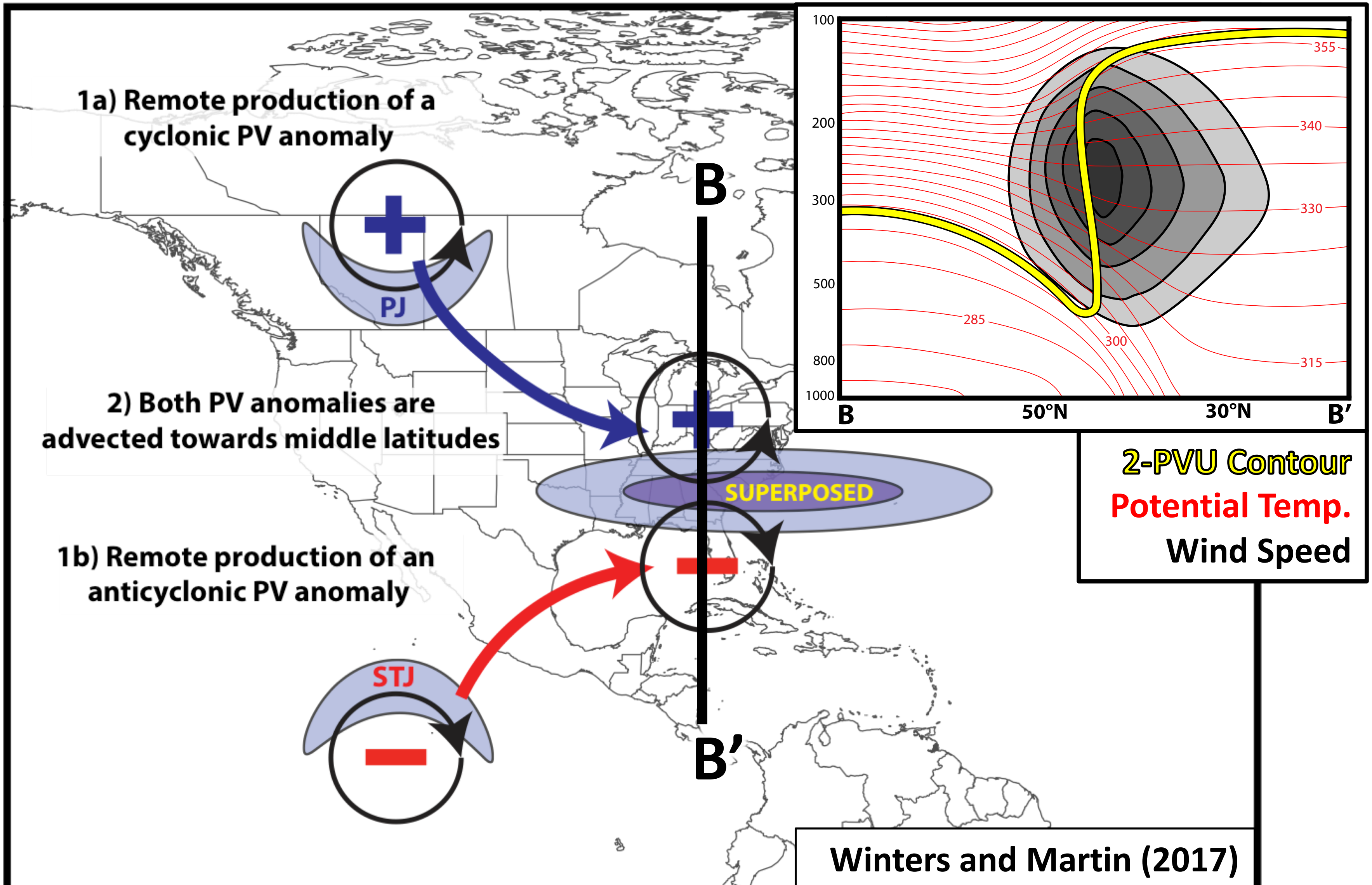

Jet Superposition Conceptual Model

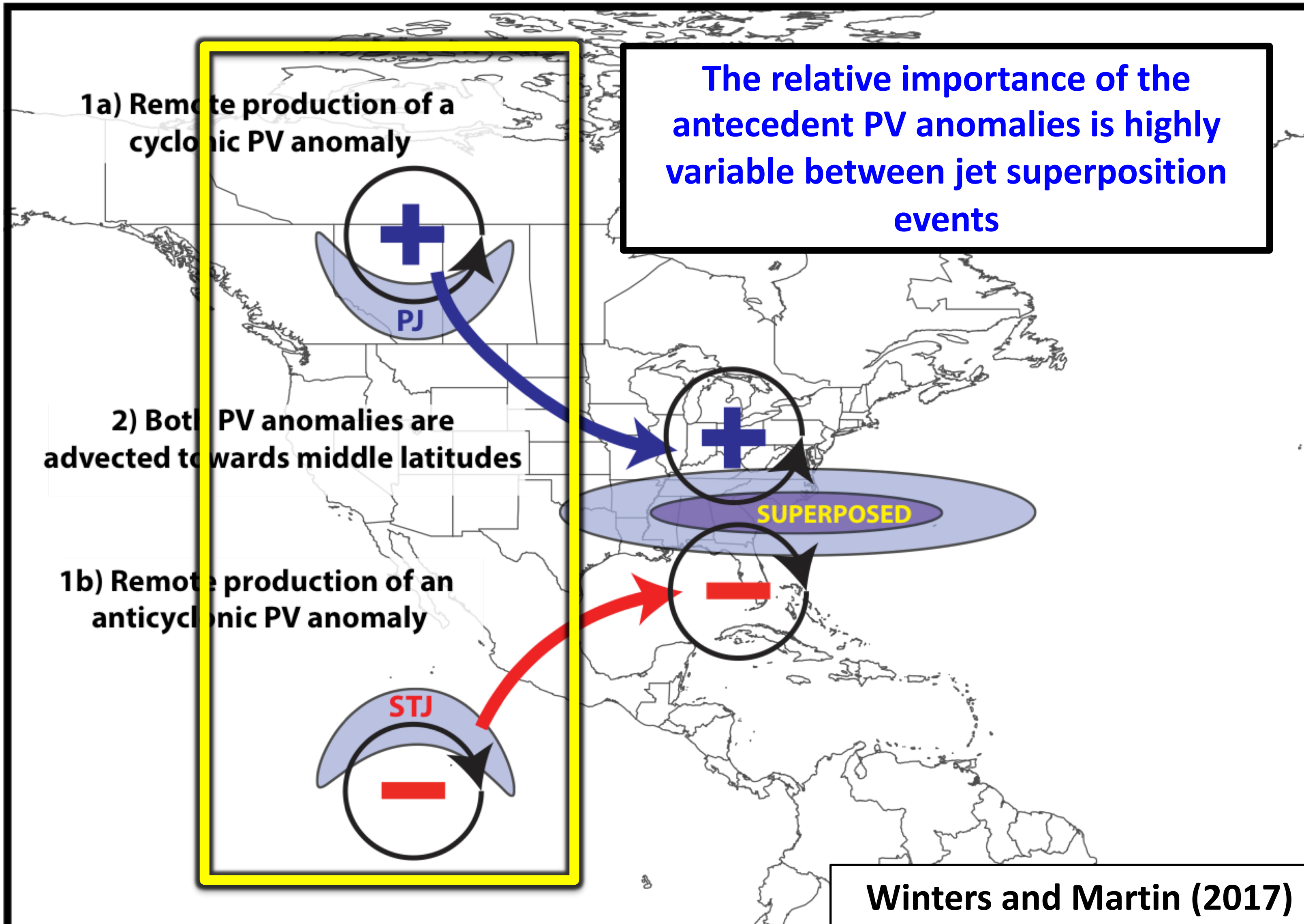

Jet Superposition Conceptual Model

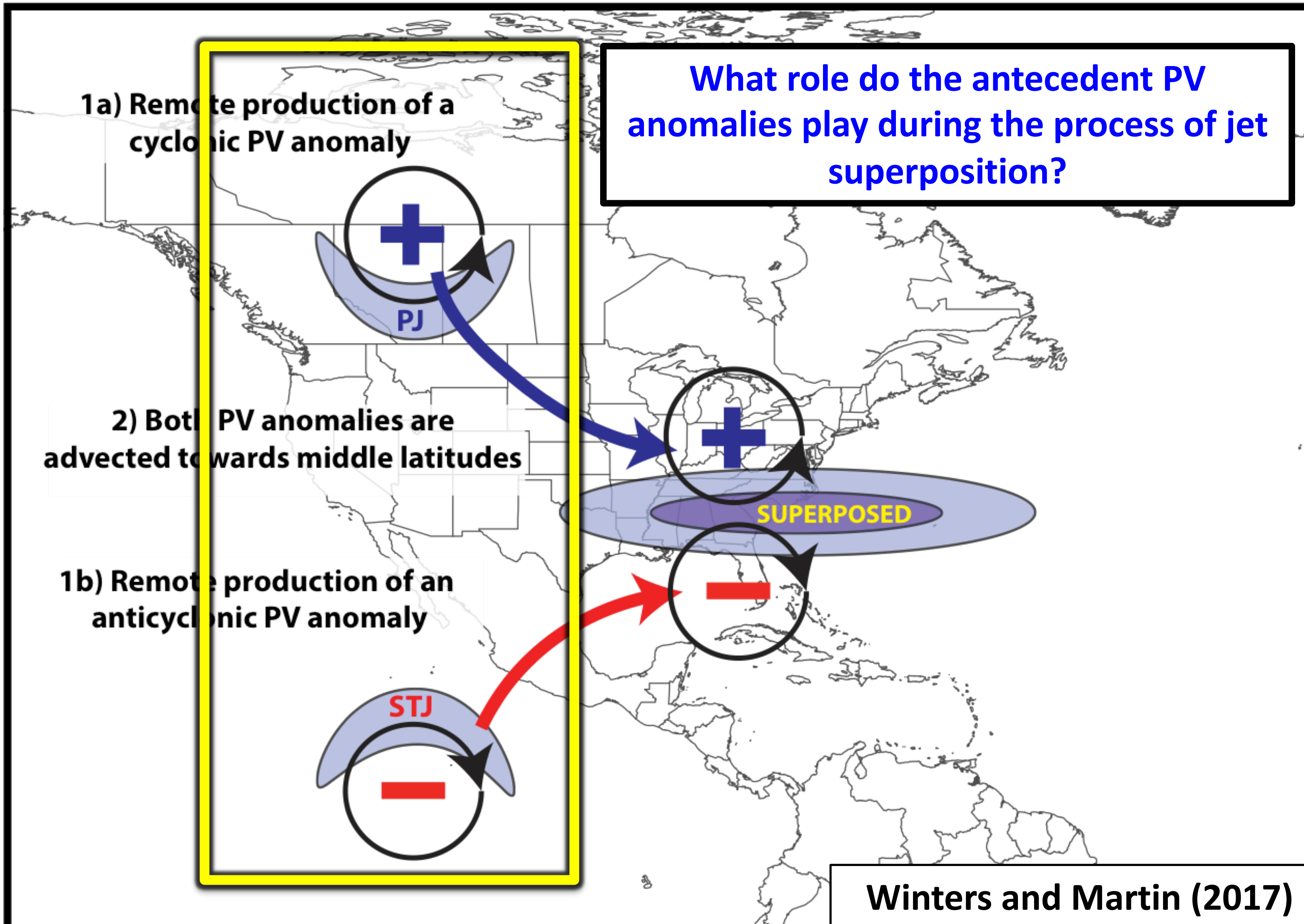

Jet Superposition Event Identification and Classification

Jet Superposition Event Identification

- Isolated NCEP CFSR (Saha et al. 2014) grid points over North America characterized by a jet superposition during Nov.–Mar. 1979–2010 using the Christenson et al. (2017) scheme.
- Retained analysis times that rank in the top 10% in terms of the number of grid points characterized by a jet superposition.
- Filtered retained analysis times to group together jet superpositions that are < 30 h and < 1500 km apart.

326 jet superposition events

Jet Superposition Event Identification

- Isolated NCEP CFSR (Saha et al. 2014) grid points over North America characterized by a jet superposition during Nov.–Mar. 1979–2010 using the Christenson et al. (2017) scheme.
- Retained analysis times that rank in the top 10% in terms of the number of grid points characterized by a jet superposition.
- Filtered retained analysis times to group together jet superpositions that are < 30 h and < 1500 km apart.
- Classified jet superposition events based on the deviations of the polar and subtropical jets from their respective climatological latitude bands at the time of jet superposition.

Jet Superposition Event Classification

1. Determined the mean position of the 2-PVU contour on the 320-K and 350-K surfaces at each analysis time in the CFSR.

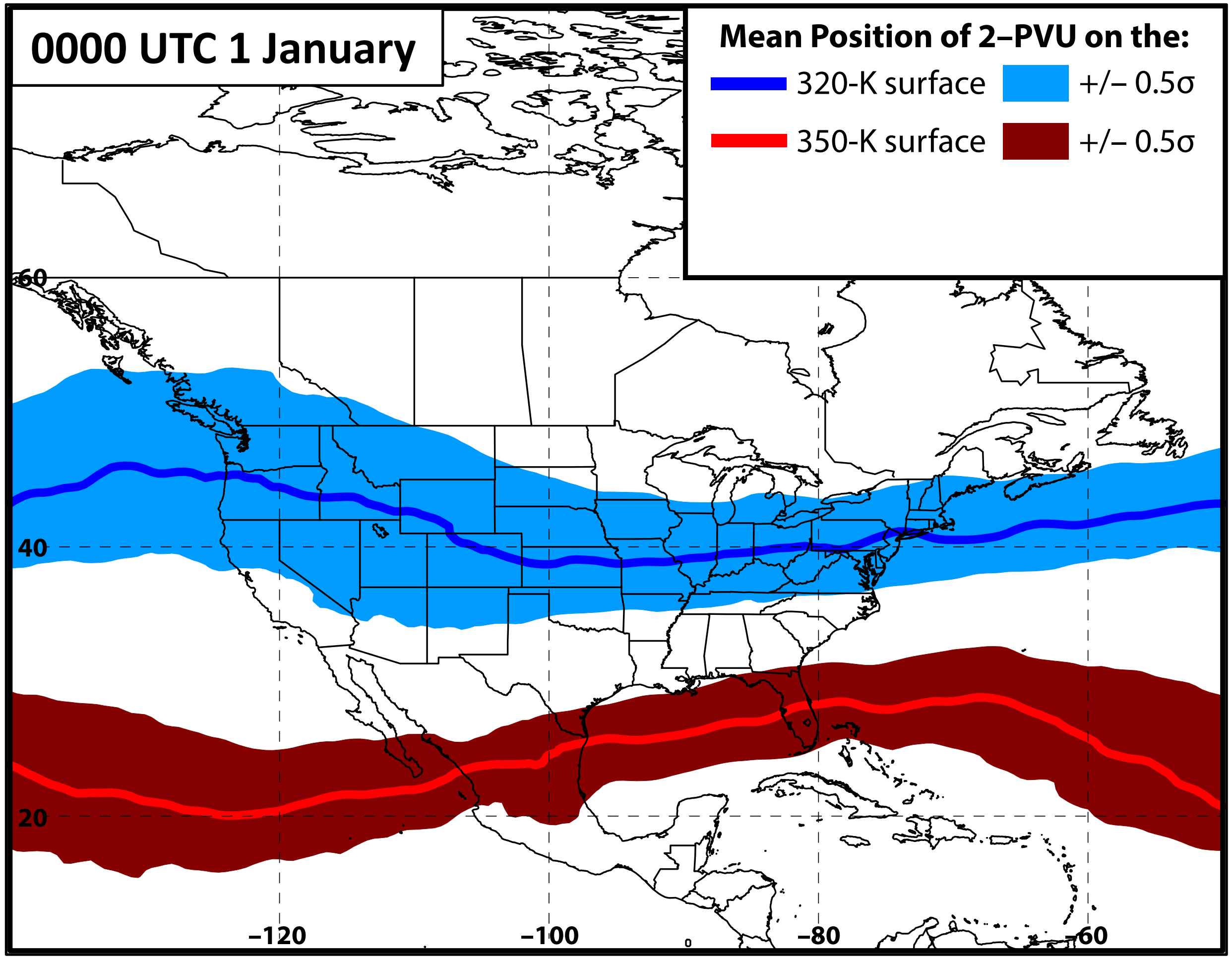

Jet Superposition Event Classification

1. Determined the mean position of the 2-PVU contour on the 320-K and 350-K surfaces at each analysis time in the CFSR.

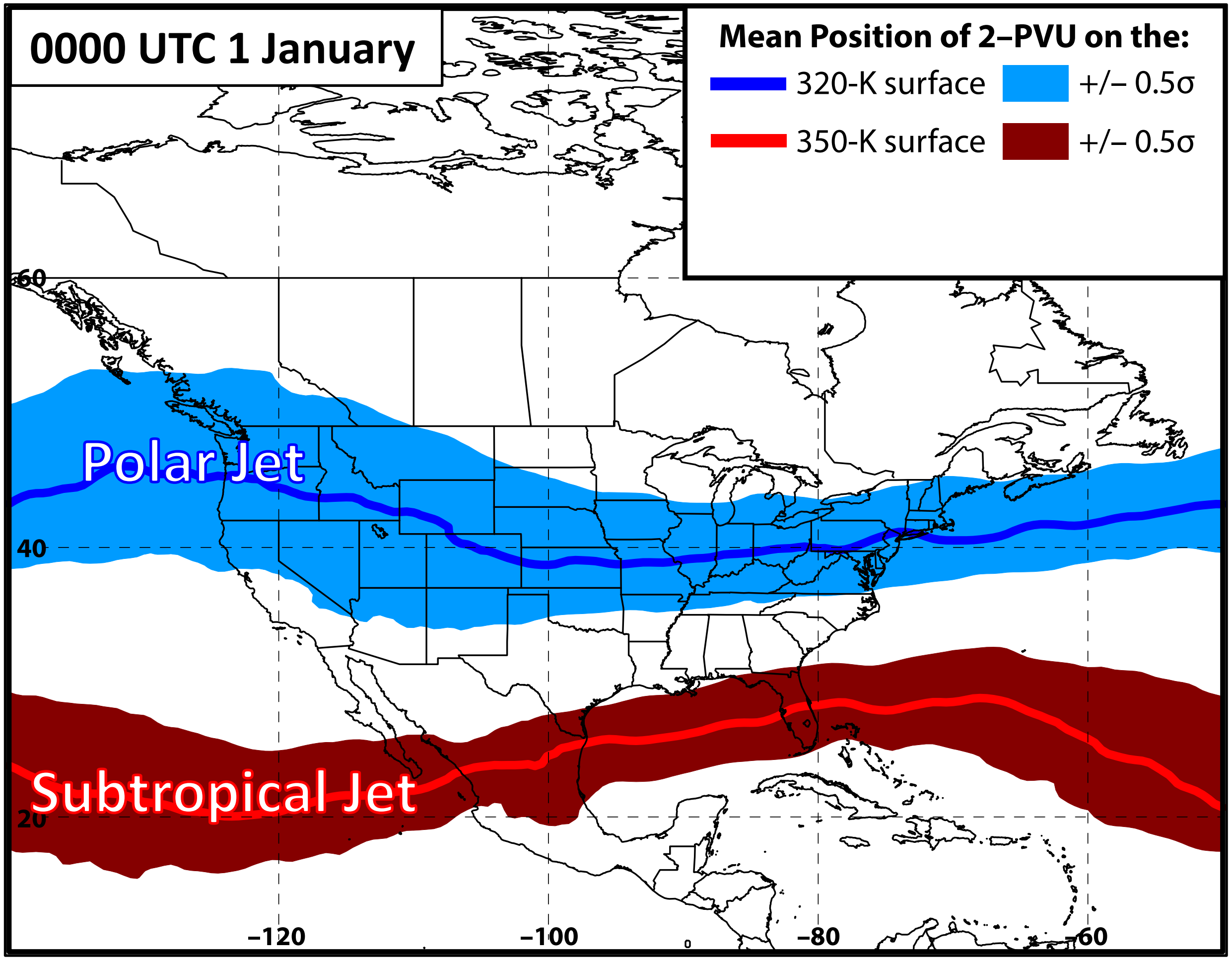

Jet Superposition Event Classification

1. Determined the mean position of the 2-PVU contour on the 320-K and 350-K surfaces at each analysis time in the CFSR.

2. Compared the position of the jet superposition centroid at the start of each event against the climatological position of the 2-PVU contour.

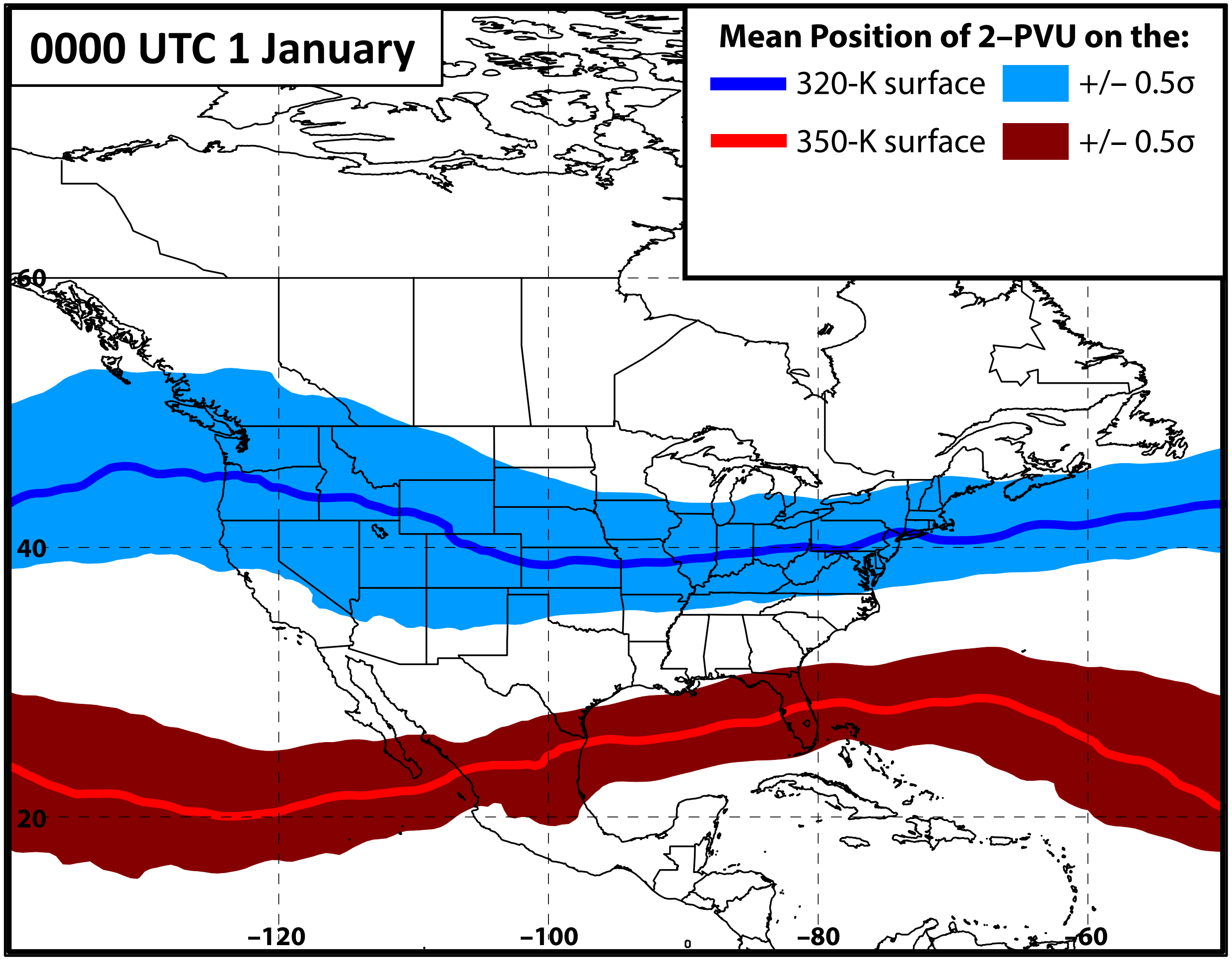

Jet Superposition Event Classification

1. Determined the mean position of the 2-PVU contour on the 320-K and 350-K surfaces at each analysis time in the CFSR.

2. Compared the position of the jet superposition centroid at the start of each event against the climatological position of the 2-PVU contour.

- **Polar Dominant**

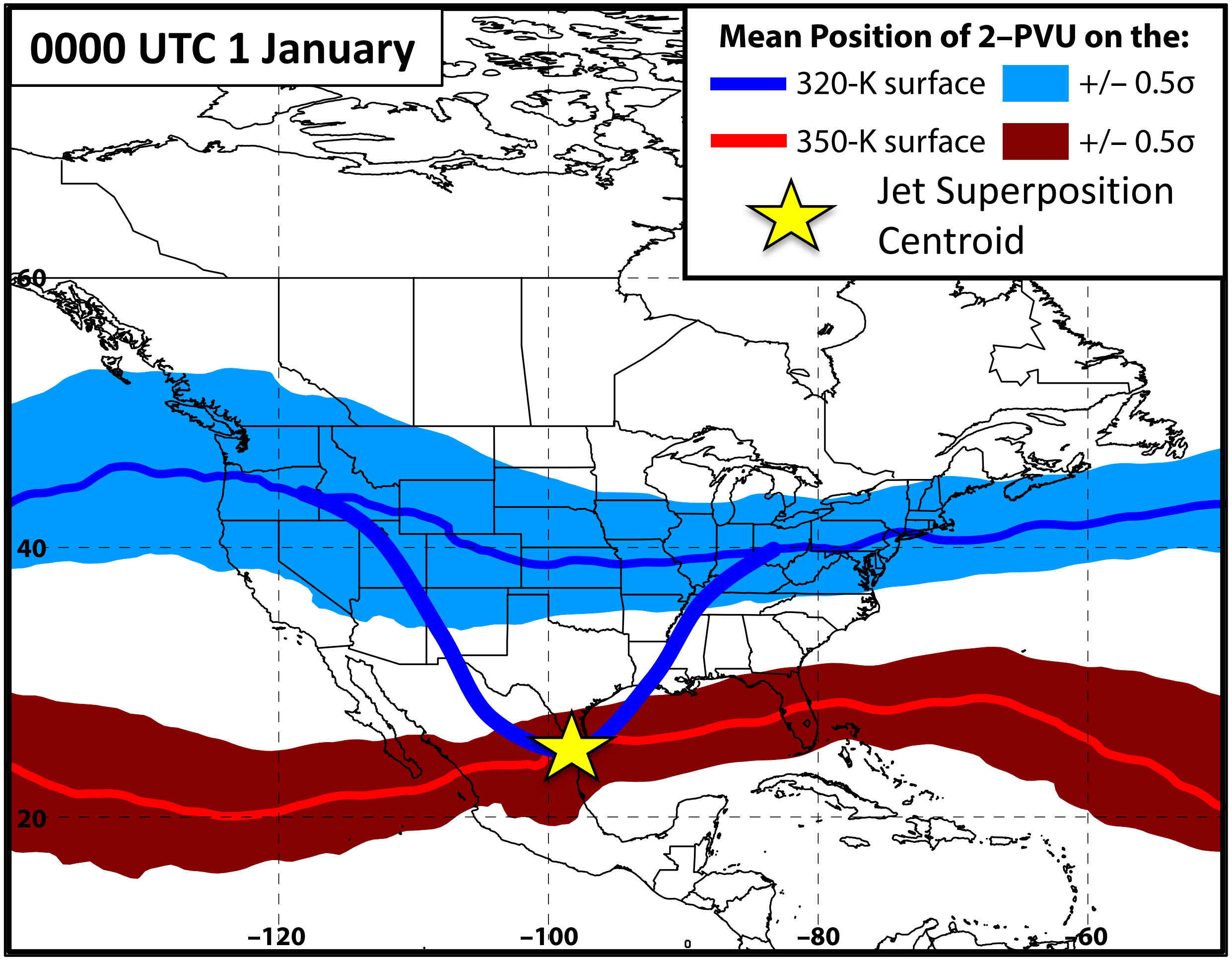

Jet Superposition Event Classification

1. Determined the mean position of the 2-PVU contour on the 320-K and 350-K surfaces at each analysis time in the CFSR.

2. Compared the position of the jet superposition centroid at the start of each event against the climatological position of the 2-PVU contour.

- Polar Dominant
- **Subtropical Dominant**

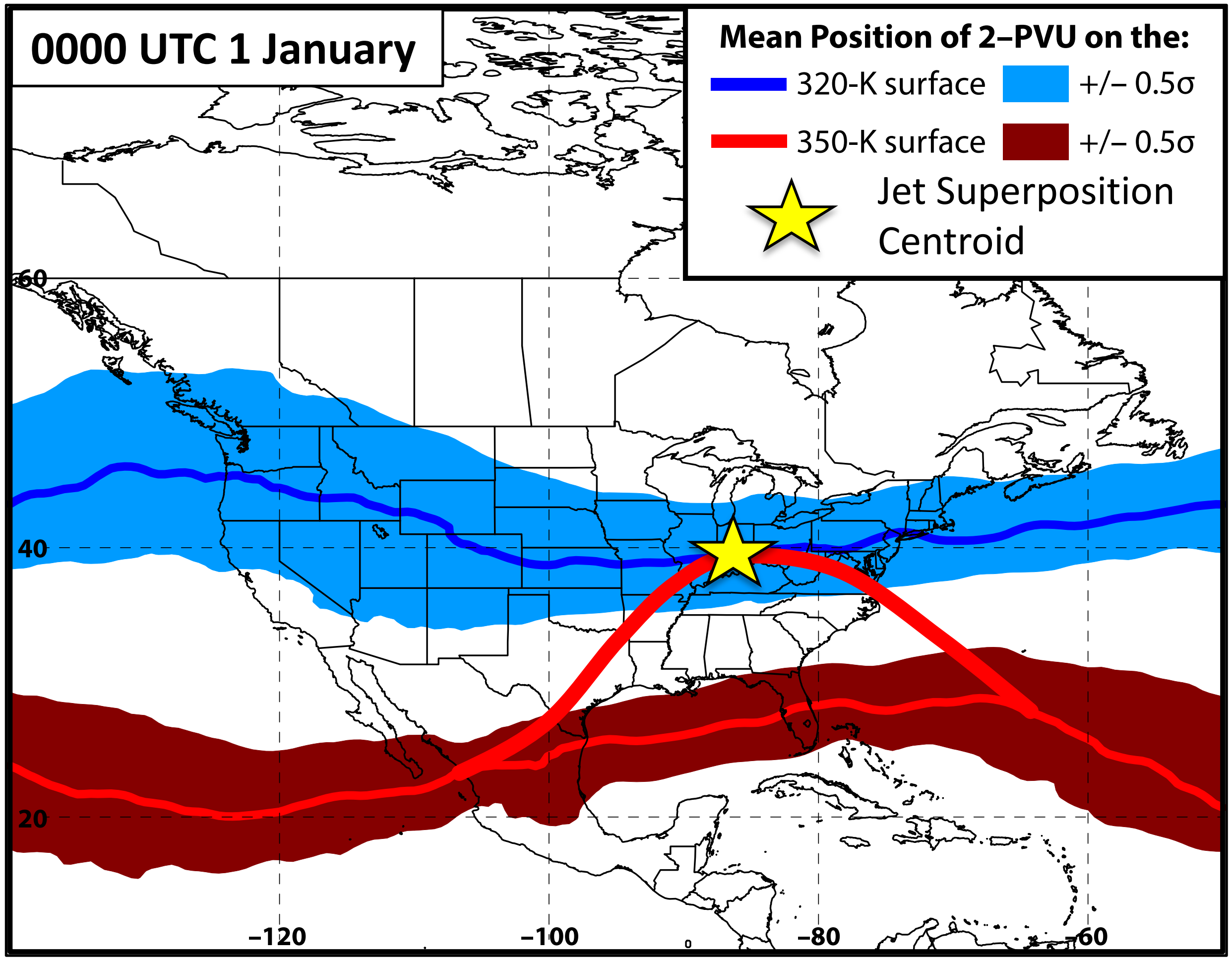

Jet Superposition Event Classification

1. Determined the mean position of the 2-PVU contour on the 320-K and 350-K surfaces at each analysis time in the CFSR.

2. Compared the position of the jet superposition centroid at the start of each event against the climatological position of the 2-PVU contour.

- Polar Dominant
- Subtropical Dominant
- **Hybrid**

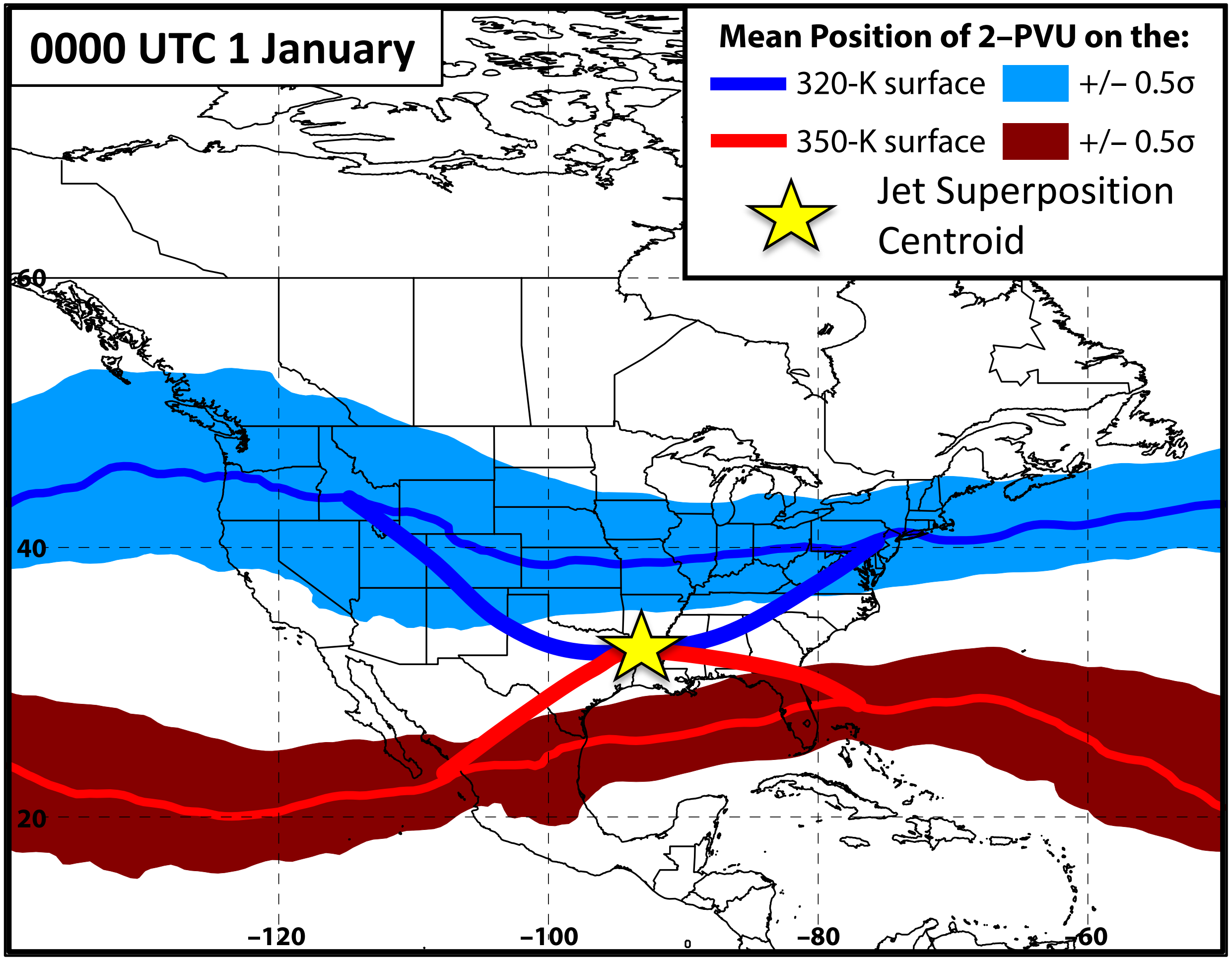

Jet Superposition Event Classification

Frequency of
Polar Dominant
Jet Superposition Events

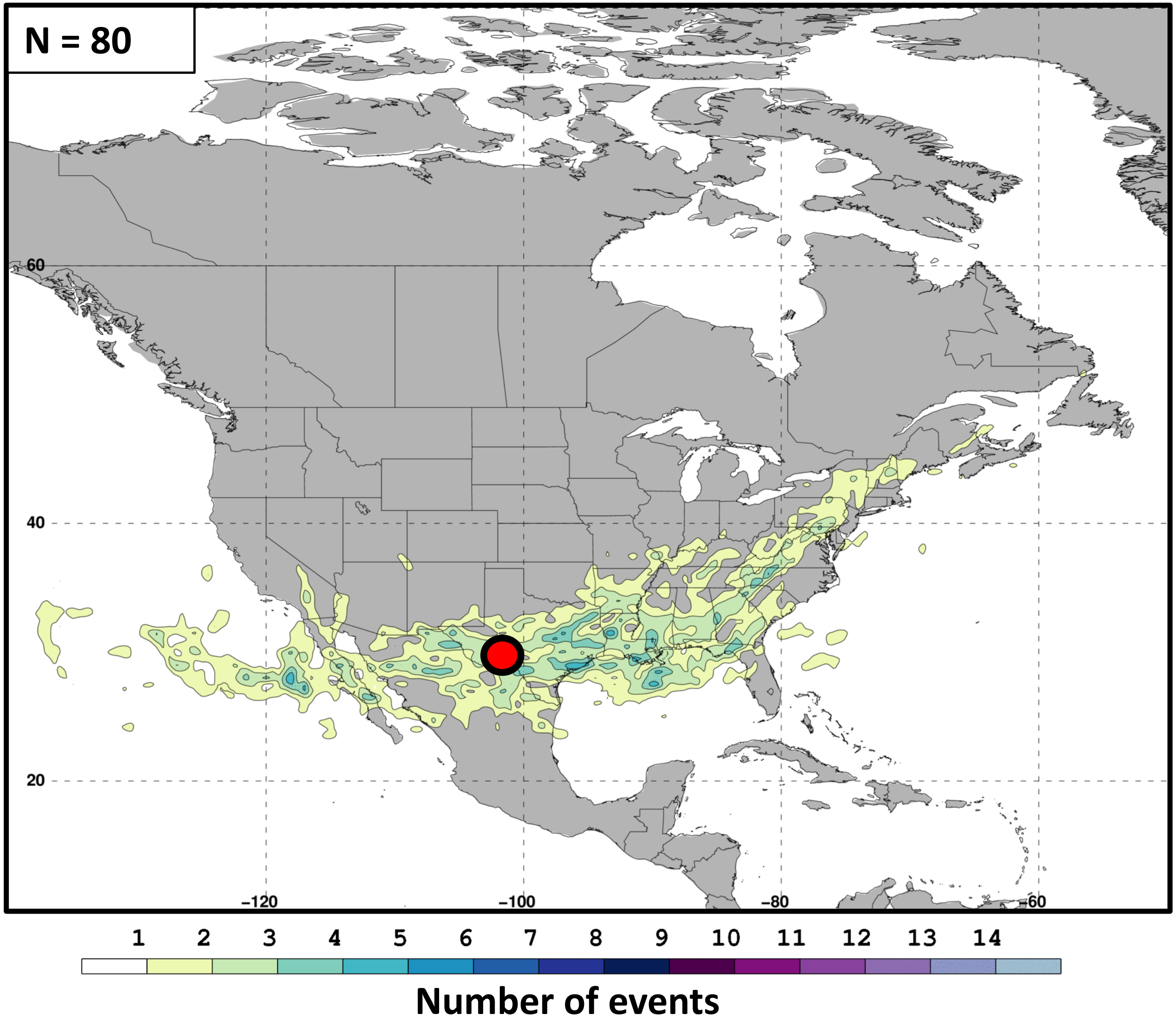

Legend	
●	Avg. Location of Superposition

Jet Superposition Event Classification

Frequency of
Hybrid
Jet
Superposition
Events

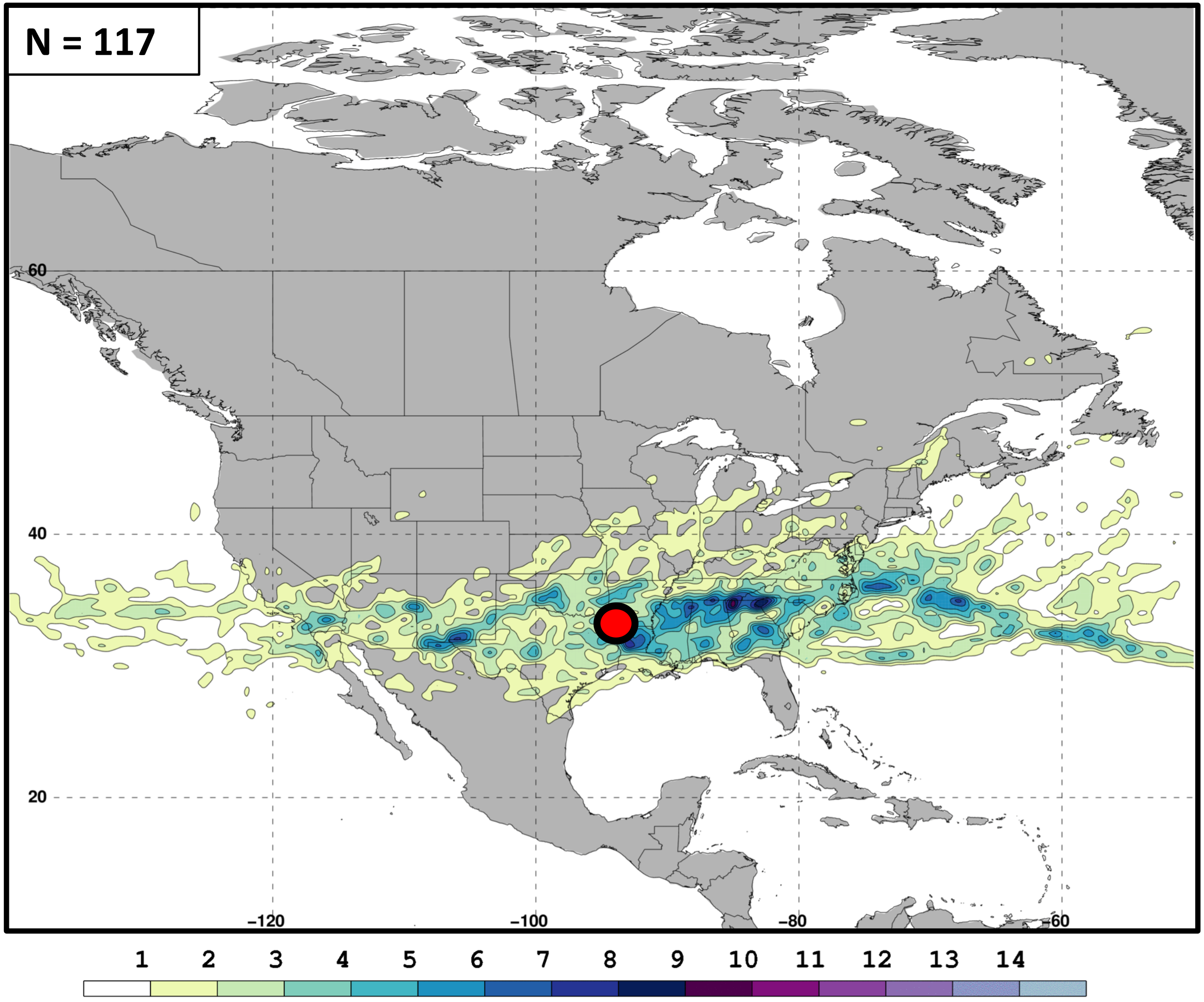

Legend
Avg. Location of Superposition

Jet Superposition Event Classification

Frequency of Subtropical Dominant Jet Superposition Events

Legend
Avg. Location of Superposition

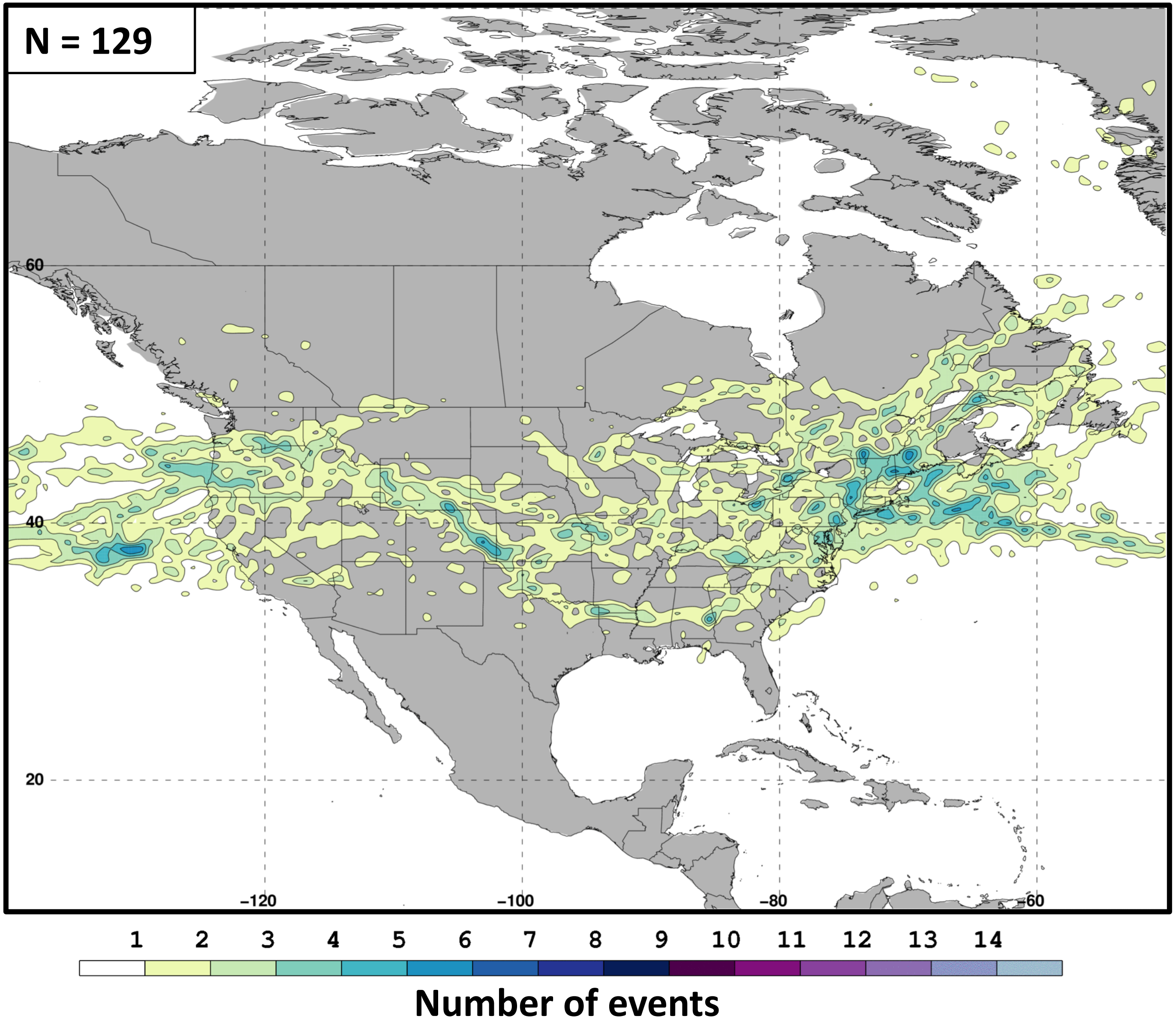

Jet Superposition Event Classification

Frequency of Subtropical Dominant Jet Superposition Events

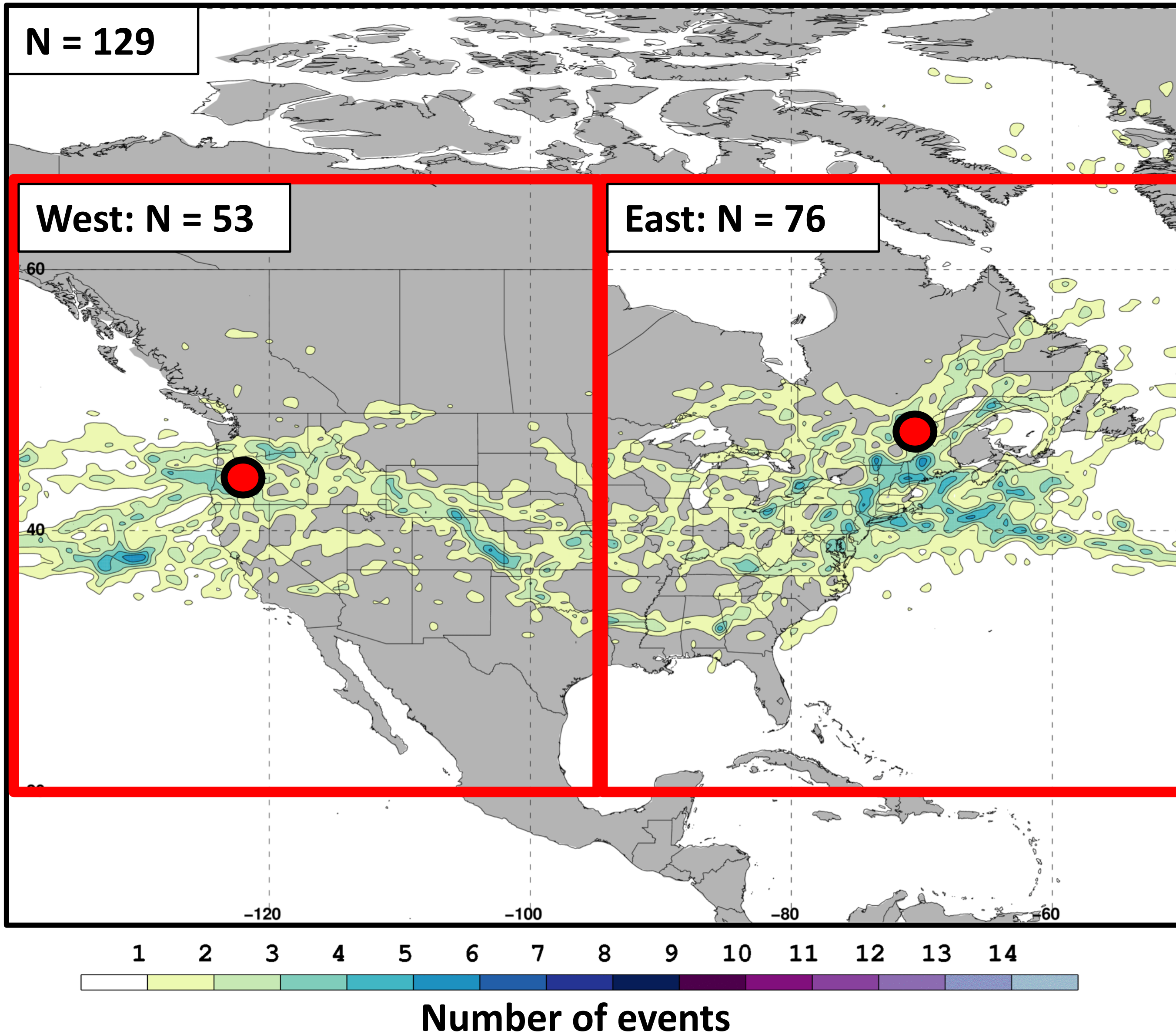

Legend

Avg. Location of Superposition

Jet Superposition Event Composites

Jet Superposition Event Composites

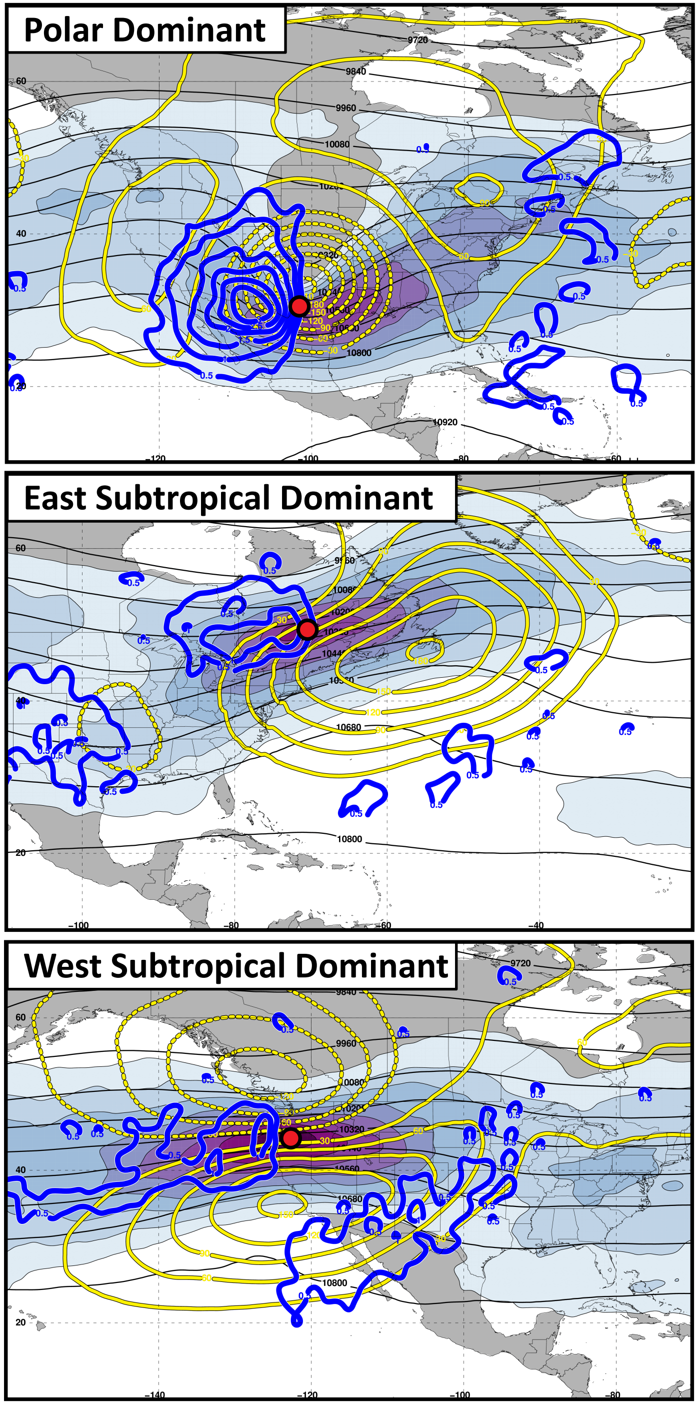

250-hPa Geo. Height

250-hPa Geo. Height Anomalies

500-hPa Descent

Avg. Location of Superposition

20 25 30 35 40 45 50 55 m s[-1] Wind Speed

Jet Superposition Event Composites

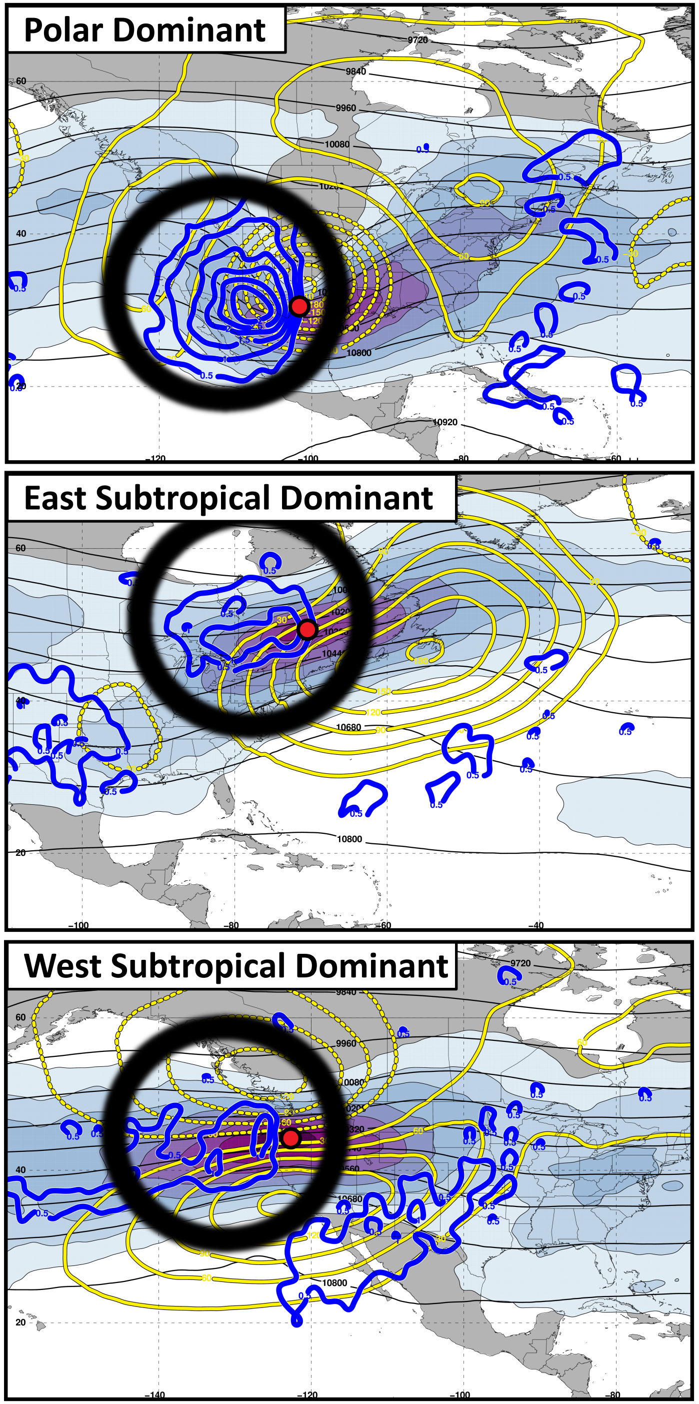

- Descent beneath the jet-entrance region is a common element among the jet superposition event composites.

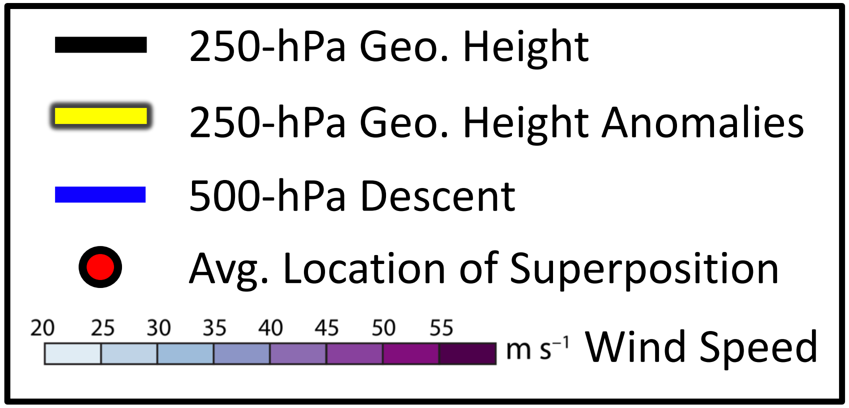

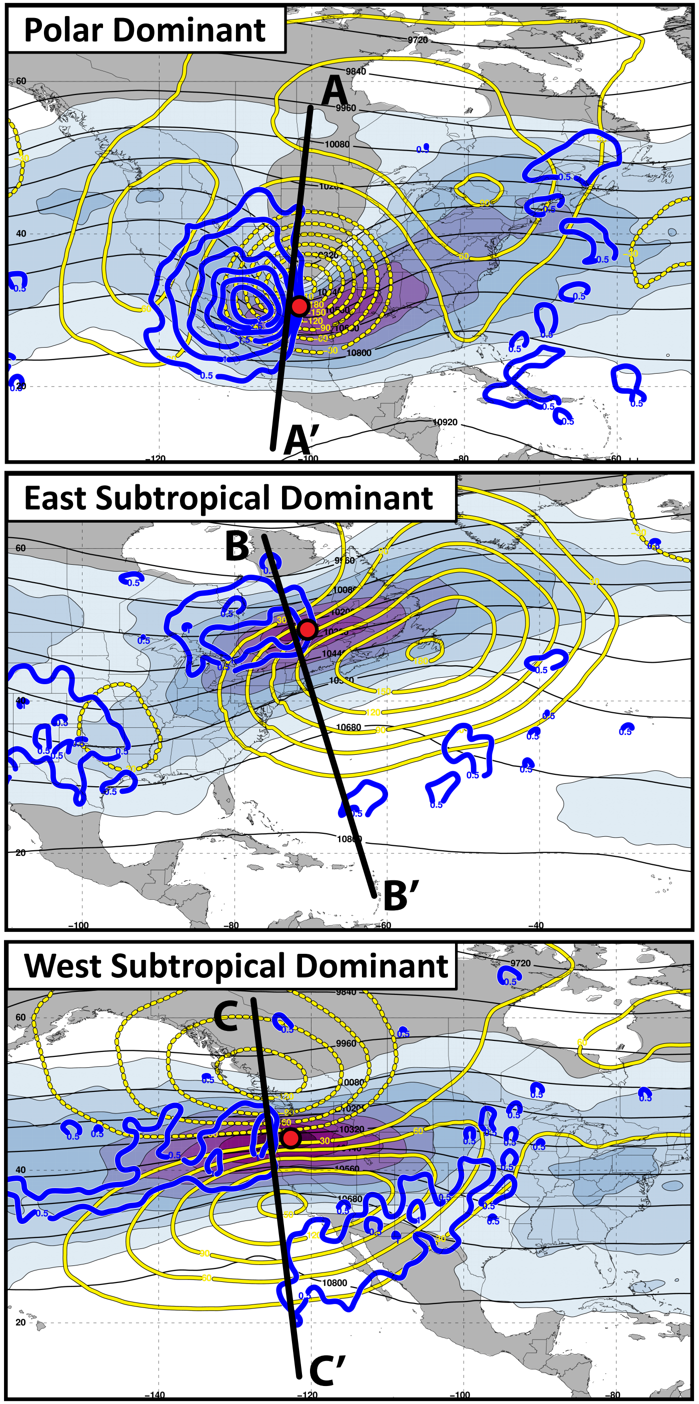

Jet Superposition Event Composites

- Descent beneath the jet-entrance region is a common element among the jet superposition event composites.

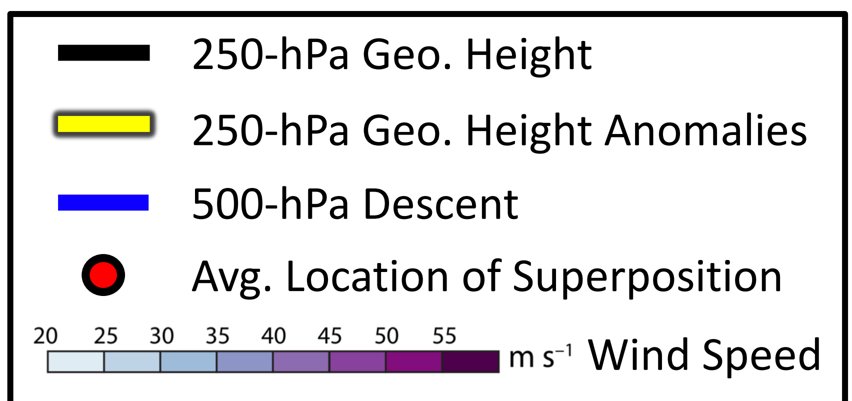

Jet Superposition Event Composites

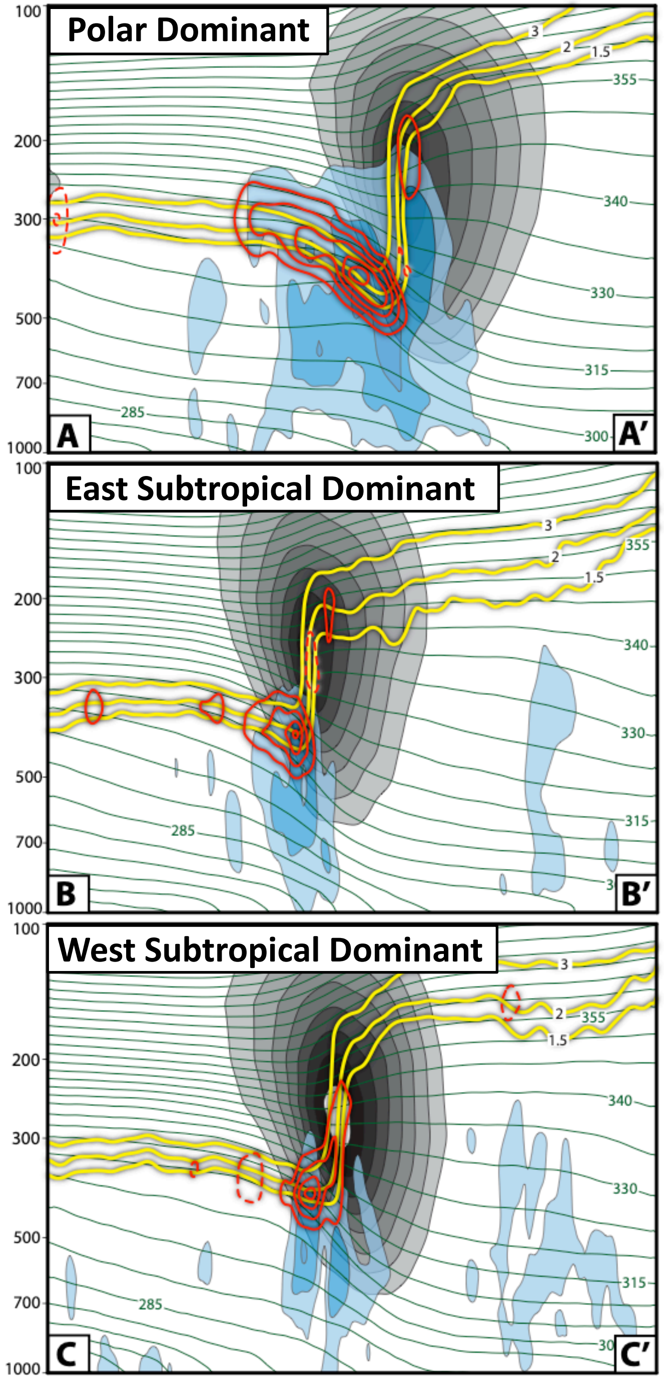

- Descent beneath the jet-entrance region is a common element among the jet superposition event composites.
- Descent results in downward PV advection within the developing tropopause fold, which steepens the tropopause.

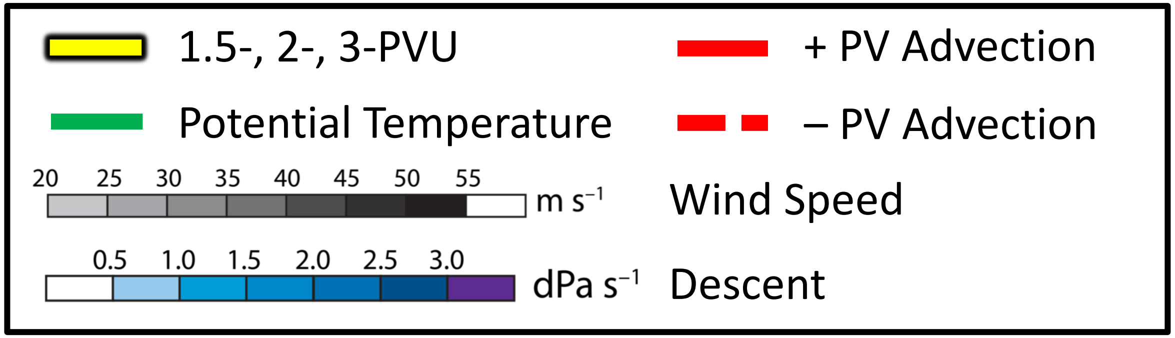

Jet Superposition Event Composites

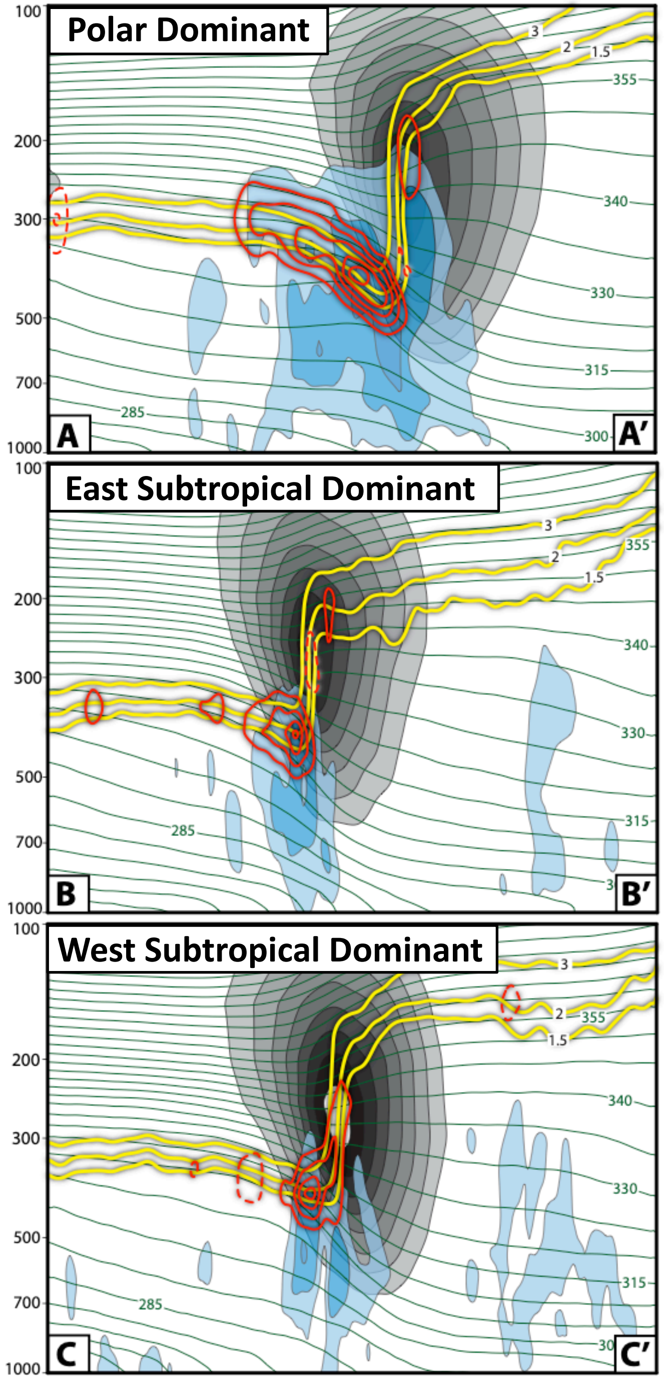

- Descent beneath the jet-entrance region is a common element among the jet superposition event composites.
- Descent results in downward PV advection within the developing tropopause fold, which steepens the tropopause.
- The consistent role of descent motivates further investigation of the dynamical mechanisms responsible for the descent.

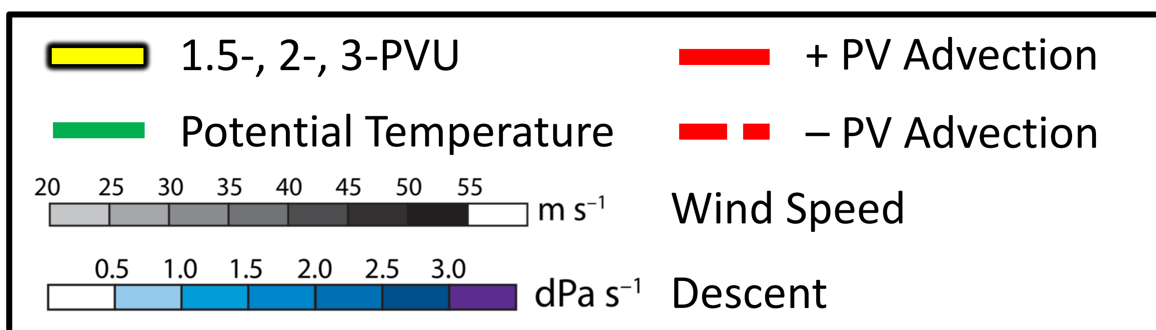

Piecewise QGPV Inversion

Piecewise QGPV Inversion

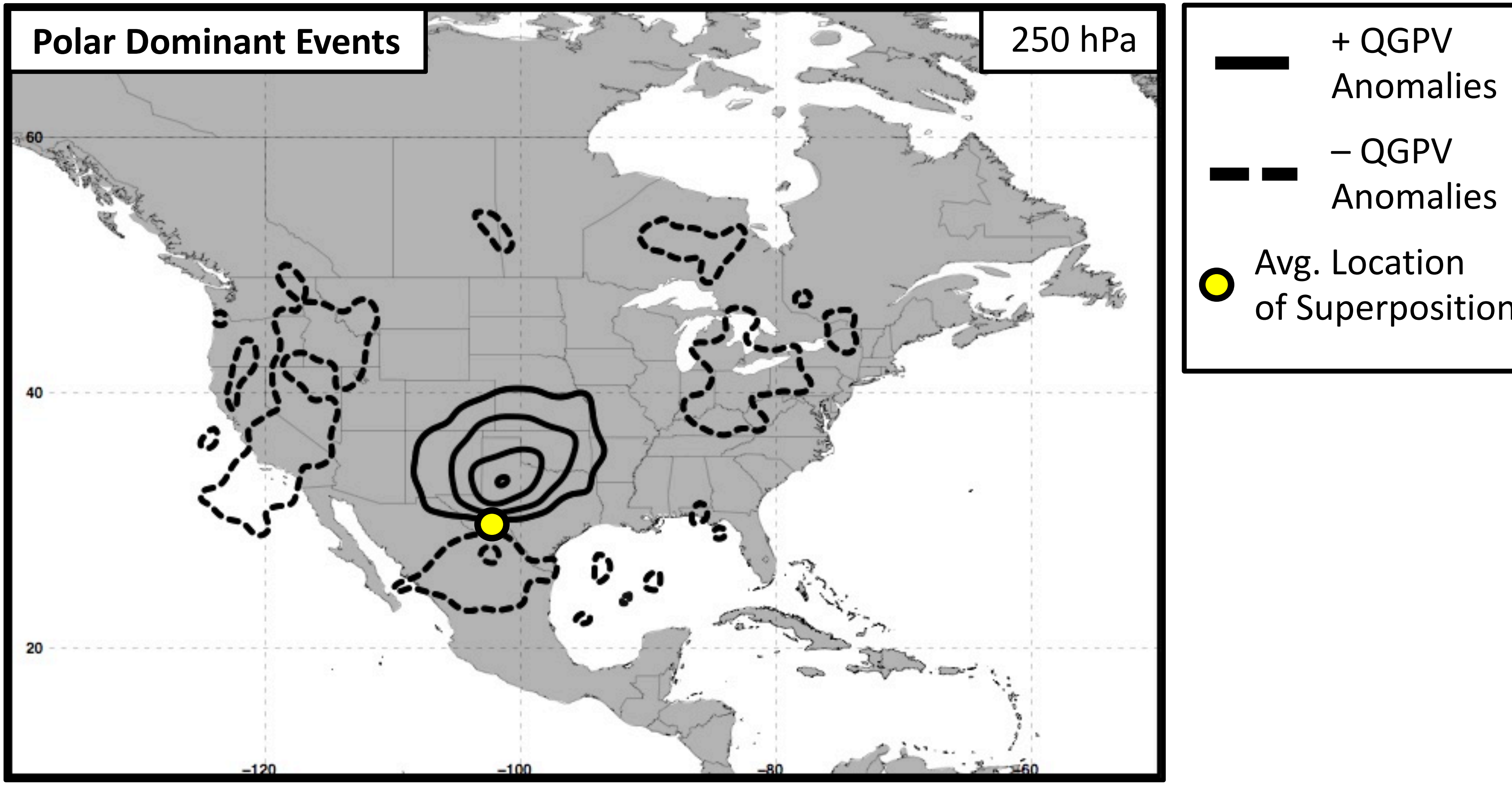

The descent characterizing each jet superposition event composite is examined further by isolating quasi-geostrophic (QG) PV anomalies in the vicinity of the jet superposition.

Piecewise QGPV Inversion

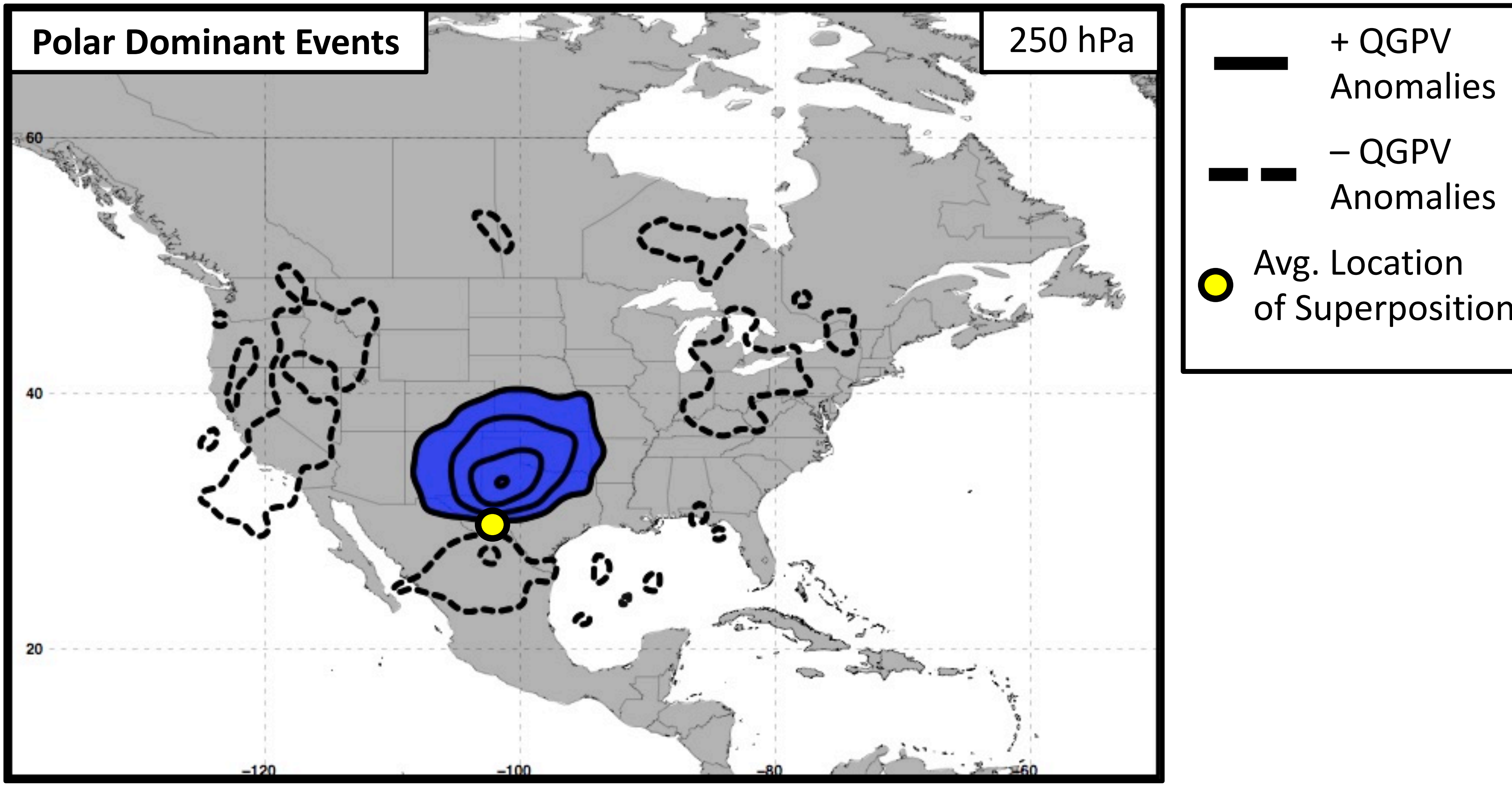

Polar Cyclonic QGPV Anomalies

Piecewise QGPV Inversion

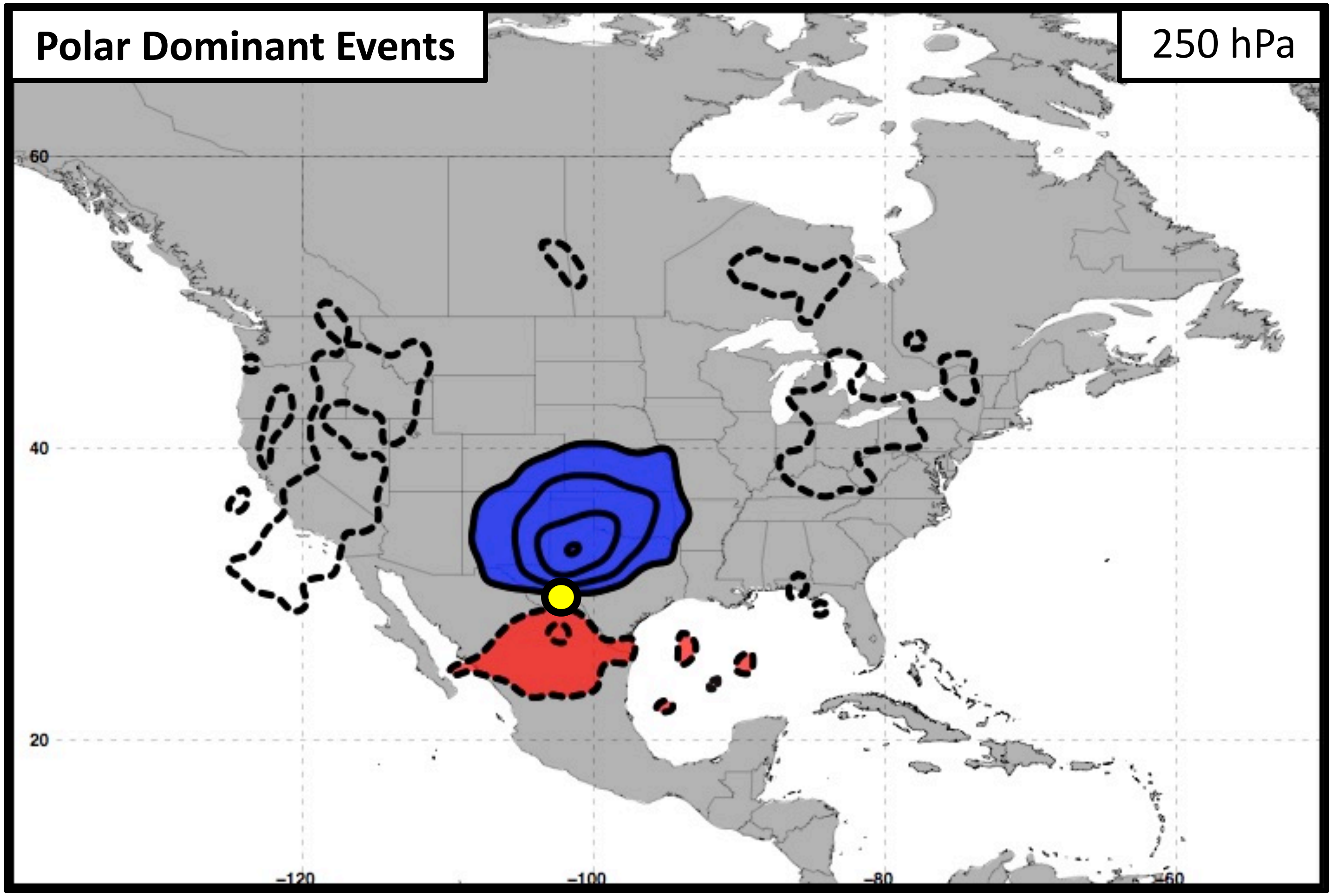

+ QGPV Anomalies

– QGPV Anomalies

Avg. Location of Superposition

Polar Cyclonic QGPV Anomalies

Tropical Anticyclonic QGPV Anomalies

Piecewise QGPV Inversion

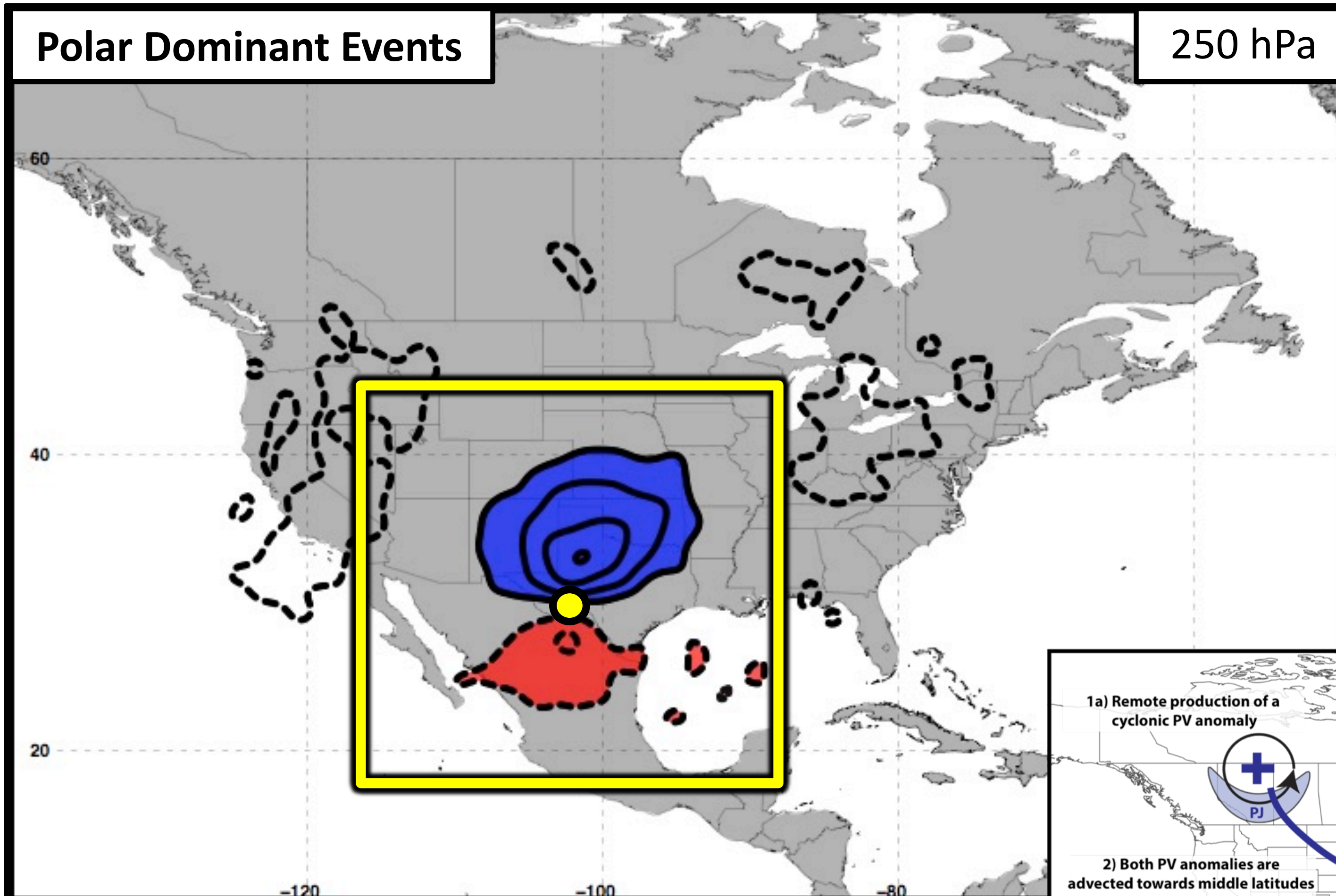

+ QGPV Anomalies

– QGPV Anomalies

Avg. Location of Superposition

Polar Cyclonic QGPV Anomalies

Tropical Anticyclonic QGPV Anomalies

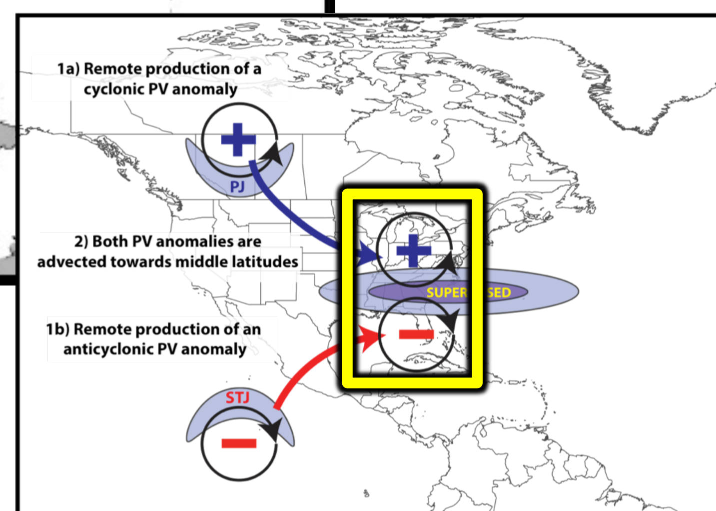

Piecewise QGPV Inversion

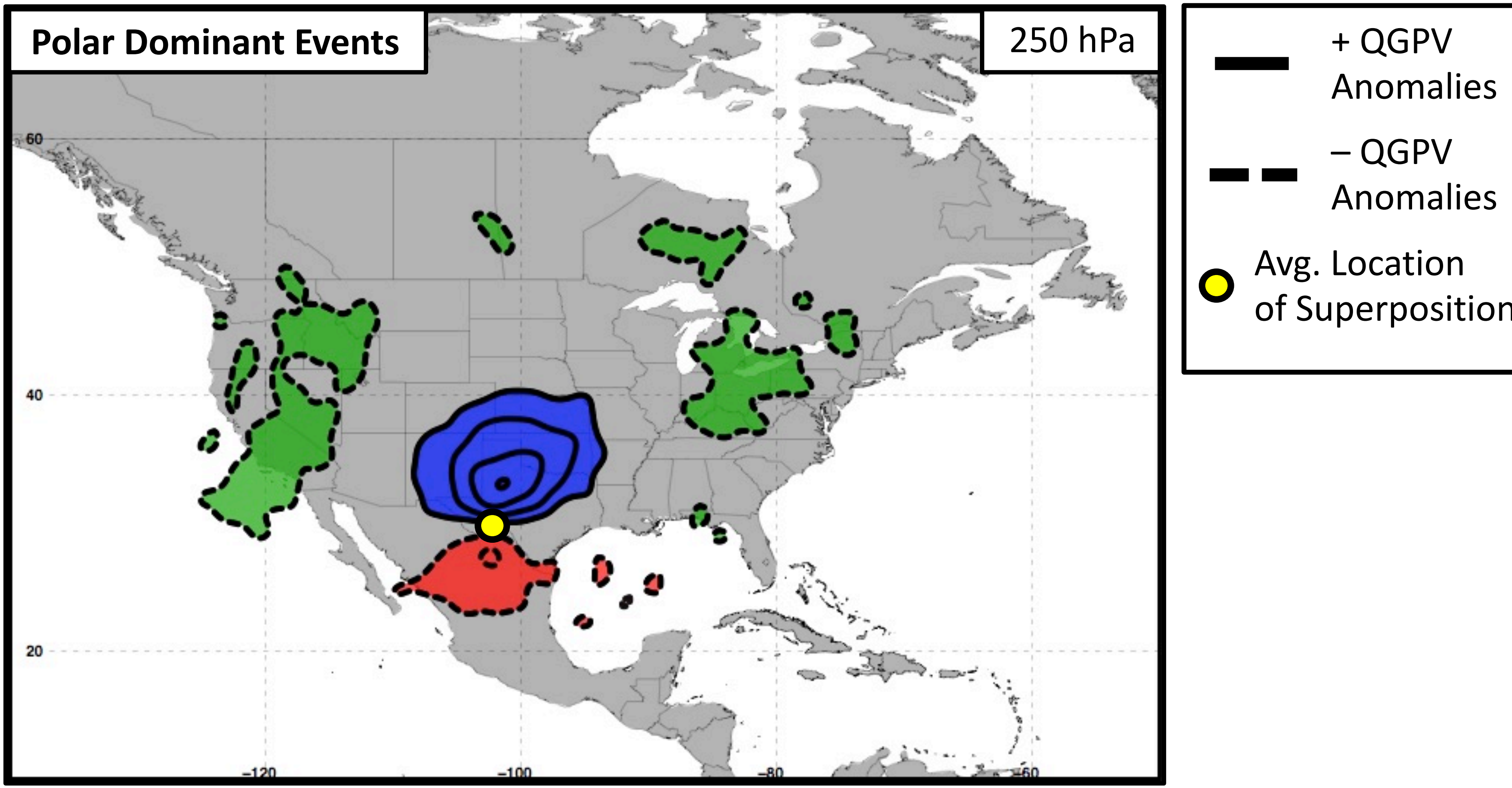

Polar Cyclonic QGPV Anomalies

Tropical Anticyclonic QGPV Anomalies

Residual Upper-Tropospheric QGPV Anomalies

Piecewise QGPV Inversion

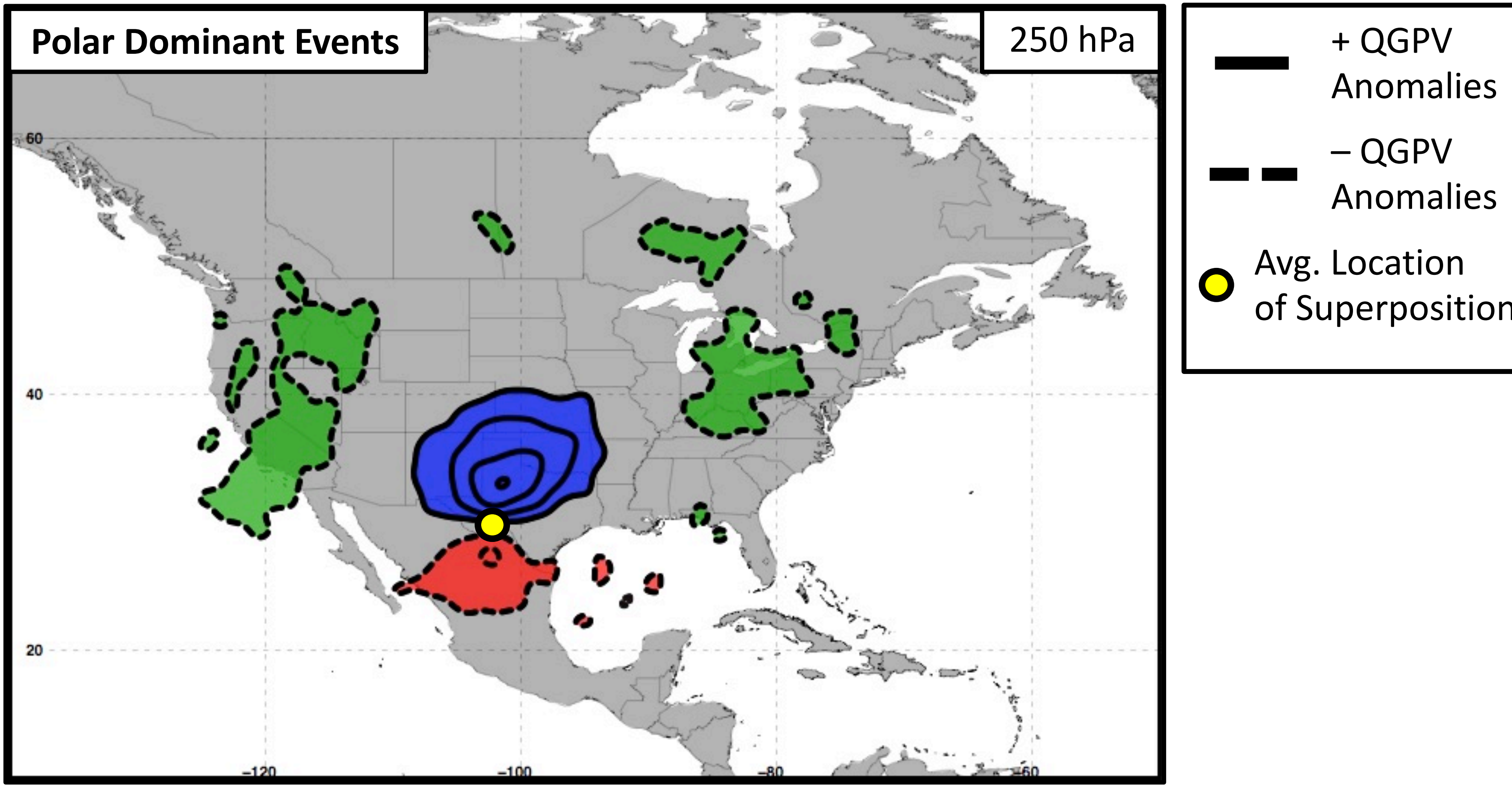

Polar Cyclonic QGPV Anomalies
Tropical Anticyclonic QGPV Anomalies
Residual Upper-Tropospheric QGPV Anomalies
Lower-Tropospheric QGPV Anomalies

Piecewise QGPV Inversion

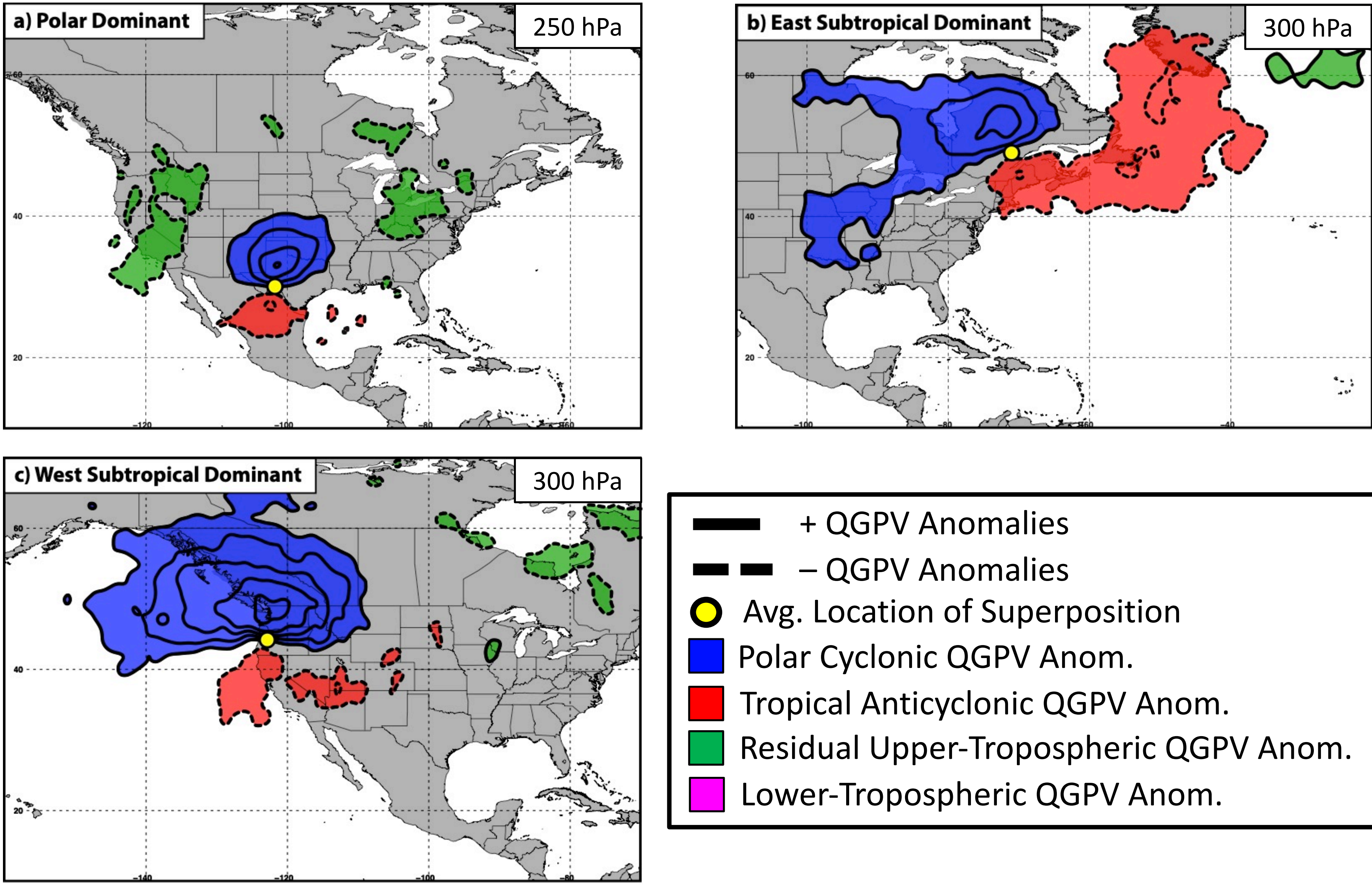

Piecewise QGPV Inversion

Each category of QGPV anomalies (q_i') is inverted to determine its associated perturbation geopotential (ϕ_i') field:

$$q_i' = \frac{1}{f_0}\nabla^2\phi_i' + f_0\frac{\partial}{\partial p}\left(\frac{1}{\sigma_r}\frac{\partial\phi_i'}{\partial p}\right)$$

where

f_0 = *Reference Coriolis Parameter*

σ_r = *Static Stability of the U.S. Std. Atm.*

Piecewise QGPV Inversion

Each category of QGPV anomalies (q_i') is inverted to determine its associated perturbation geopotential (ϕ_i') field:

$$q_i' = \frac{1}{f_0}\nabla^2\phi_i' + f_0\frac{\partial}{\partial p}\left(\frac{1}{\sigma_r}\frac{\partial\phi_i'}{\partial p}\right)$$

where

f_0 = *Reference Coriolis Parameter*

σ_r = *Static Stability of the U.S. Std. Atm.*

The perturbation geopotential fields and the composite temperature (T) field are used to determine the QG vertical motion (ω_i) associated with each category of QGPV:

$$\sigma_r\nabla^2\omega_i + f_0^2\frac{\partial^2\omega_i}{\partial p^2} = -2\nabla\cdot\vec{Q}_i$$

where

$$\vec{V_{gi}'} = -(1/f_0)(\hat{k}\times\nabla\phi_i')$$

$$\vec{Q}_i = -\frac{R}{p}\left[\left(\frac{\partial\vec{V_{gi}'}}{\partial x}\cdot\nabla T\right),\left(\frac{\partial\vec{V_{gi}'}}{\partial y}\cdot\nabla T\right)\right]$$

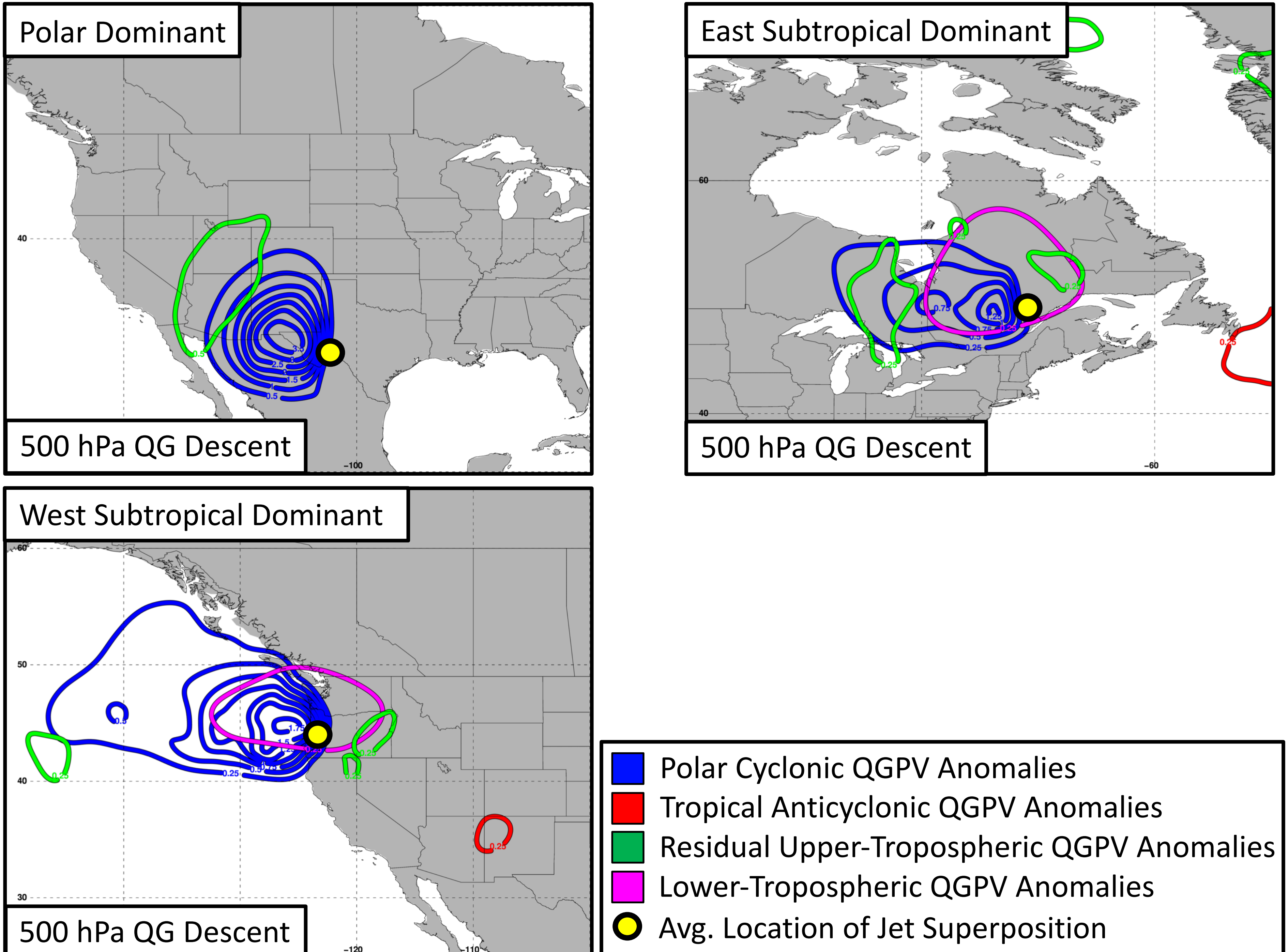

Polar Dominant
500 hPa QG Descent
East Subtropical Dominant
500 hPa QG Descent
West Subtropical Dominant
500 hPa QG Descent
Polar Cyclonic QGPV Anomalies
Tropical Anticyclonic QGPV Anomalies
Residual Upper-Tropospheric QGPV Anomalies
Lower-Tropospheric QGPV Anomalies
Avg. Location of Jet Superposition

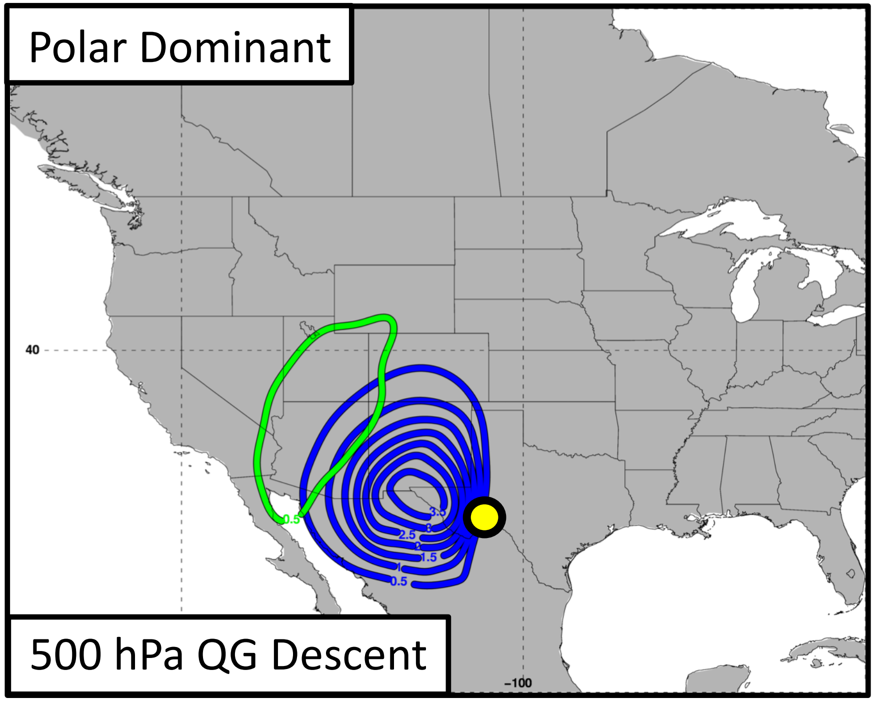

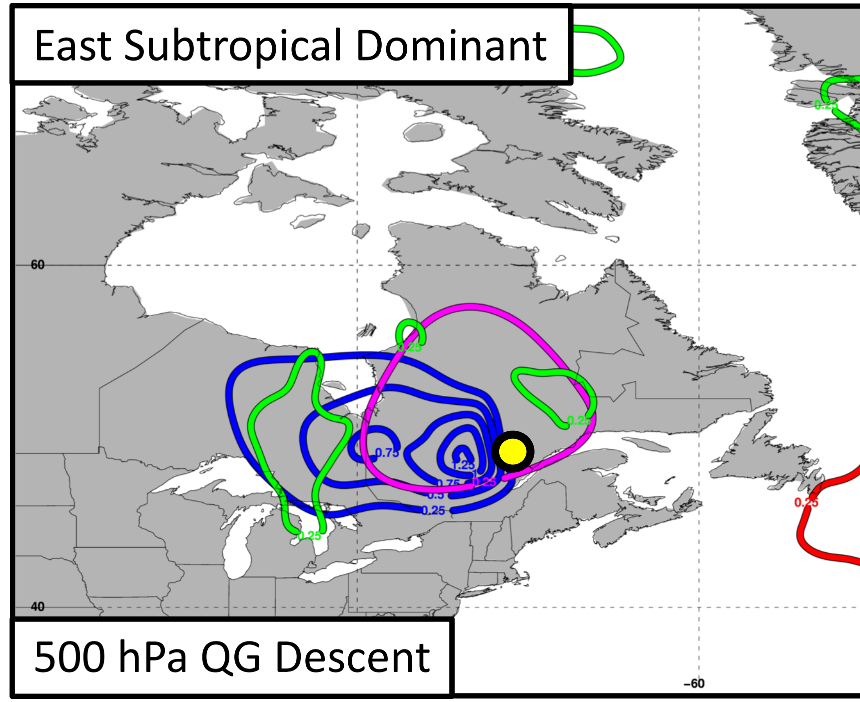

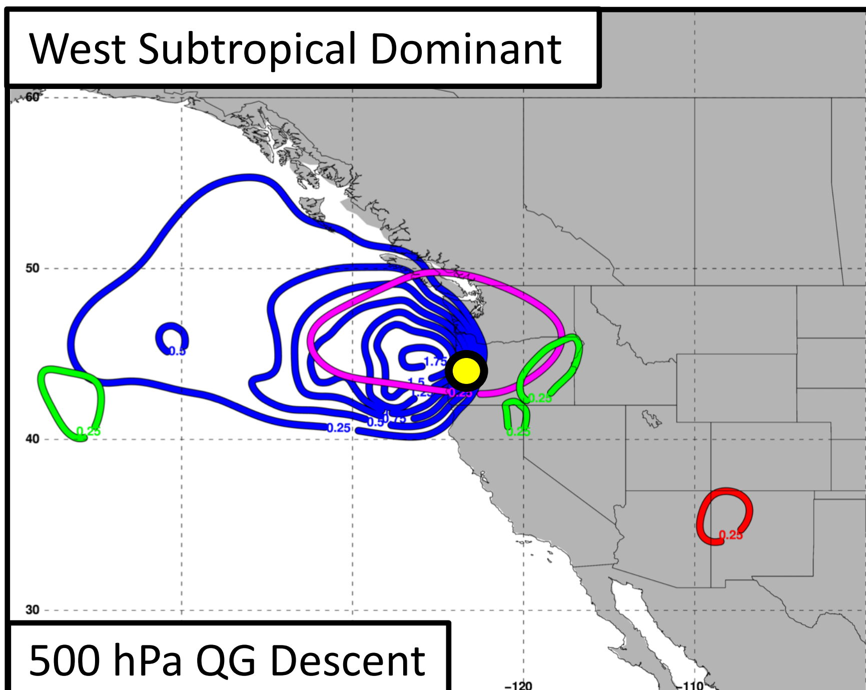

Descent is primarily associated with polar cyclonic QGPV anomalies.

- Polar Cyclonic QGPV Anomalies
- Tropical Anticyclonic QGPV Anomalies
- Residual Upper-Tropospheric QGPV Anomalies
- Lower-Tropospheric QGPV Anomalies
- Avg. Location of Jet Superposition

Piecewise QGPV Inversion

$$\sigma_r \nabla^2 \omega_i + f_0^2 \frac{\partial^2 \omega_i}{\partial p^2} = -2\nabla \cdot \vec{Q}_i \quad \textit{where} \quad \begin{aligned} \overrightarrow{V'_{gi}} &= -(1/f_0)(\hat{k} \times \nabla \phi'_i) \\ \vec{Q}_i &= -\frac{R}{p}\left[\left(\frac{\partial \overrightarrow{V'_{gi}}}{\partial x} \cdot \nabla T\right), \left(\frac{\partial \overrightarrow{V'_{gi}}}{\partial y} \cdot \nabla T\right)\right] \end{aligned}$$

The prior analyses only consider the interaction of each perturbation geostrophic wind ($\overrightarrow{V'_{gi}}$) field with the composite temperature field (T).

Piecewise QGPV Inversion

$$\sigma_r \nabla^2 \omega_i + f_0^2 \frac{\partial^2 \omega_i}{\partial p^2} = -2\nabla \cdot \vec{Q}_i \quad \textit{where} \quad \begin{aligned} \overrightarrow{V'_{gi}} &= -(1/f_0)(\hat{k} \times \nabla \phi'_i) \\ \vec{Q}_i &= -\frac{R}{p}\left[\left(\frac{\partial \overrightarrow{V'_{gi}}}{\partial x} \cdot \nabla T\right), \left(\frac{\partial \overrightarrow{V'_{gi}}}{\partial y} \cdot \nabla T\right)\right] \end{aligned}$$

The prior analyses only consider the interaction of each perturbation geostrophic wind ($\overrightarrow{V'_{gi}}$) field with the composite temperature field (T).

Each perturbation geopotential field (ϕ'_i) is also accompanied by a perturbation temperature field (T'_i) .

Piecewise QGPV Inversion

$$\sigma_r \nabla^2 \omega_i + f_0^2 \frac{\partial^2 \omega_i}{\partial p^2} = -2\nabla \cdot \vec{Q}_i$$

where

$$\overrightarrow{V'_{gi}} = -(1/f_0)(\hat{k} \times \nabla \phi'_i)$$

$$\vec{Q}_i = -\frac{R}{p}\left[\left(\frac{\partial \overrightarrow{V'_{gi}}}{\partial x} \cdot \boxed{\nabla T'_i}\right), \left(\frac{\partial \overrightarrow{V'_{gi}}}{\partial y} \cdot \boxed{\nabla T'_i}\right)\right]$$

The prior analyses only consider the interaction of each perturbation geostrophic wind ($\overrightarrow{V'_{gi}}$) field with the composite temperature field (T).

Each perturbation geopotential field (ϕ'_i) is also accompanied by a perturbation temperature field (T'_i) .

Substituting the perturbation temperature fields (T'_i) into the QG-ω equation permits a determination of the QG vertical motion that results from interactions between each category of QGPV anomalies.

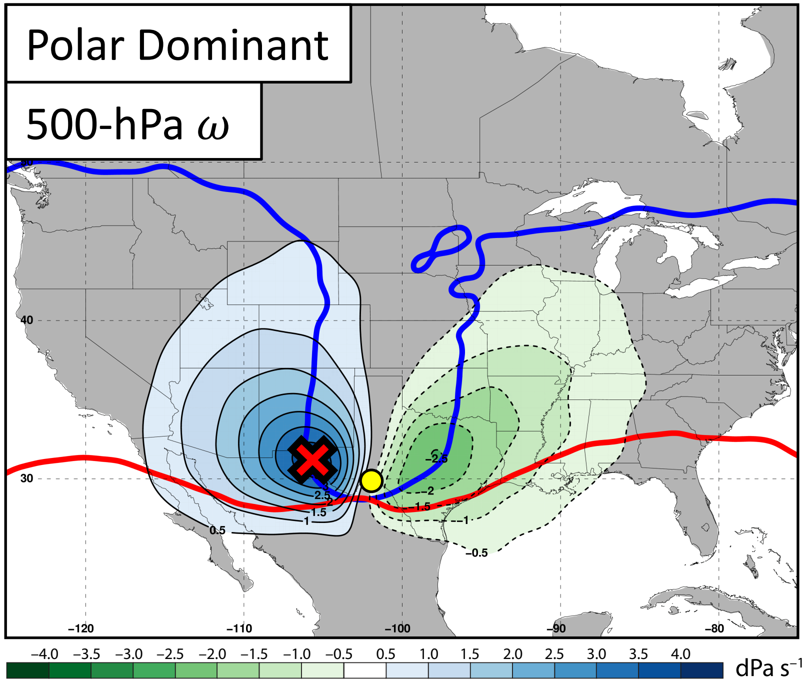

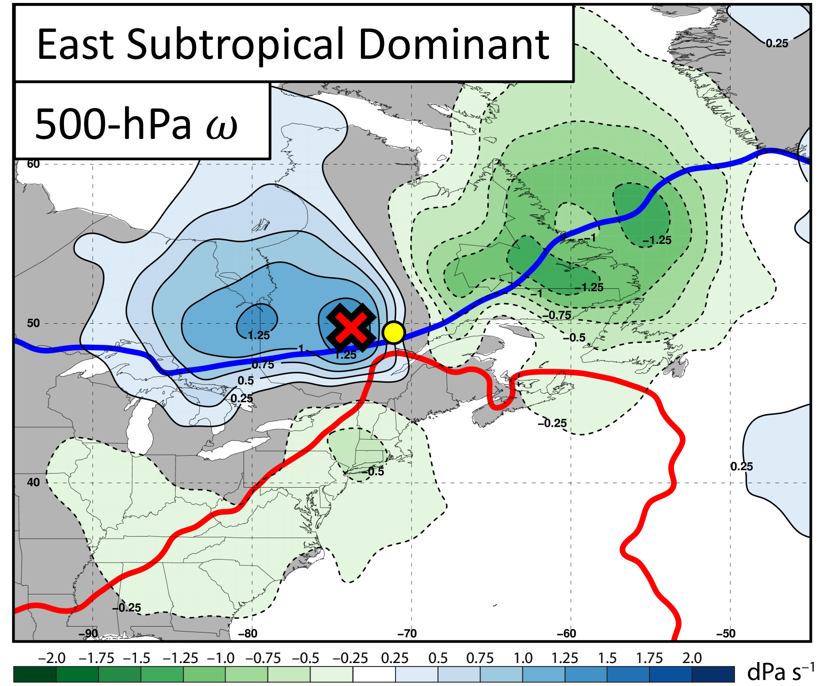

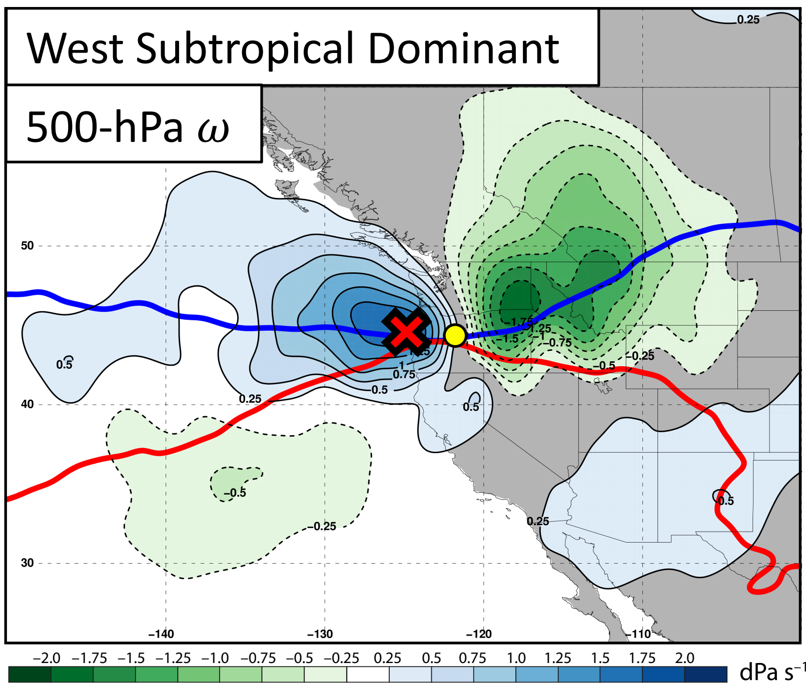

Consider the QG ω associated with each interaction term at the location of maximum descent.

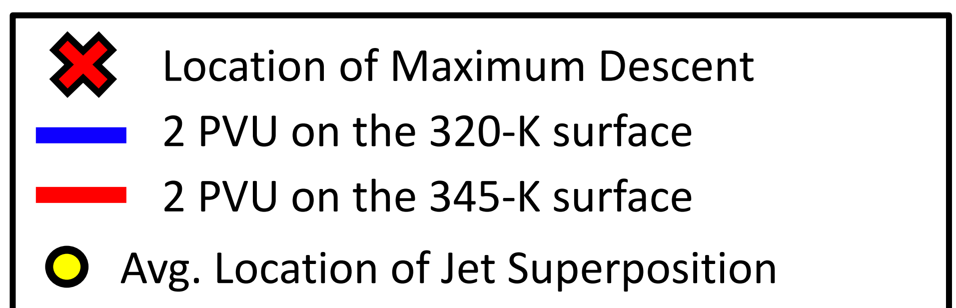

Piecewise QGPV Inversion

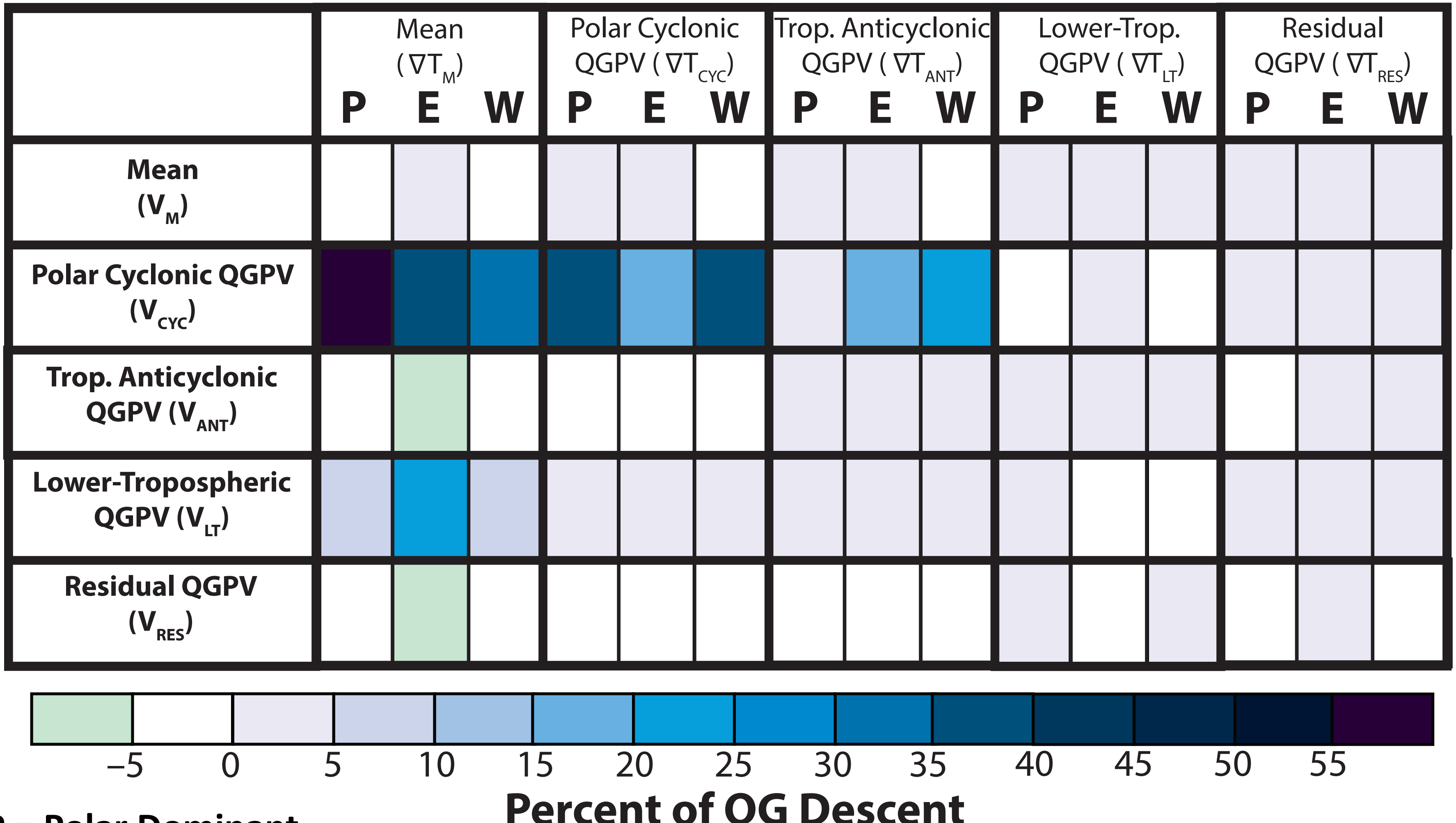

P = Polar Dominant

E = East Subtropical Dominant

W = West Subtropical Dominant

Piecewise QGPV Inversion

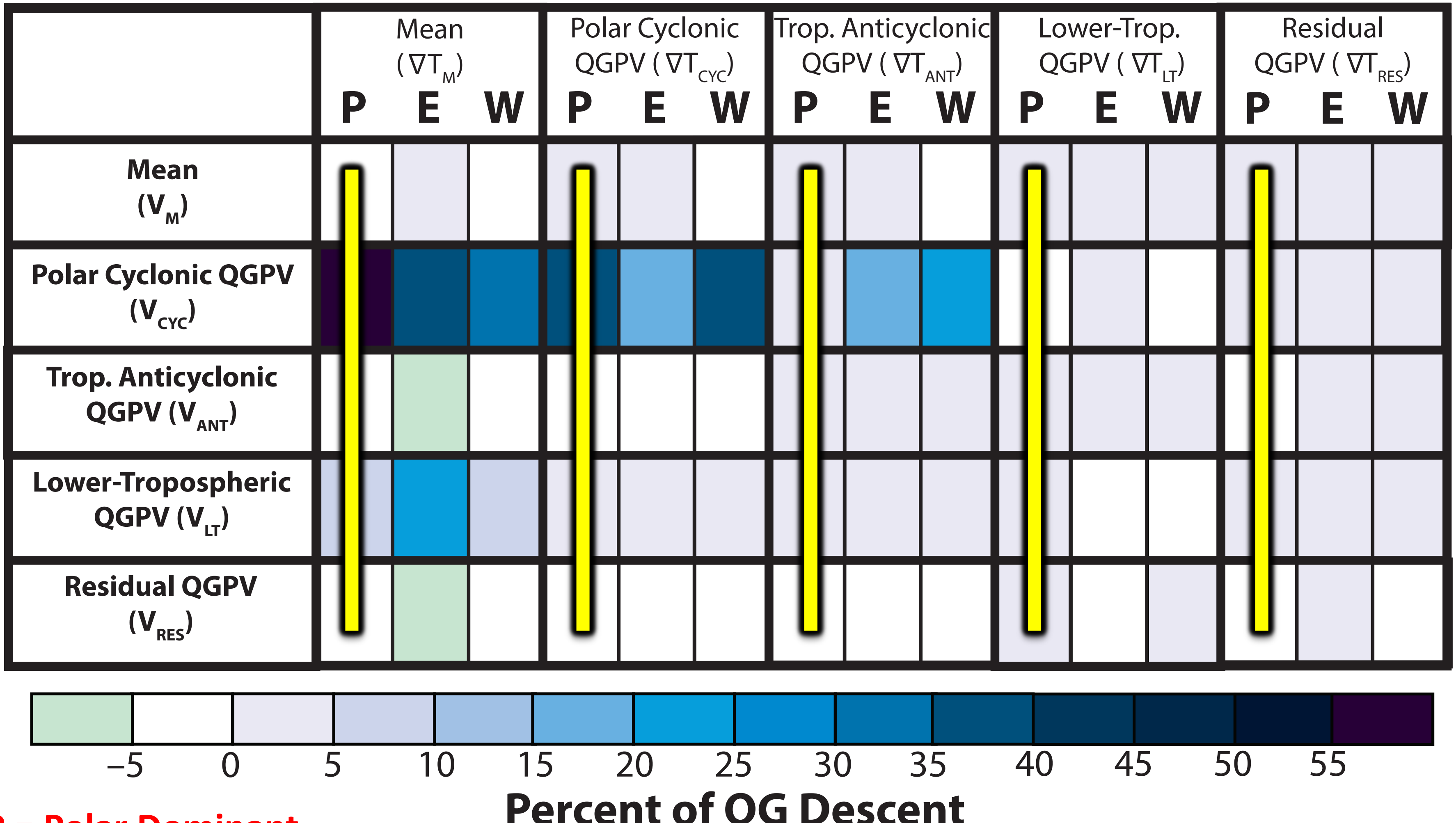

P = Polar Dominant

E = East Subtropical Dominant

W = West Subtropical Dominant

Piecewise QGPV Inversion

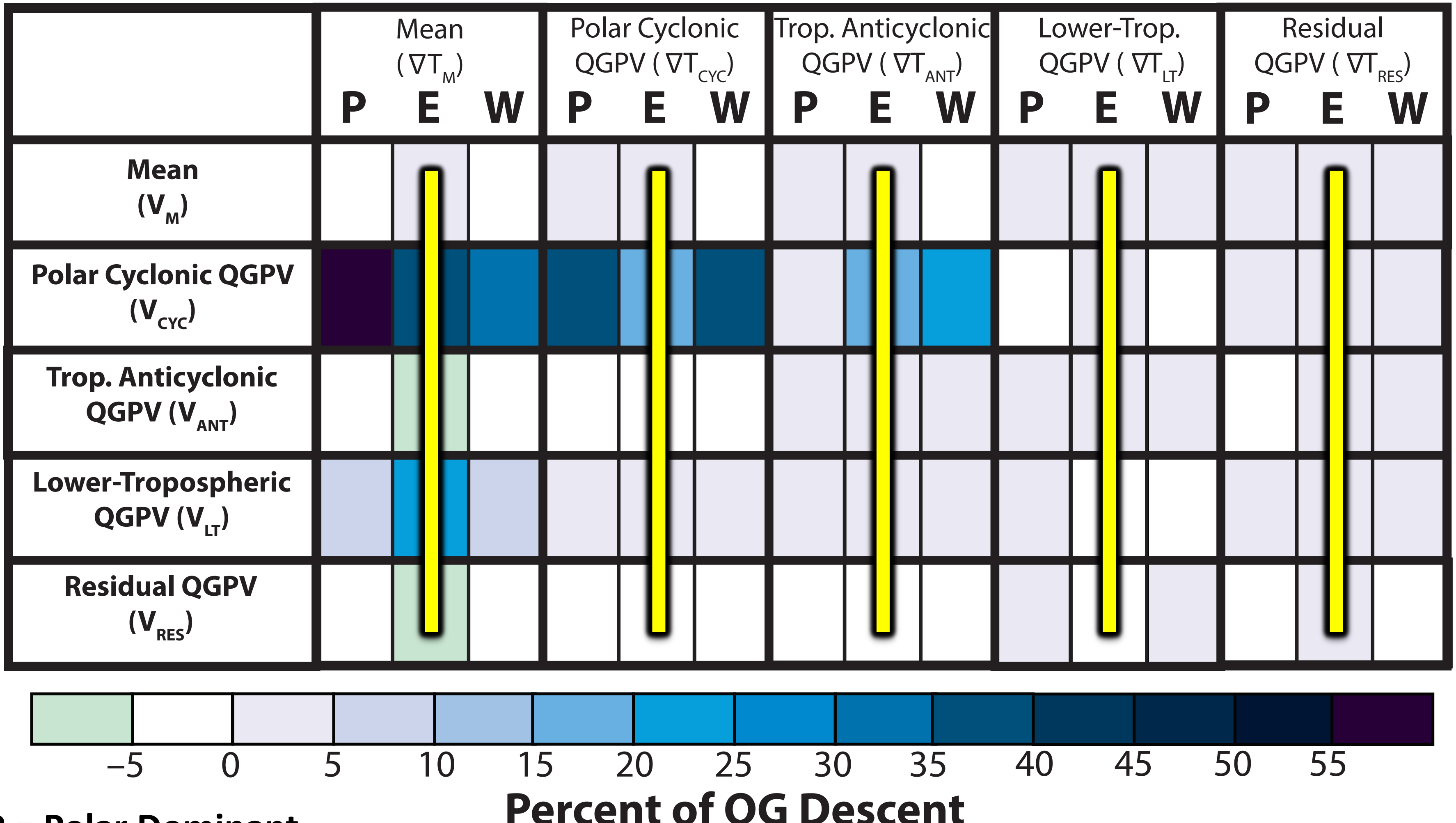

P = Polar Dominant

E = East Subtropical Dominant

W = West Subtropical Dominant

Piecewise QGPV Inversion

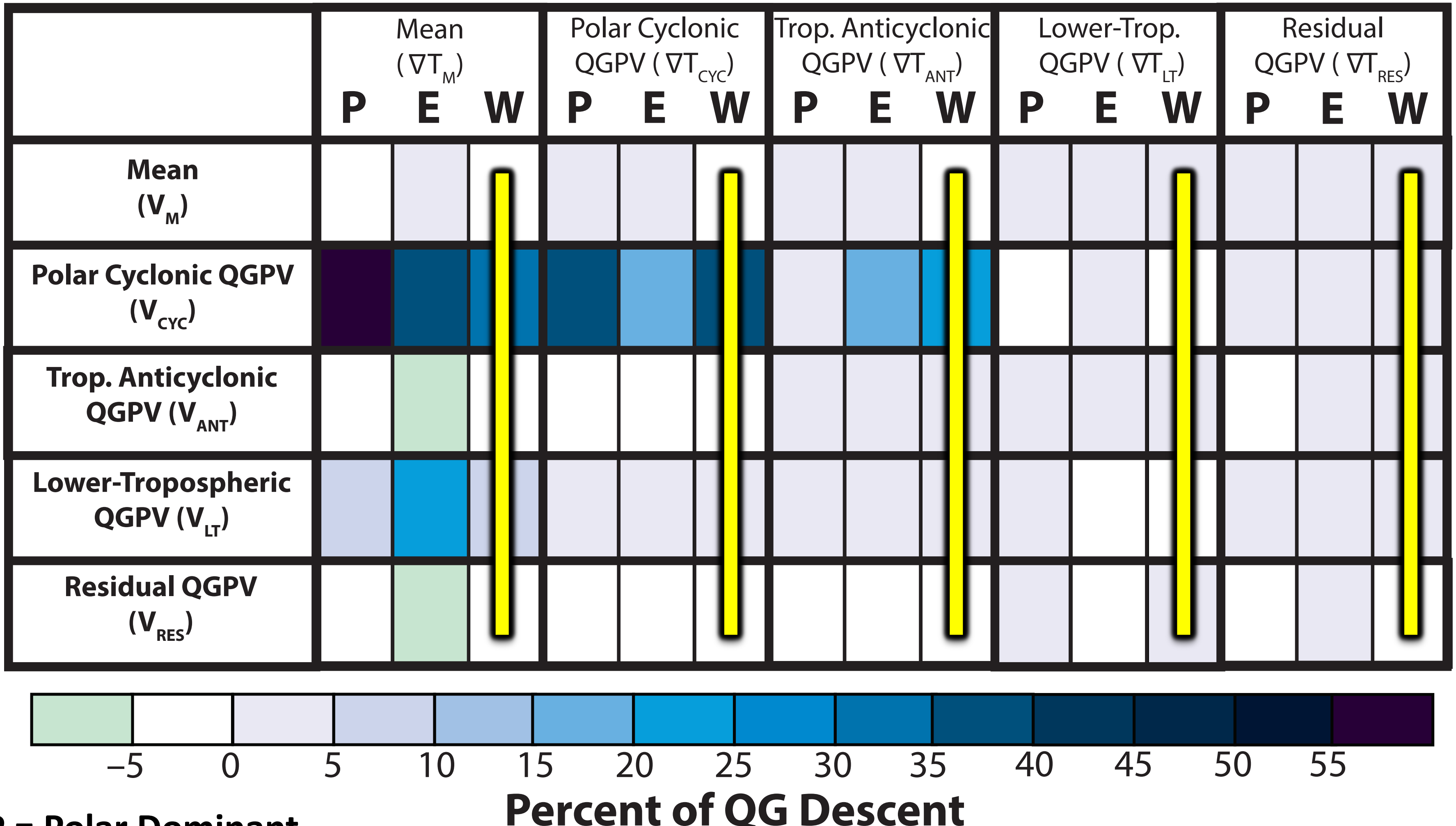

P = Polar Dominant

E = East Subtropical Dominant

W = West Subtropical Dominant

Piecewise QGPV Inversion

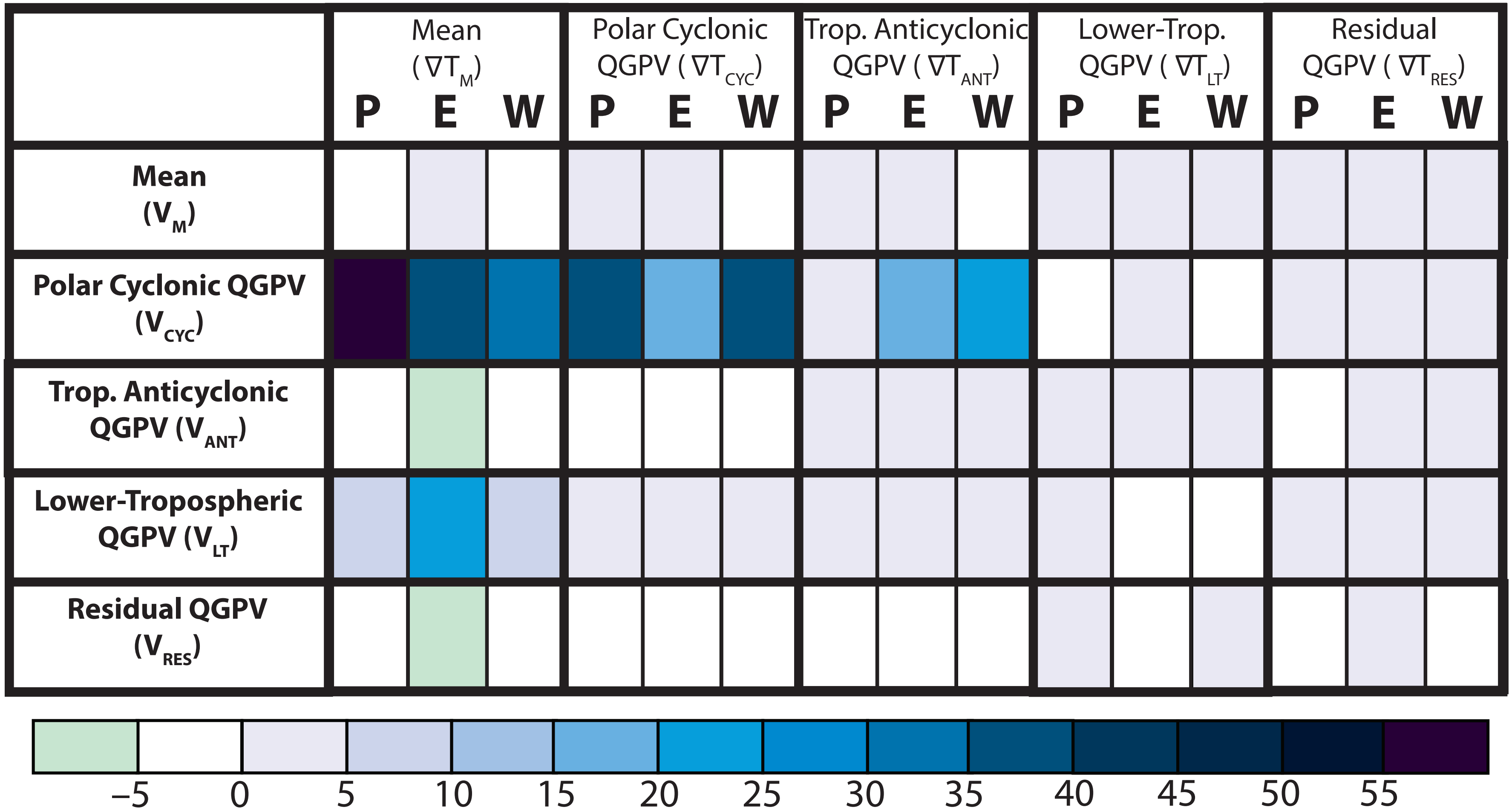

P = Polar Dominant
E = East Subtropical Dominant
W = West Subtropical Dominant

Piecewise QGPV Inversion

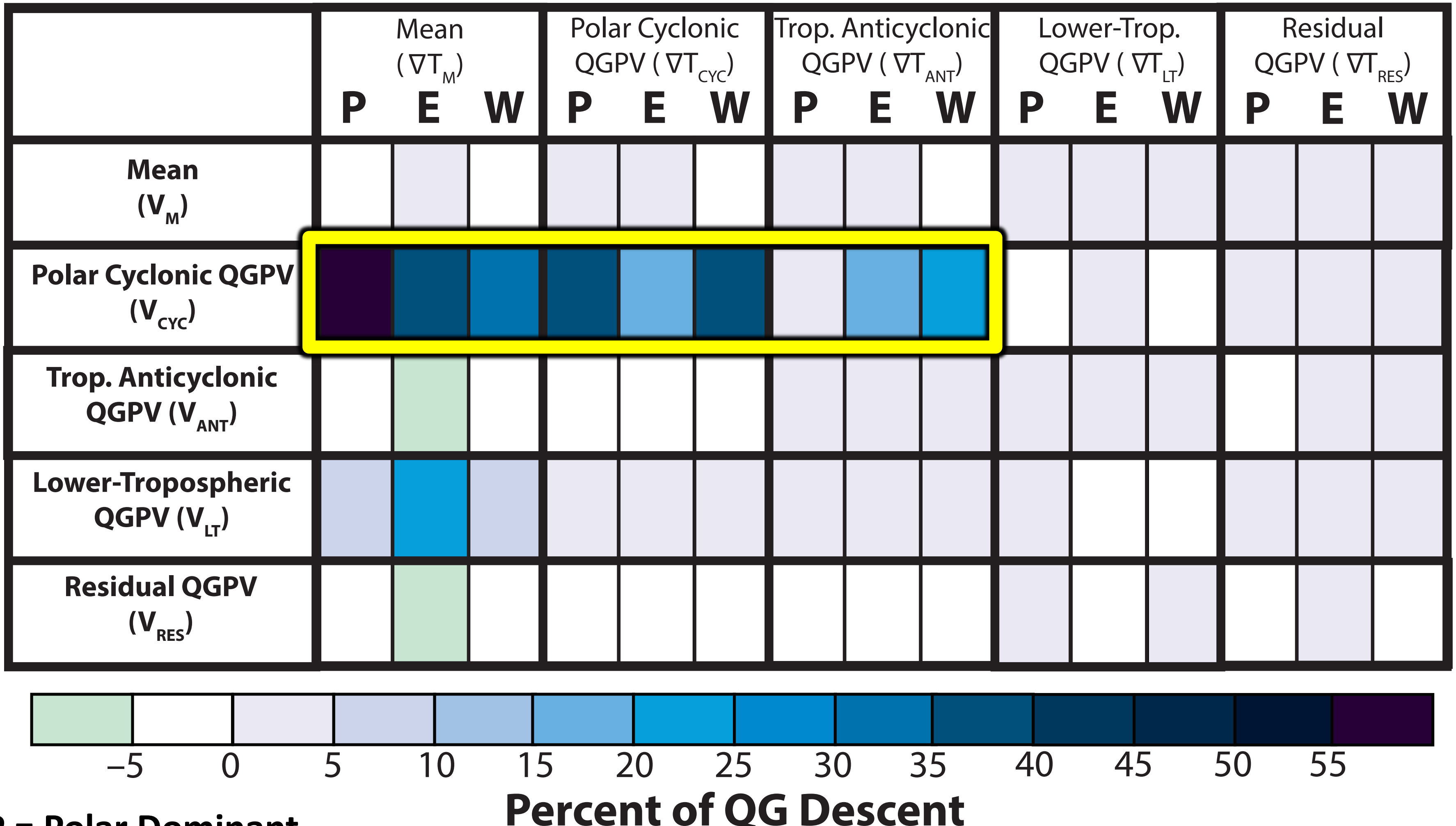

P = Polar Dominant
E = East Subtropical Dominant
W = West Subtropical Dominant

Piecewise QGPV Inversion

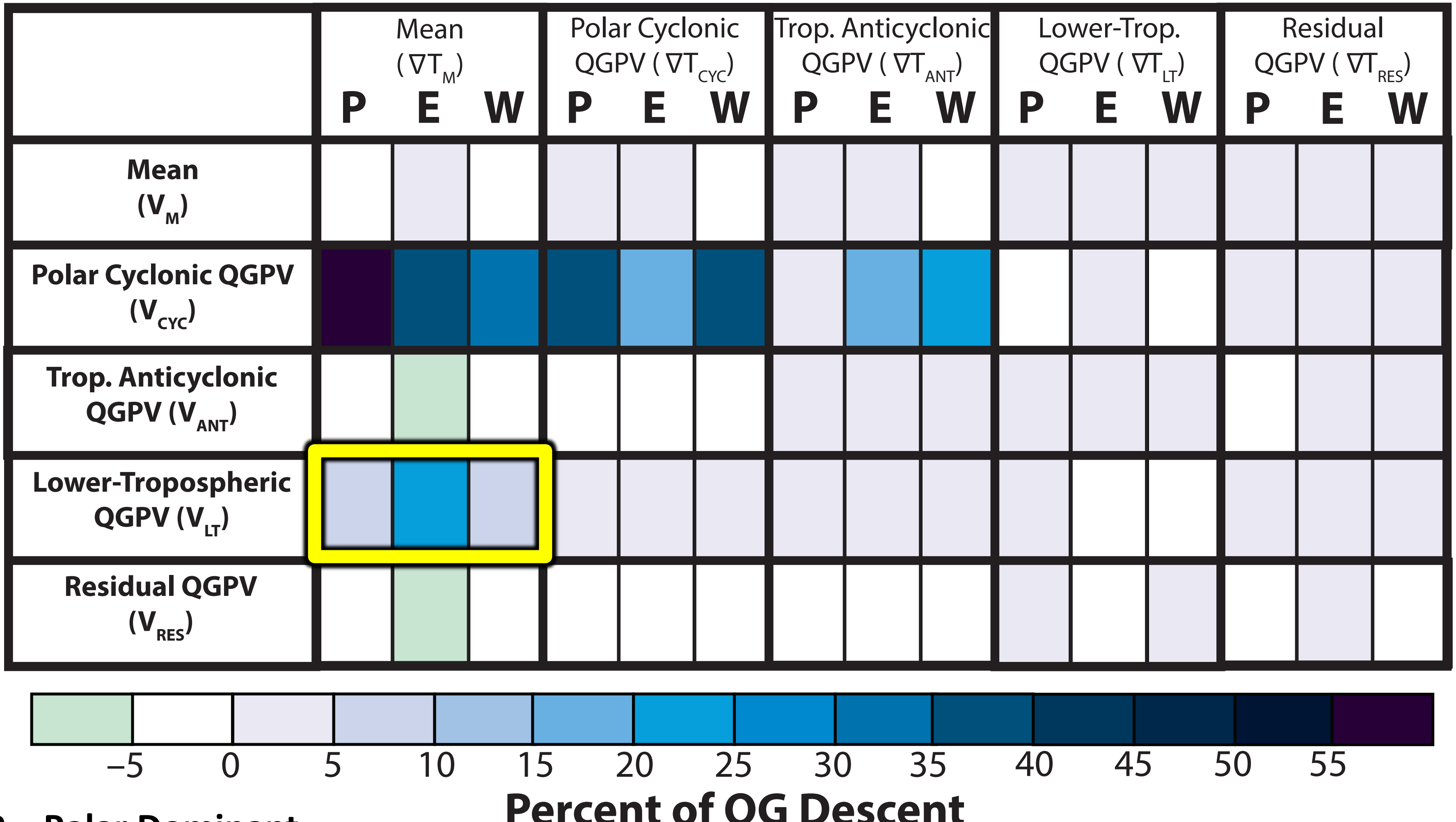

P = Polar Dominant
E = East Subtropical Dominant
W = West Subtropical Dominant

Summary

- Jet superpositions establish a dynamical and thermodynamic environment that is particularly conducive to high-impact weather.
- Descent within the jet-entrance region is a common element among jet superpositions, regardless of the event type.
- Descent is primarily associated with the geostrophic flow attributed to polar cyclonic QGPV anomalies, and the interaction of that geostrophic flow with ∇T_M and ∇T_{CYC}.
- The latter result underscores the critical role that polar cyclonic QGPV anomalies play during jet superpositions.

Summary

- Jet superpositions establish a dynamical and thermodynamic environment that is particularly conducive to high-impact weather.
- Descent within the jet-entrance region is a common element among jet superpositions, regardless of the event type.
- Descent is primarily associated with the geostrophic flow attributed to polar cyclonic QGPV anomalies, and the interaction of that geostrophic flow with ∇T_M and ∇T_{CYC}.
- The latter result underscores the critical role that polar cyclonic QGPV anomalies play during jet superpositions.

Contact: andrew.c.winters@colorado.edu

Supplementary Slides

References

Cavallo, S. M., and G. J. Hakim, 2010: Composite structure of tropopause polar cyclones. *Mon. Wea. Rev.*, **138,** 3840–3857.

Christenson, C. E., J. E. Martin, and Z. J. Handlos, 2017: A synoptic-climatology of Northern Hemisphere, cold season polar and subtropical jet superposition events. *J. Climate*, **30**, 7231-7246.

Pyle, M. E., D. Keyser, and L. F. Bosart, 2004: A diagnostic study of jet streaks: Kinematic signatures and relationship to coherent tropopause disturbances. *Mon. Wea. Rev.*, **132,** 297–319.

Saha, S. and co-authors, 2014: The NCEP Climate Forecast System Version 2. *J. Climate*, **27,** 2185–2208.

Winters, A. C., and J. E. Martin, 2017: Diagnosis of a North American polar/subtropical jet superposition employing piecewise potential vorticity inversion. *Mon. Wea. Rev.*,**145**, 1853-1873.

Shearwise and Transverse QG Omega

Shearwise and Transverse QG Omega

Polar Dominant Events

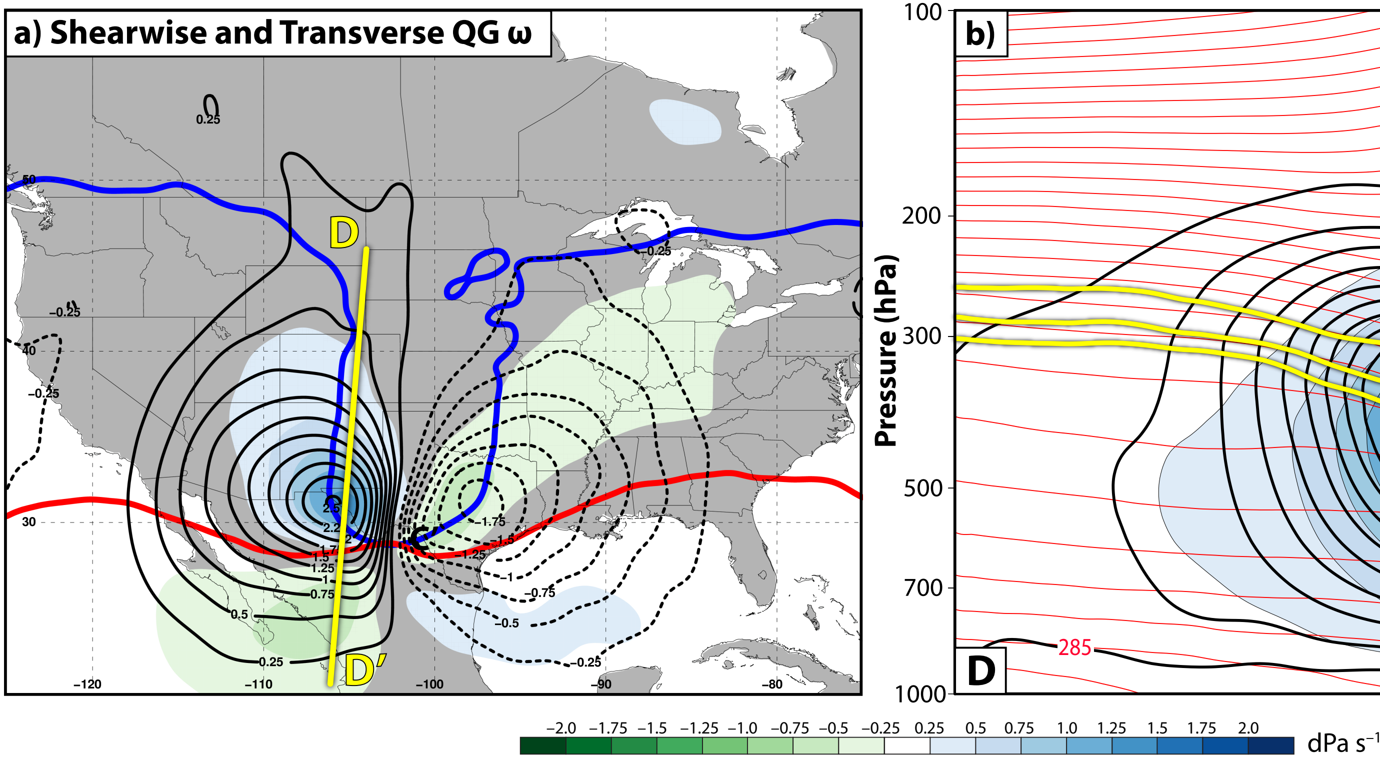

Contours – Shearwise QG omega
Shading – Transverse QG omega

Shearwise and Transverse QG Omega

East Subtropical Dominant Events

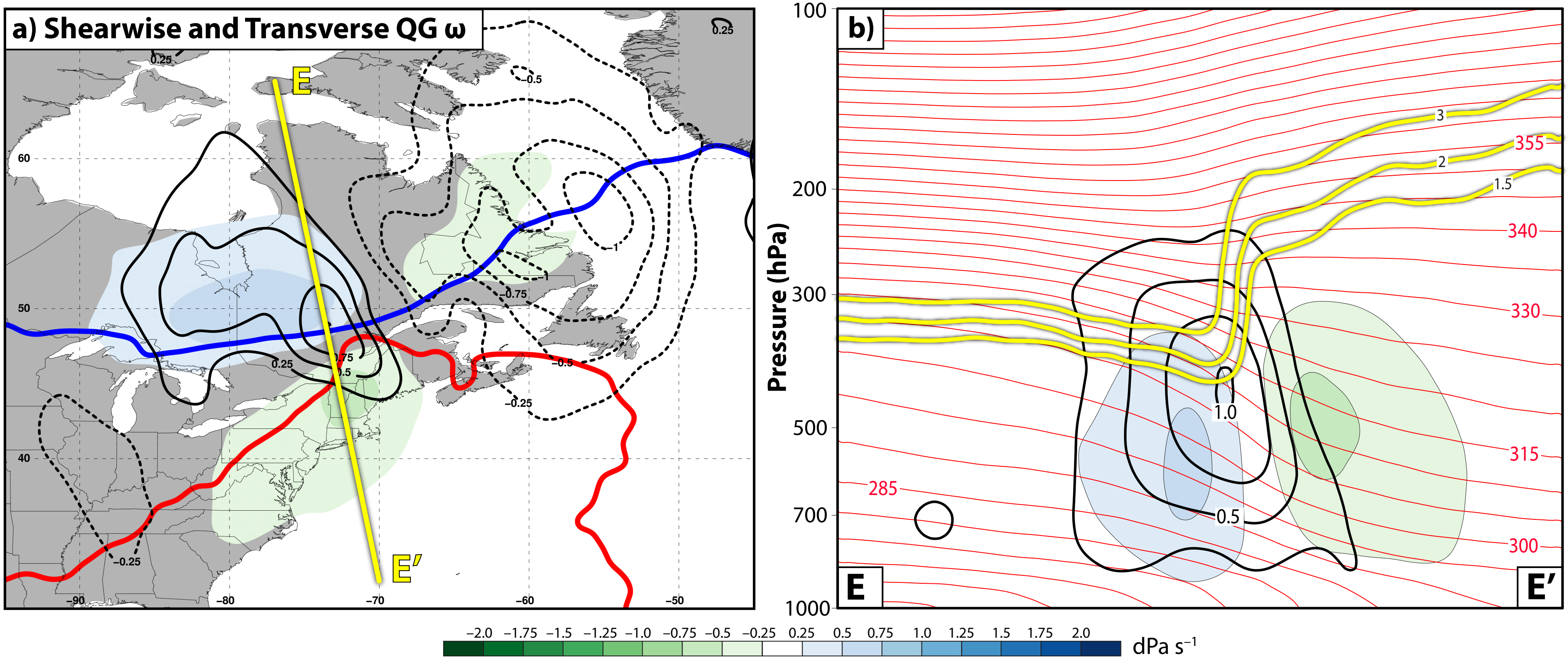

Contours – Shearwise QG omega
Shading – Transverse QG omega

Shearwise and Transverse QG Omega

West Subtropical Dominant Events

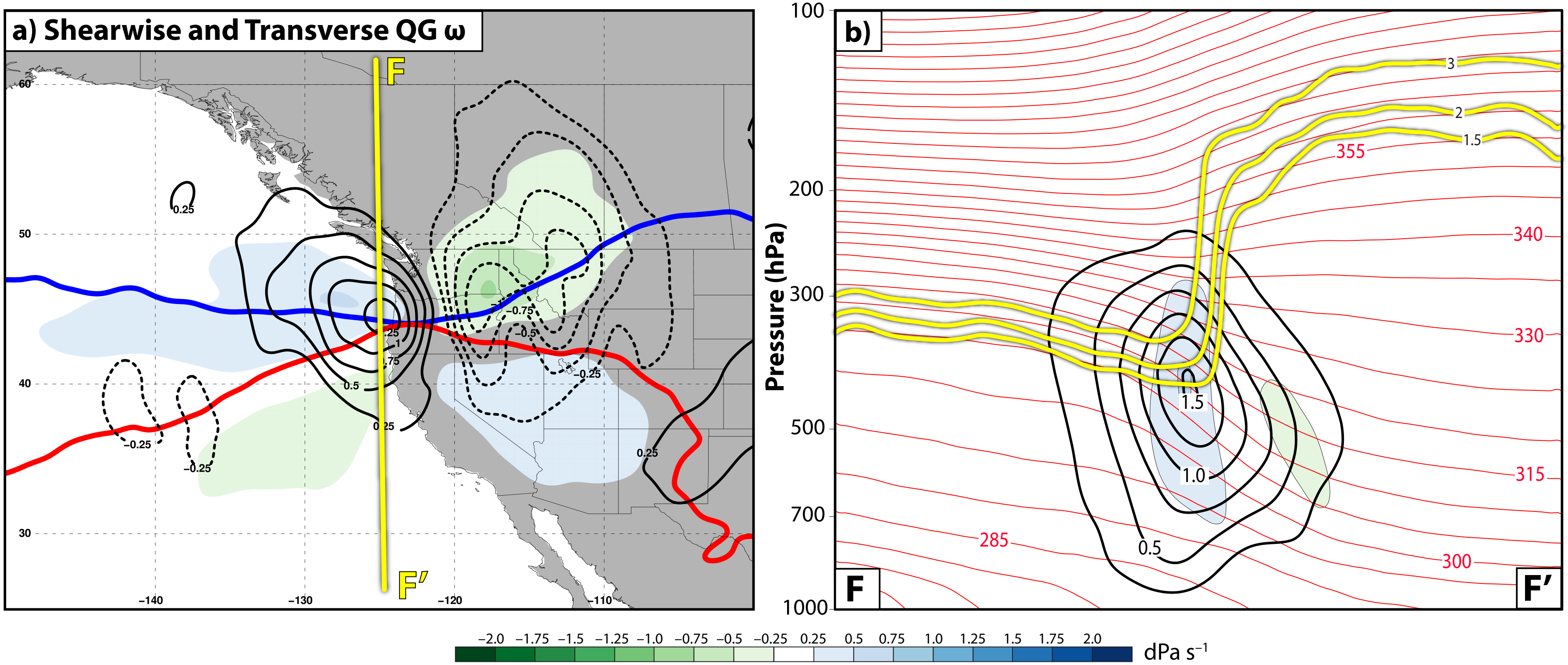

Contours – Shearwise QG omega
Shading – Transverse QG omega

Psi Vector Partition
of the Full Vertical Motion

Psi Vectors

Keyser et al. 1989

$$\mathbf{V}_{agirr} = -\frac{\partial \psi}{\partial p}, \quad \omega = \nabla_p \cdot \psi.$$

- A vector streamfunction field can be defined that describes the horizontal irrotational flow and vertical velocity.
- The vector streamfunction can be determined uniquely from the vertical velocity field and by assuming suitable boundary conditions.
- The projection of the "psi vector" onto planes in the along- and across-front directions can be used to examine the character of the three-dimensional vertical circulation

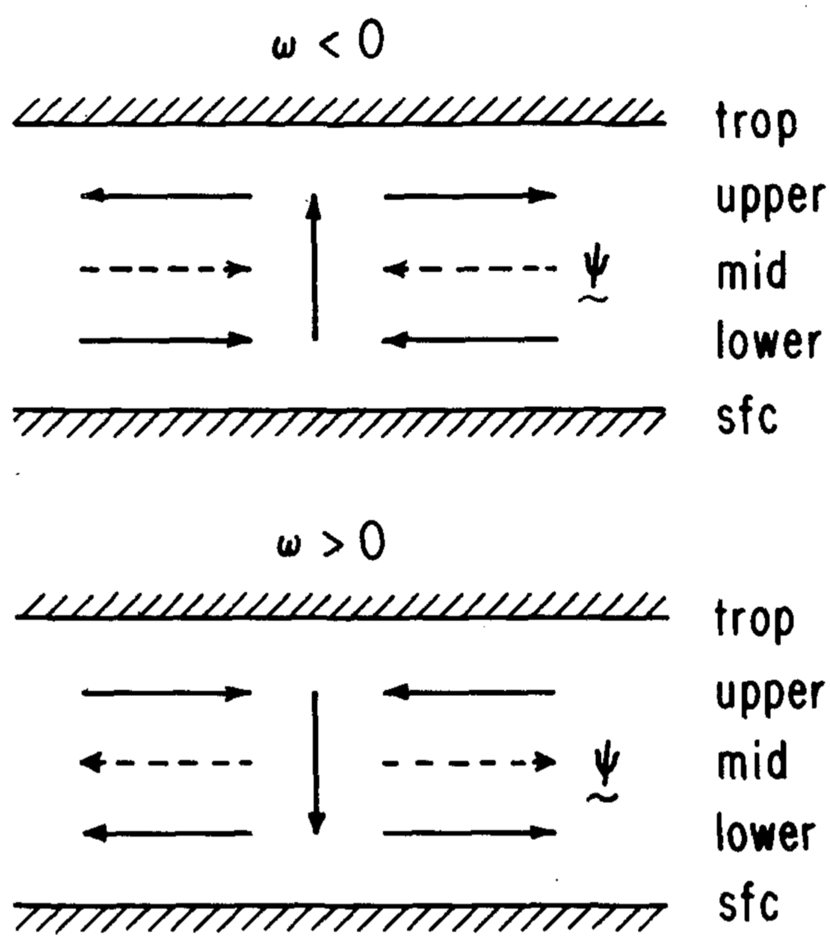

Keyser, D., B. D. Schmidt, and D. G. Duffy, 1989: A technique for representing three-dimensional vertical circulations in baroclinic disturbances. Mon. Wea. Rev., ***117****, 2463–2494.*

Psi Vectors

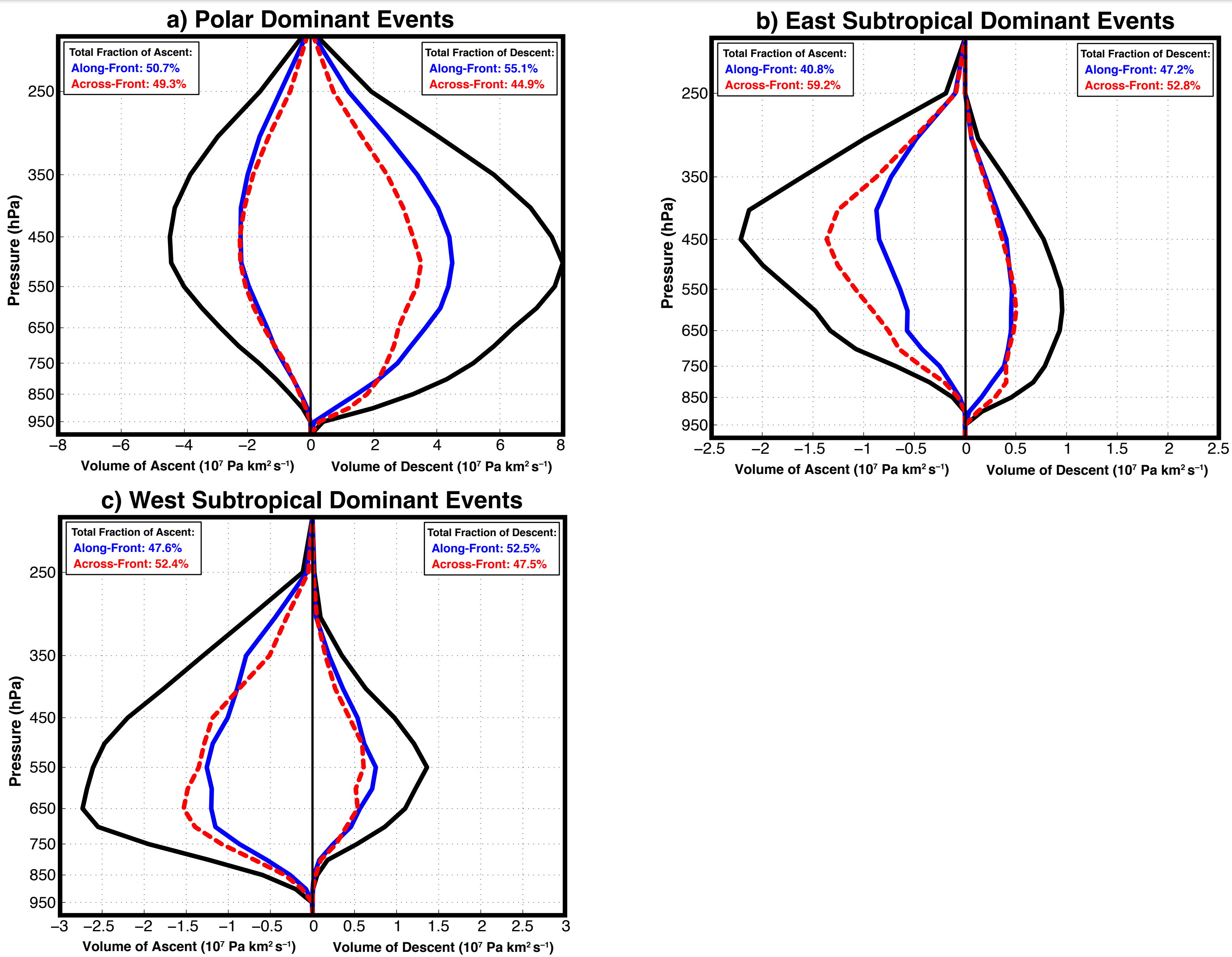

a) Polar Dominant Events
Total Fraction of Ascent:
Along-Front: 50.7%
Across-Front: 49.3%
Total Fraction of Descent:
Along-Front: 55.1%
Across-Front: 44.9%
Pressure (hPa)
250
350
450
550
650
750
850
950
−8 −6 −4 −2 0 2 4 6 8
Volume of Ascent (10⁷ Pa km² s⁻¹)
Volume of Descent (10⁷ Pa km² s⁻¹)
b) East Subtropical Dominant Events
Total Fraction of Ascent:
Along-Front: 40.8%
Across-Front: 59.2%
Total Fraction of Descent:
Along-Front: 47.2%
Across-Front: 52.8%
Pressure (hPa)
−2.5 −2 −1.5 −1 −0.5 0 0.5 1 1.5 2 2.5
Volume of Ascent (10⁷ Pa km² s⁻¹)
Volume of Descent (10⁷ Pa km² s⁻¹)
c) West Subtropical Dominant Events
Total Fraction of Ascent:
Along-Front: 47.6%
Across-Front: 52.4%
Total Fraction of Descent:
Along-Front: 52.5%
Across-Front: 47.5%
Pressure (hPa)
−3 −2.5 −2 −1.5 −1 −0.5 0 0.5 1 1.5 2 2.5 3
Volume of Ascent (10⁷ Pa km² s⁻¹)
Volume of Descent (10⁷ Pa km² s⁻¹)

Composite Characteristics

Jet Superposition Event Characteristics

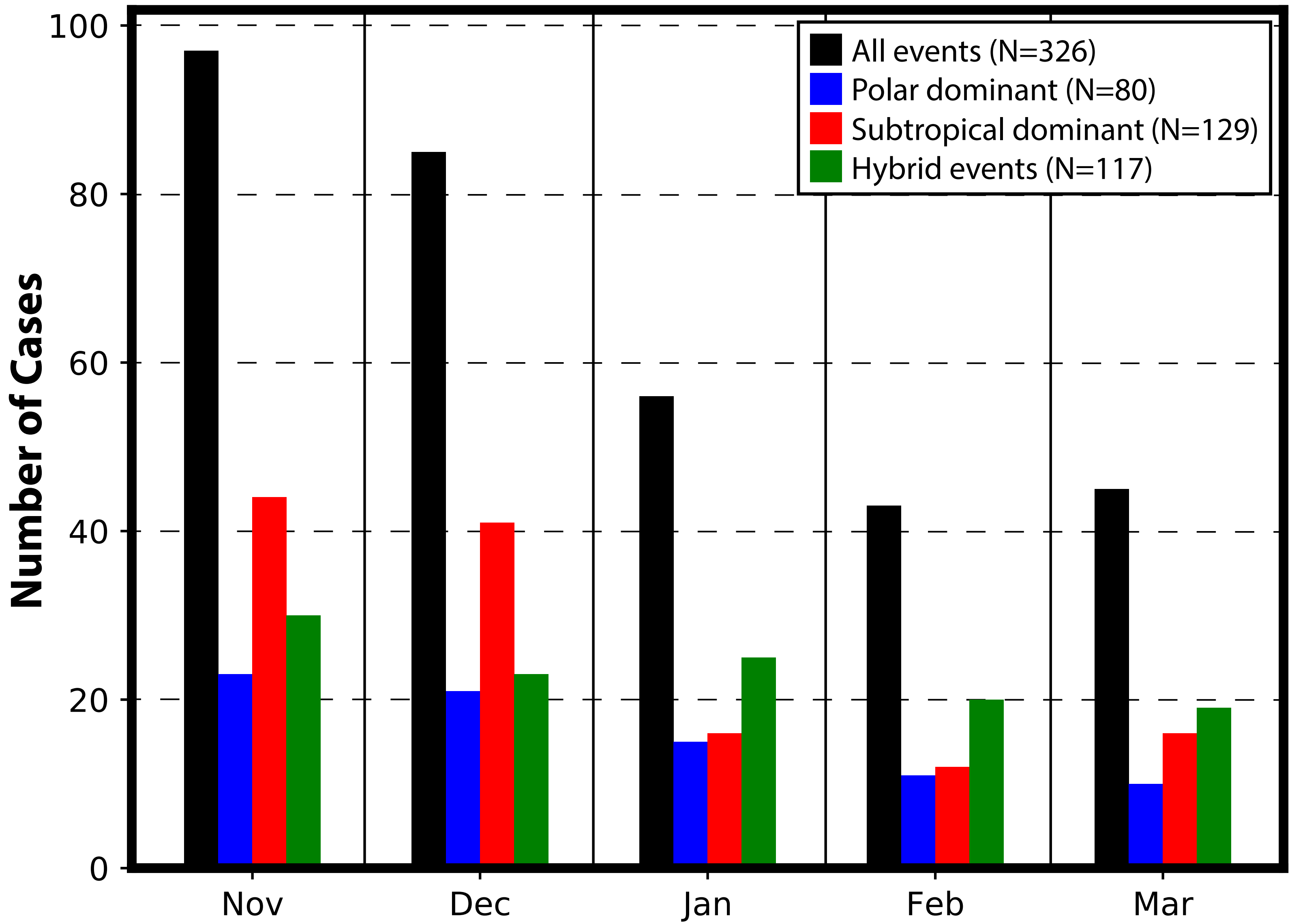

Jet Superposition Event Composites

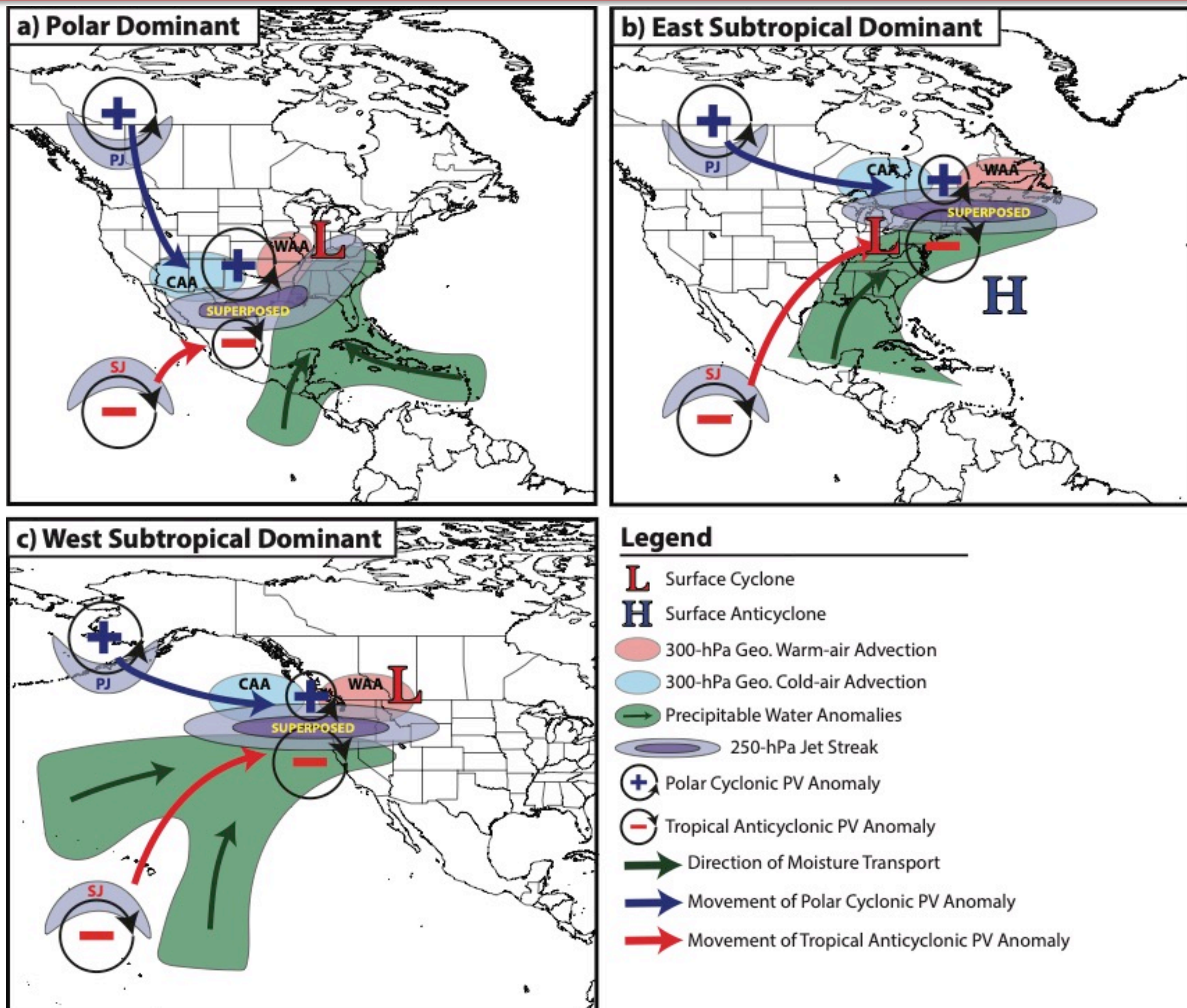

Downstream Consequences

North Atlantic Oscillation: 5 Days After Jet Superposition

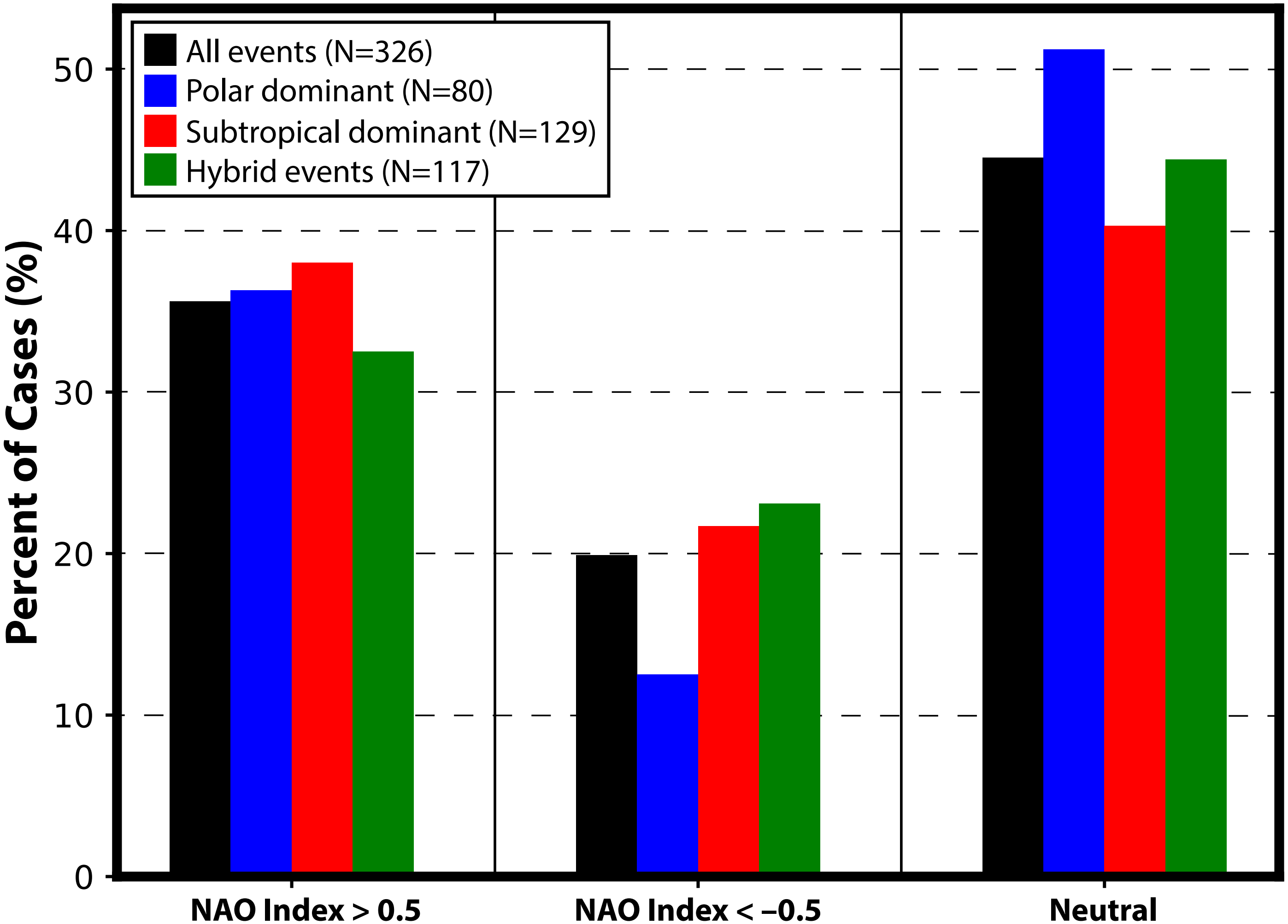

All Events ΔNAO
+0.11

Ave. Polar Dominant ΔNAO
+0.15

Ave. Subtropical Dominant ΔNAO
+0.13

Ave. Hybrid ΔNAO
+0.07

Background Material

Background

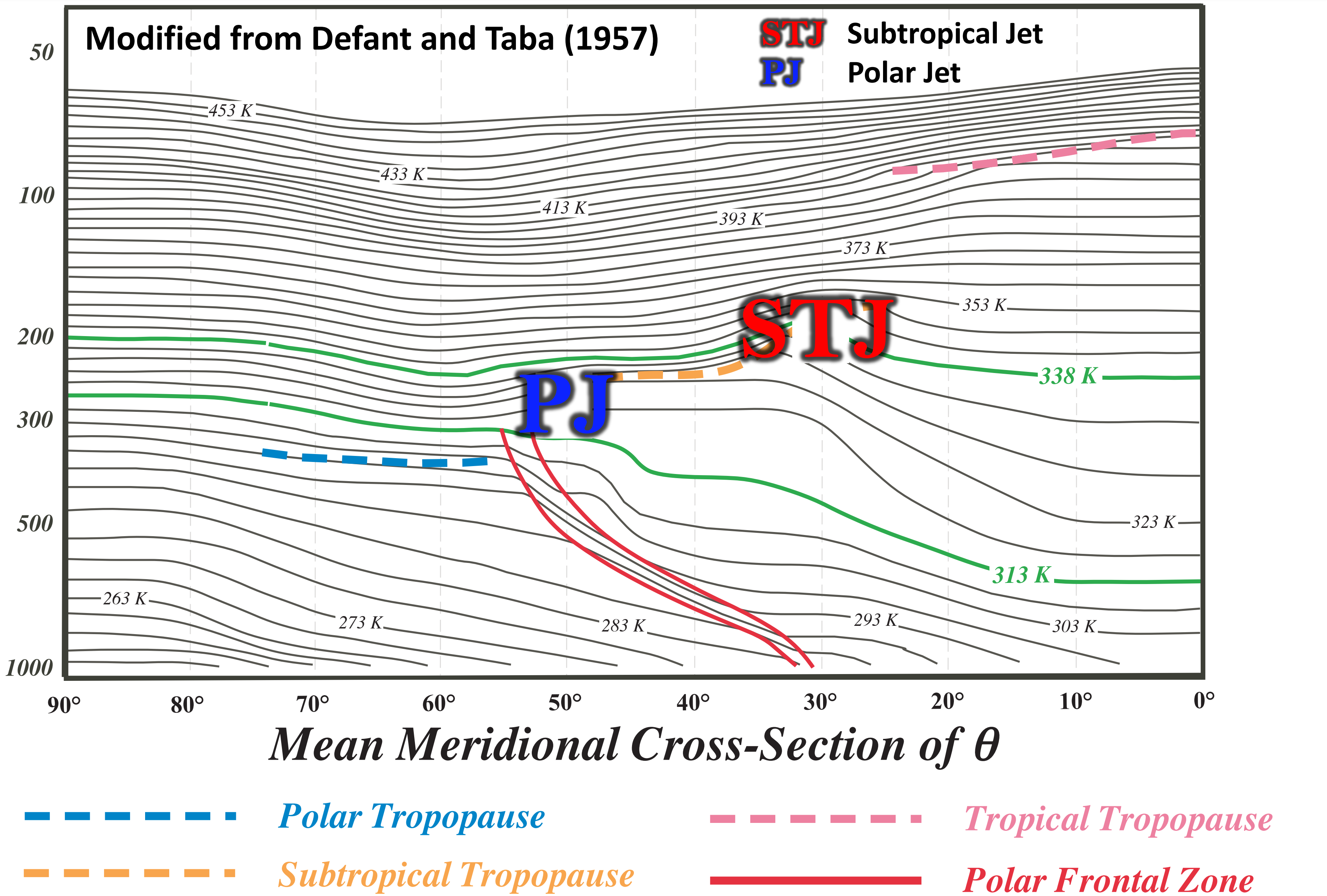

Modified from Defant and Taba (1957)
STJ Subtropical Jet
PJ Polar Jet
50
100
200
300
500
1000
453 K
433 K
413 K
393 K
373 K
353 K
338 K
323 K
313 K
303 K
293 K
283 K
273 K
263 K
STJ
PJ
90°
80°
70°
60°
50°
40°
30°
20°
10°
0°
Mean Meridional Cross-Section of θ
Polar Tropopause
Tropical Tropopause
Subtropical Tropopause
Polar Frontal Zone

Background

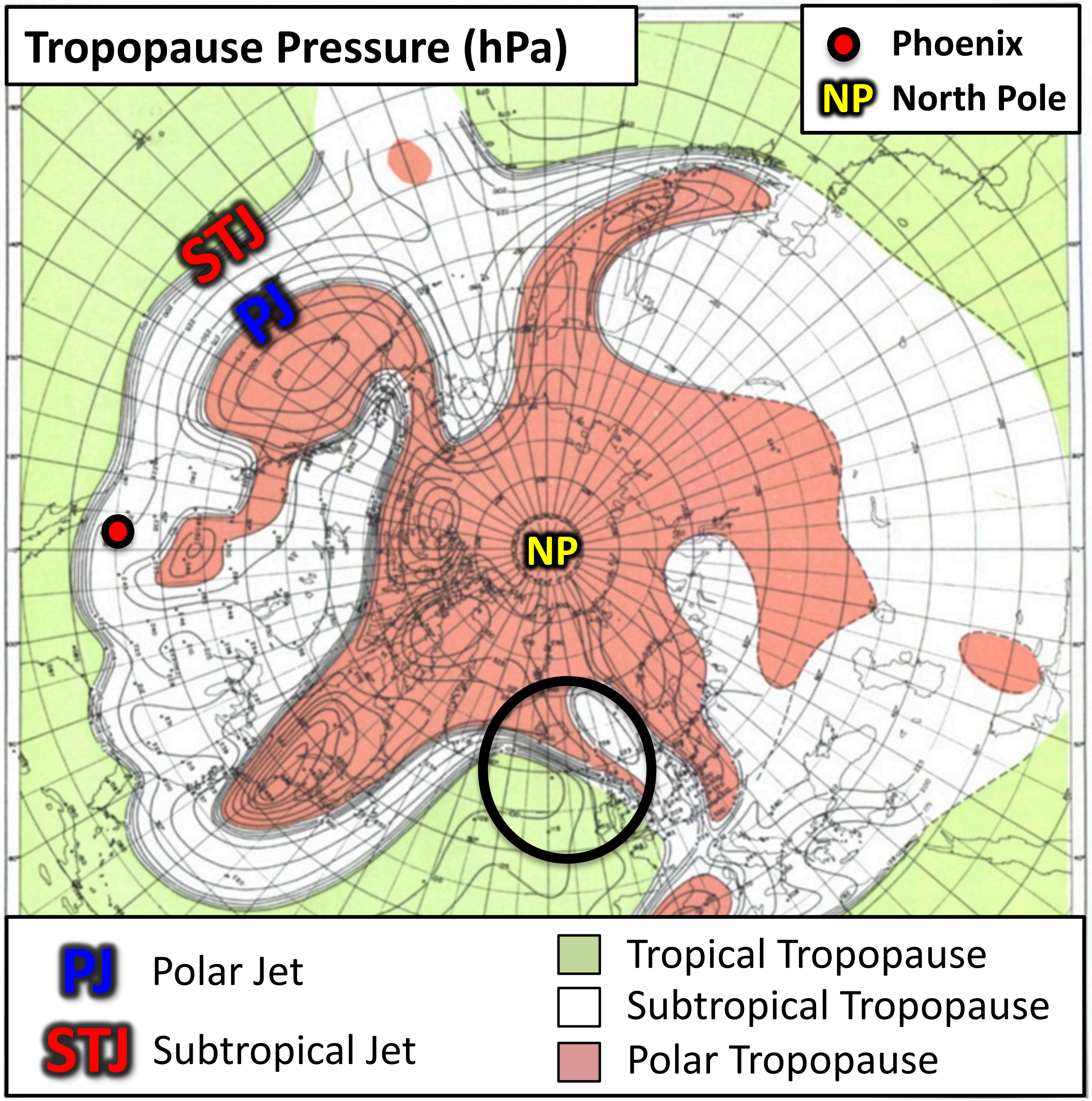

Maps of tropopause pressure help to identify the location of the jets.

While each jet occupies its own climatological latitude band, substantial meanders are common.

Occasionally, the latitudinal separation between the jets can vanish resulting in a vertical **jet superposition**.

Modified from Defant and Taba (1957)

Background

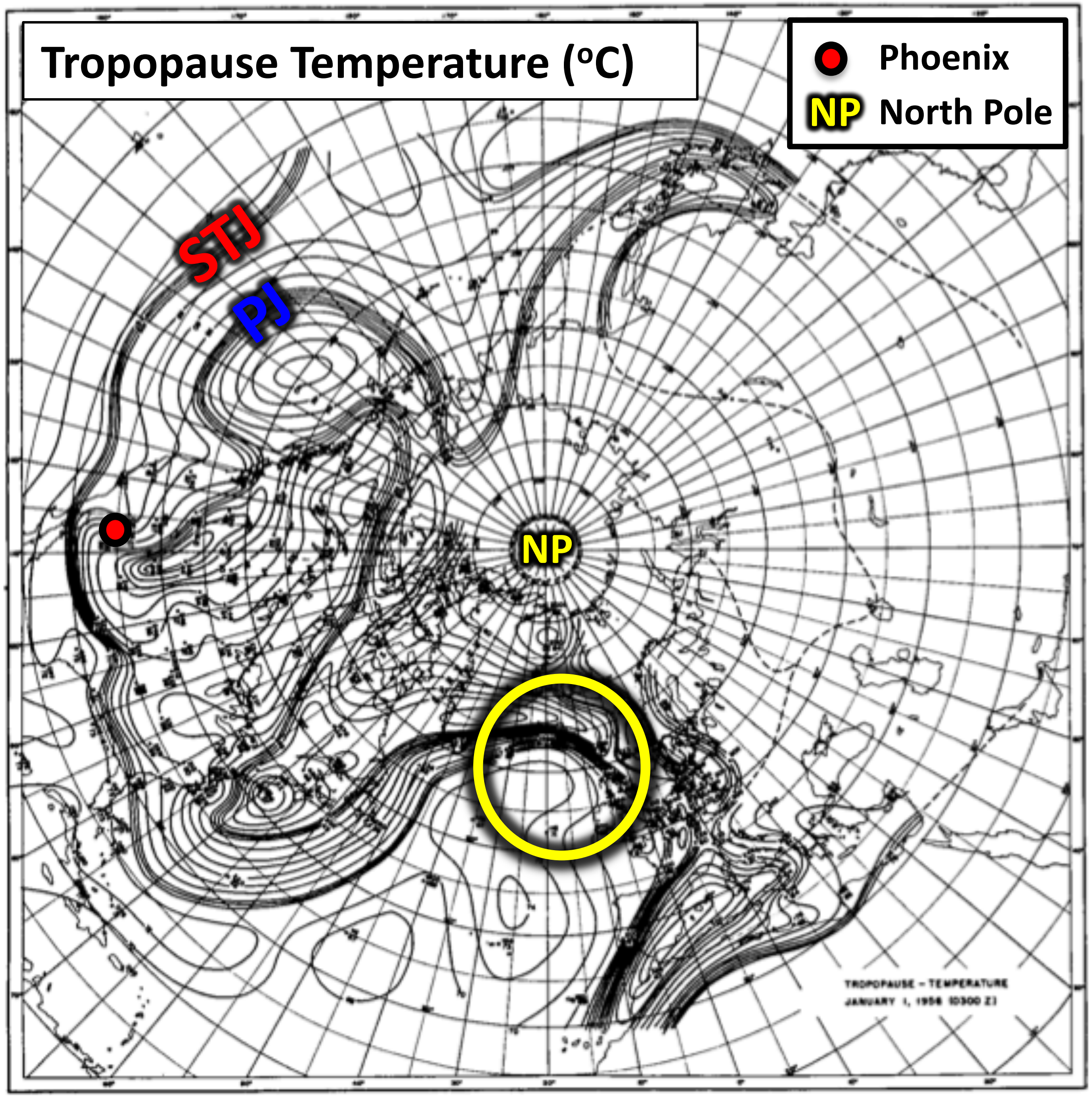

The pole-to-equator baroclinicity is combined into a much narrower zone of contrast in the vicinity of a jet superposition.

Intensified frontal structure is often attended by a strengthening of the superposed jet's transverse circulation.

Modified from Defant and Taba (1957)

Background

Christenson et al. (2017) highlight three locations that experience the greatest frequency of jet superpositions:

1) Western Pacific

2) North America

3) Northern Africa

Climatological frequency of Northern Hemisphere jet superposition events per cold season (Nov–Mar) 1960–2010

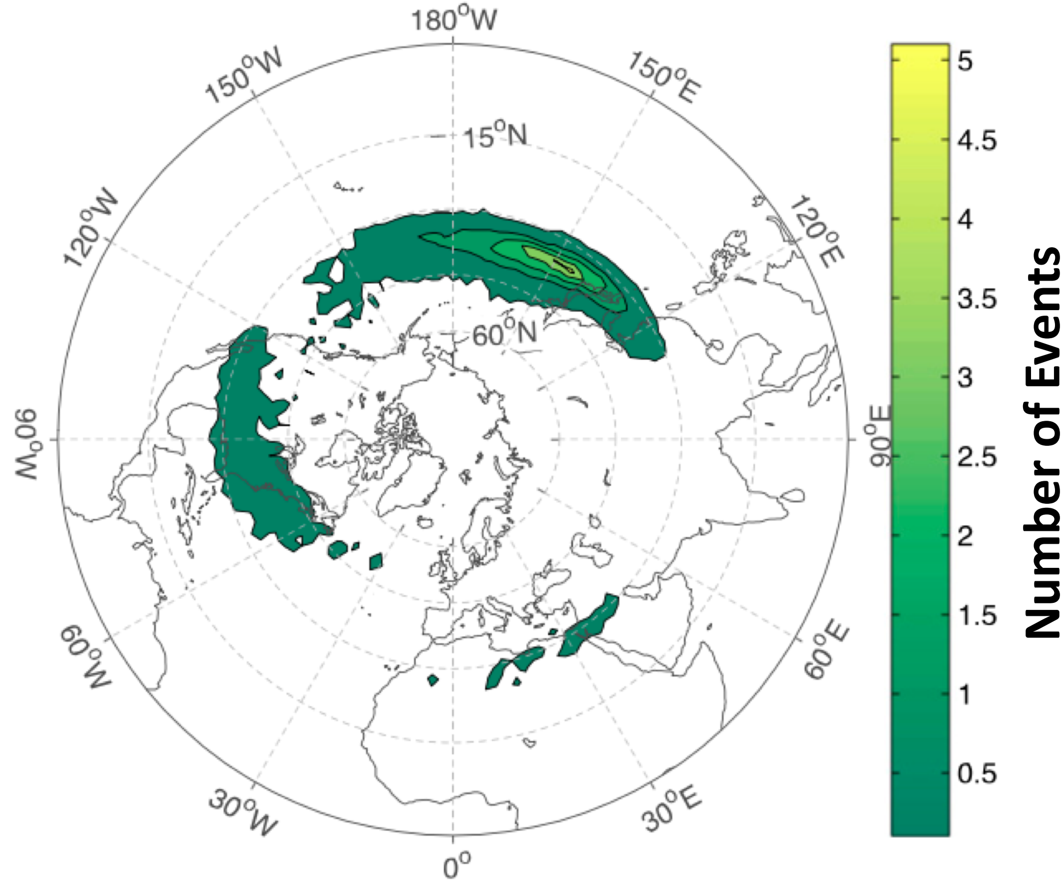

Christenson et al. (2017)

Jet Superpositions and High-Impact Weather

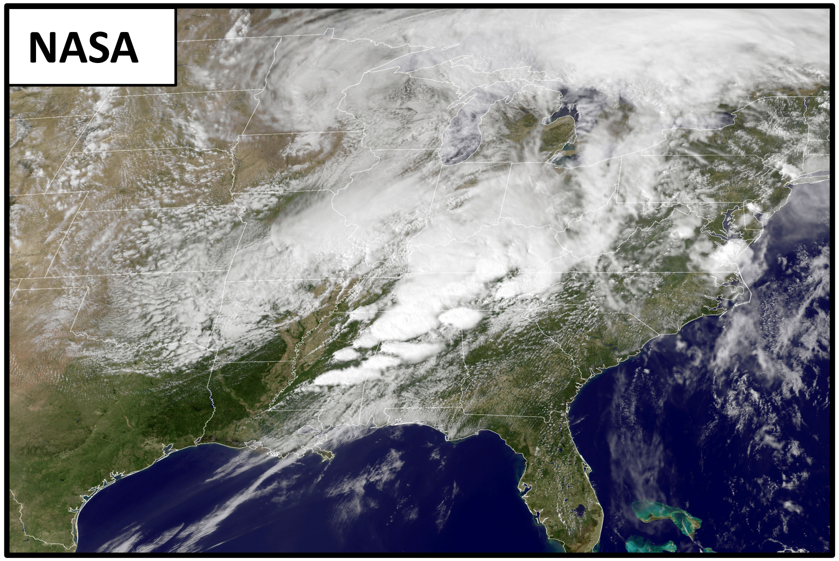

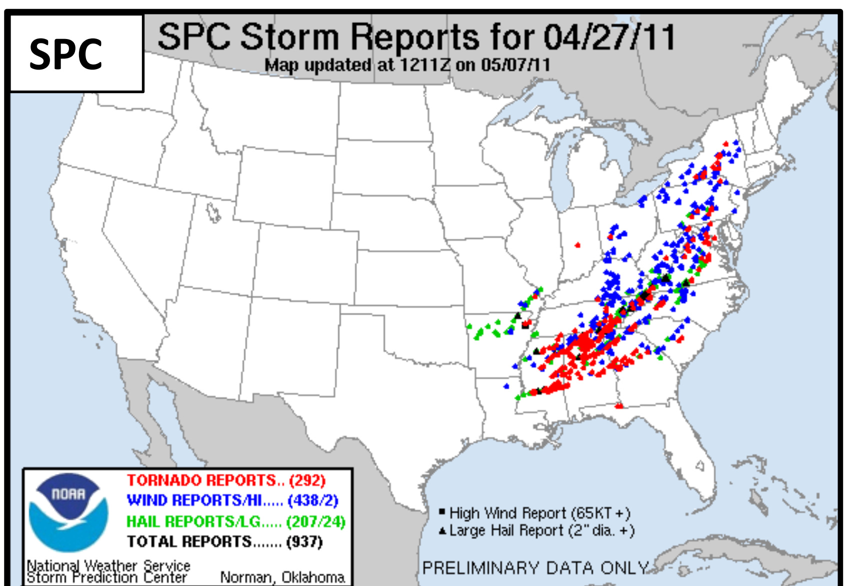

Jet superpositions can be an element of high-impact weather events

1–3 May 2010 Nashville Flood

- Jet superposition enhanced the poleward moisture transport via its ageostrophic circulation (Winters and Martin 2014; 2016).

18–20 December 2009 Mid-Atlantic Blizzard

- Jet superposition was associated with a rapidly deepening East Coast cyclone (Winters and Martin 2016; 2017).

26 October 2010: Explosive Cyclogenesis Event

- Jet superposition over the West Pacific preceded the development of an intense Midwest U.S. cyclone.

25–28 April 2011 Tornado Outbreak

- Jet superposition occurred over the West Pacific prior to the outbreak (Knupp et al. 2014; Christenson and Martin 2012).

Ageostrophic Transverse Jet Circulations

Traditional four-quadrant model

Geo. cold-air advection (CAA) along the jet axis promotes **subsidence** through the jet core

Geo. warm-air advection (WAA) along the jet axis promotes **ascent** through the jet core

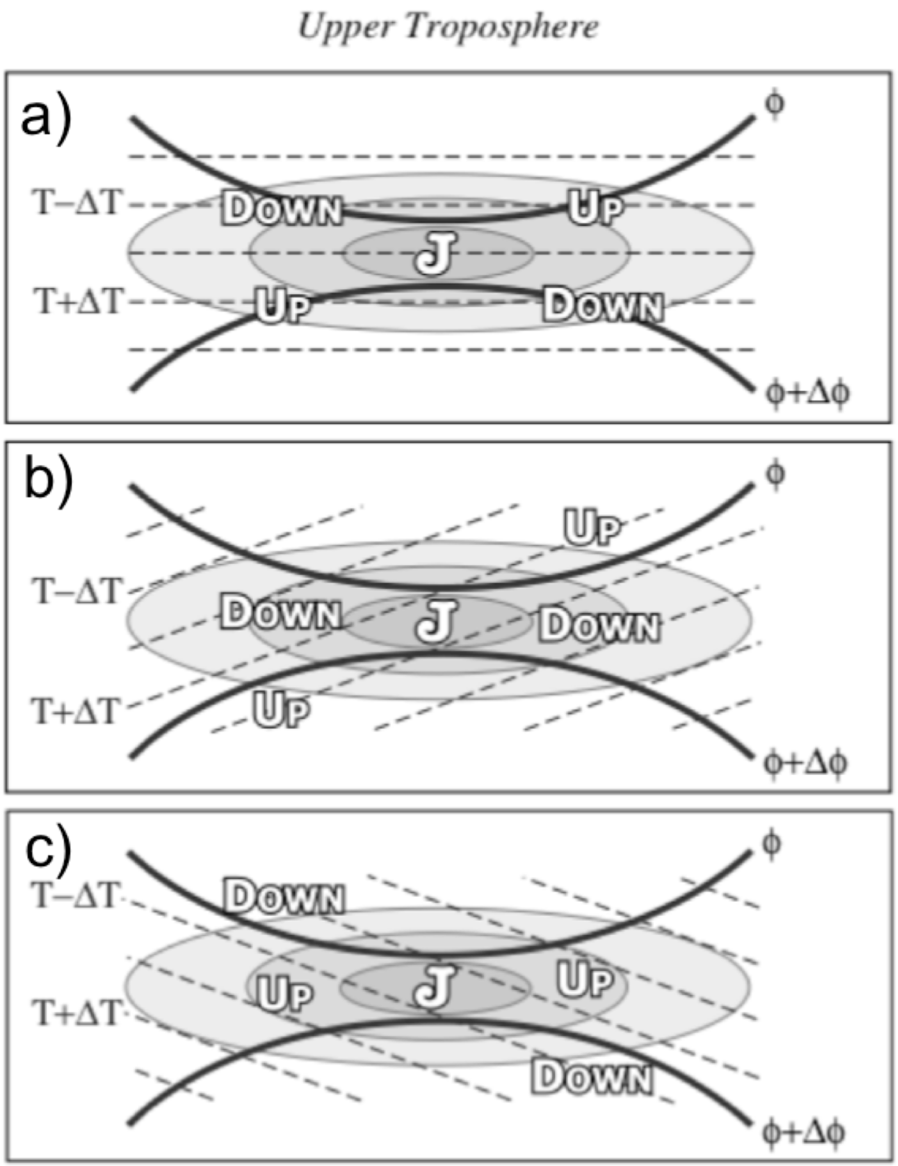

Lang and Martin (2012)

Background

Insight into how the tropopause can be restructured from a PV perspective can be found by consulting Wandishin et al. (2000)

Two processes can account for "foldogenesis":

1) **Differential vertical motions** can vertically steepen the tropopause.

2) **Convergence** or a **vertical shear** can produce a differential horizontal advection of the tropopause surface.

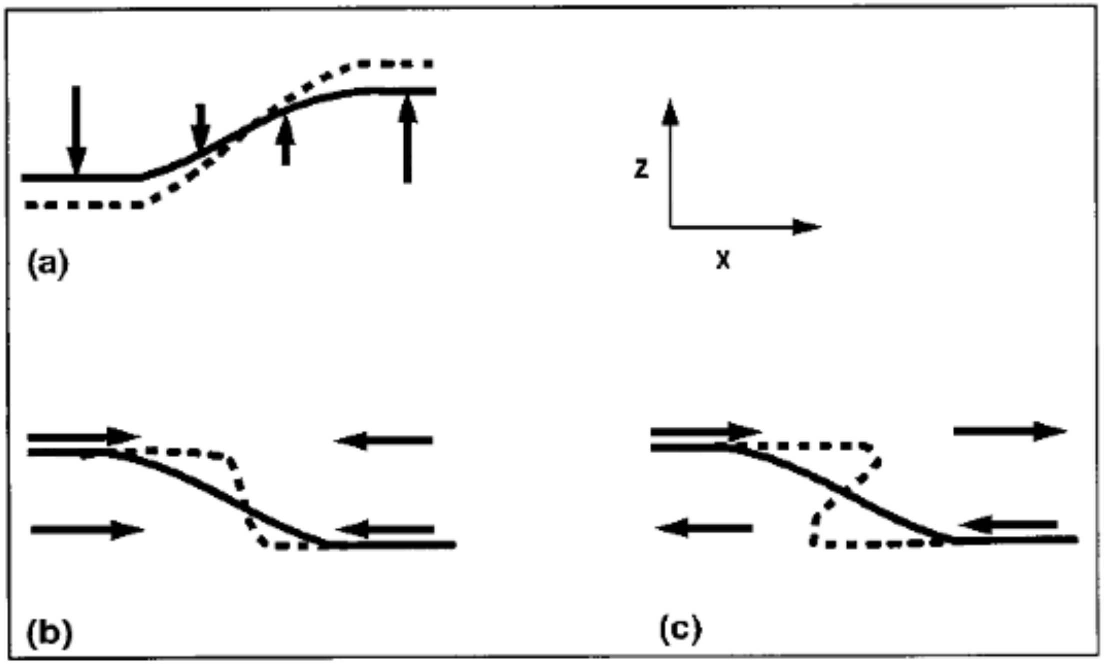

Wandishin et al. 2000

These same mechanisms are also likely to play an important role in superpositions.

Jet Identification

Jet Superposition Event Identification

0000 UTC 27 April 2010

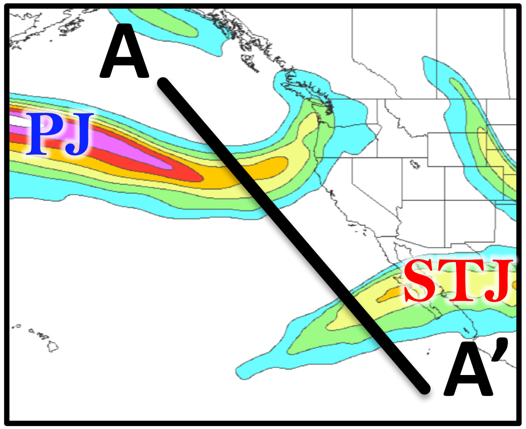

250-hPa wind speed

Isolated grid points over North America in the CFSR (Saha et al. 2014) characterized by polar and subtropical jets during Nov–Mar 1979–2010.

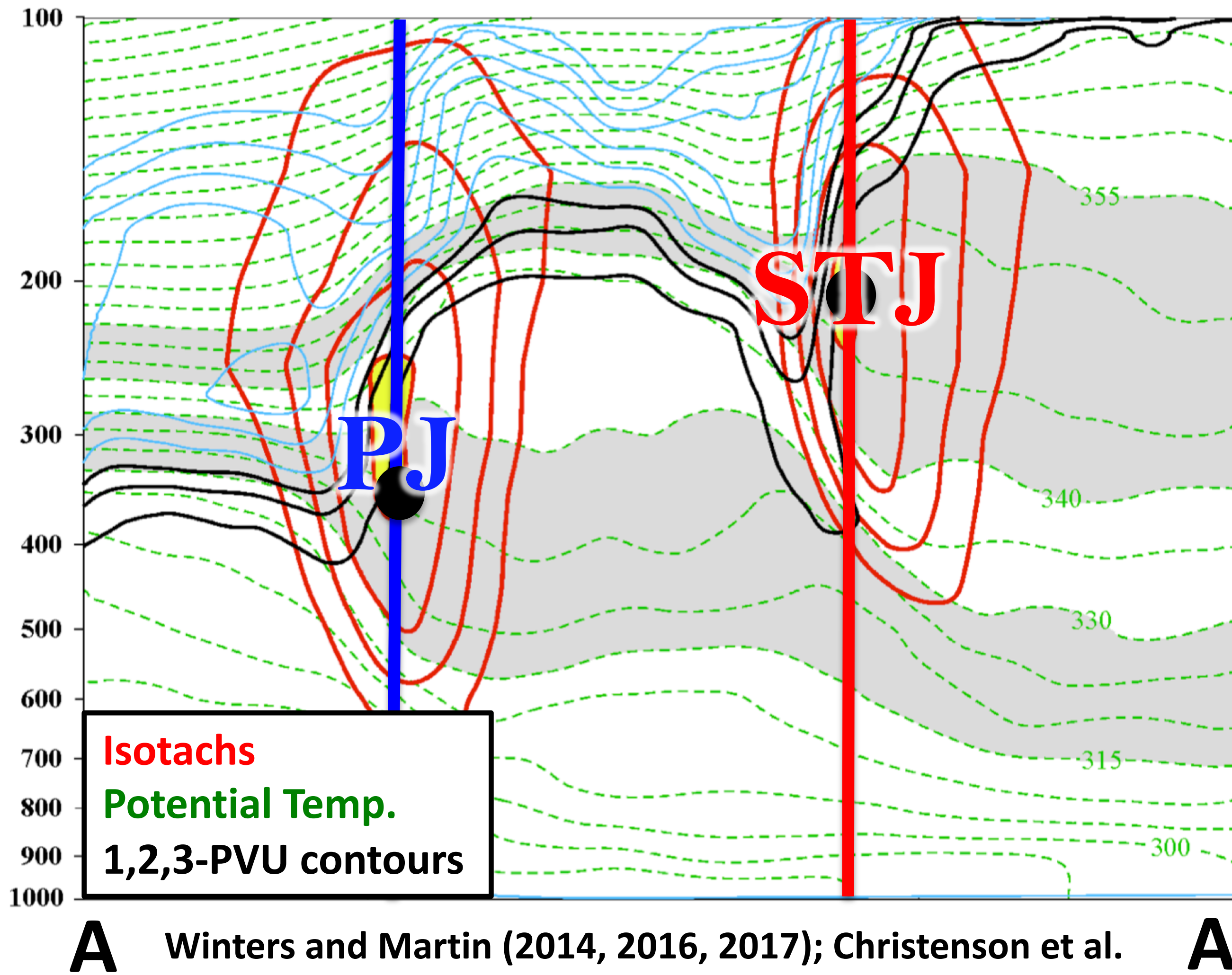

Winters and Martin (2014, 2016, 2017); Christenson et al. (2017); Handlos and Martin (2016)

Jet Superposition Event Identification

0000 UTC 27 April 2010

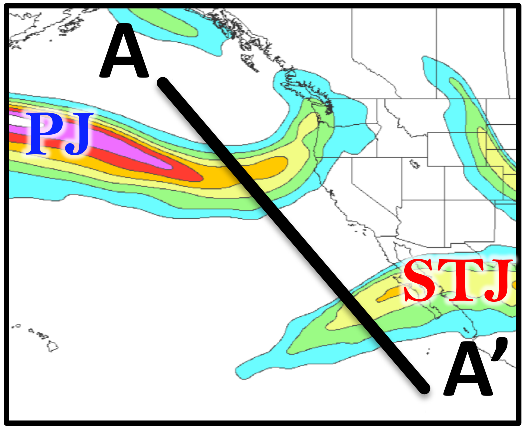

250-hPa wind speed

Isolated grid points over North America in the CFSR (Saha et al. 2014) characterized by polar and subtropical jets during Nov–Mar 1979–2010.

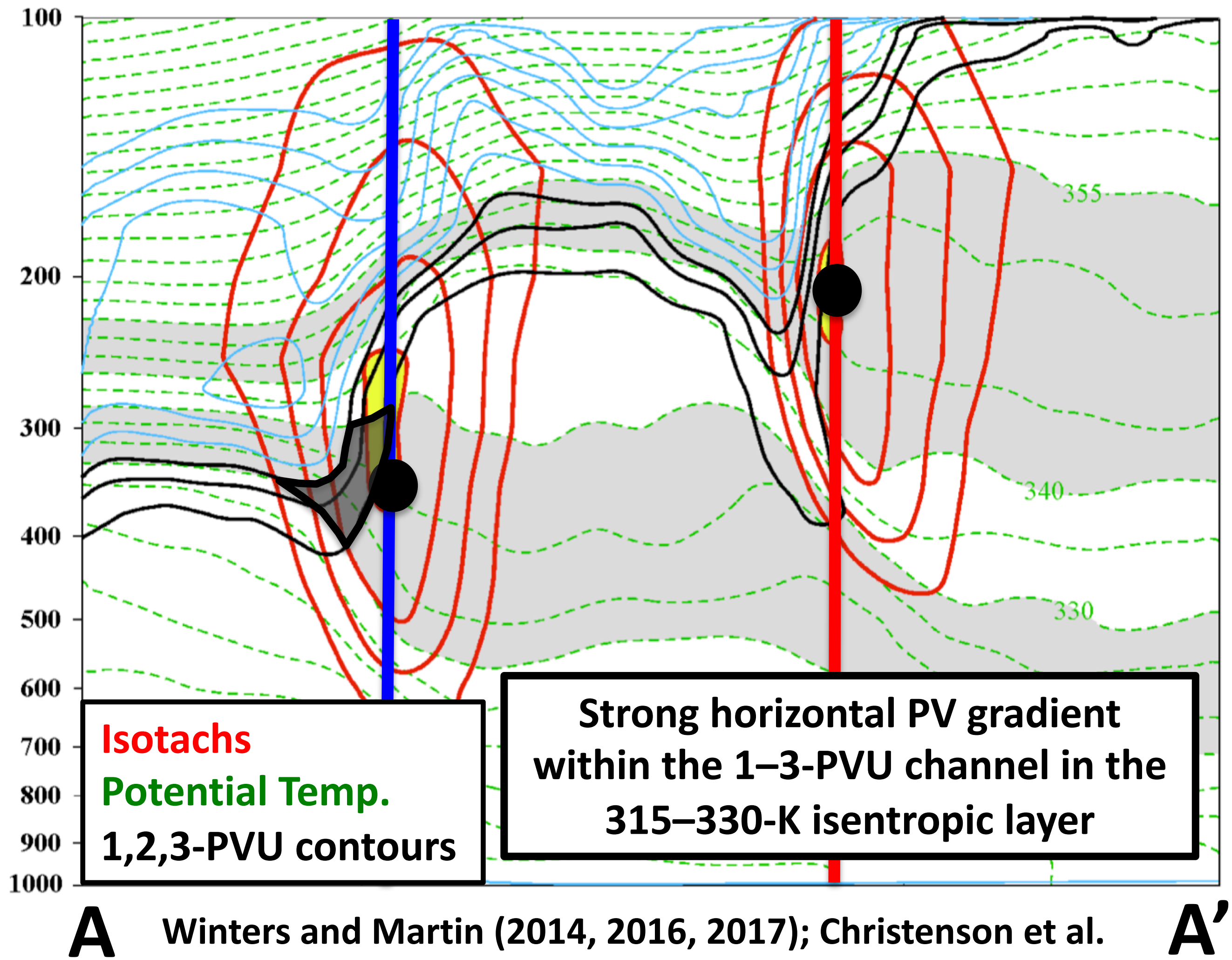

Winters and Martin (2014, 2016, 2017); Christenson et al. (2017); Handlos and Martin (2016)

Jet Superposition Event Identification

0000 UTC 27 April 2010

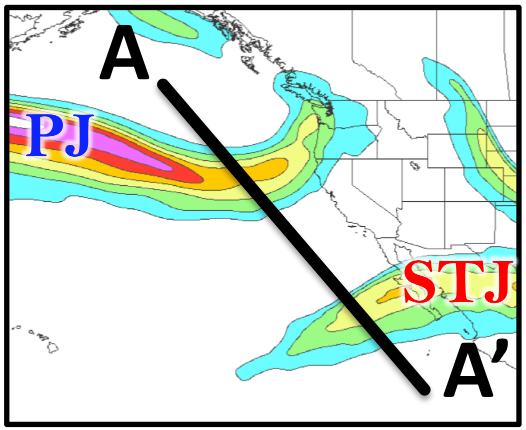

250-hPa wind speed

Isolated grid points over North America in the CFSR (Saha et al. 2014) characterized by polar and subtropical jets during Nov–Mar 1979–2010.

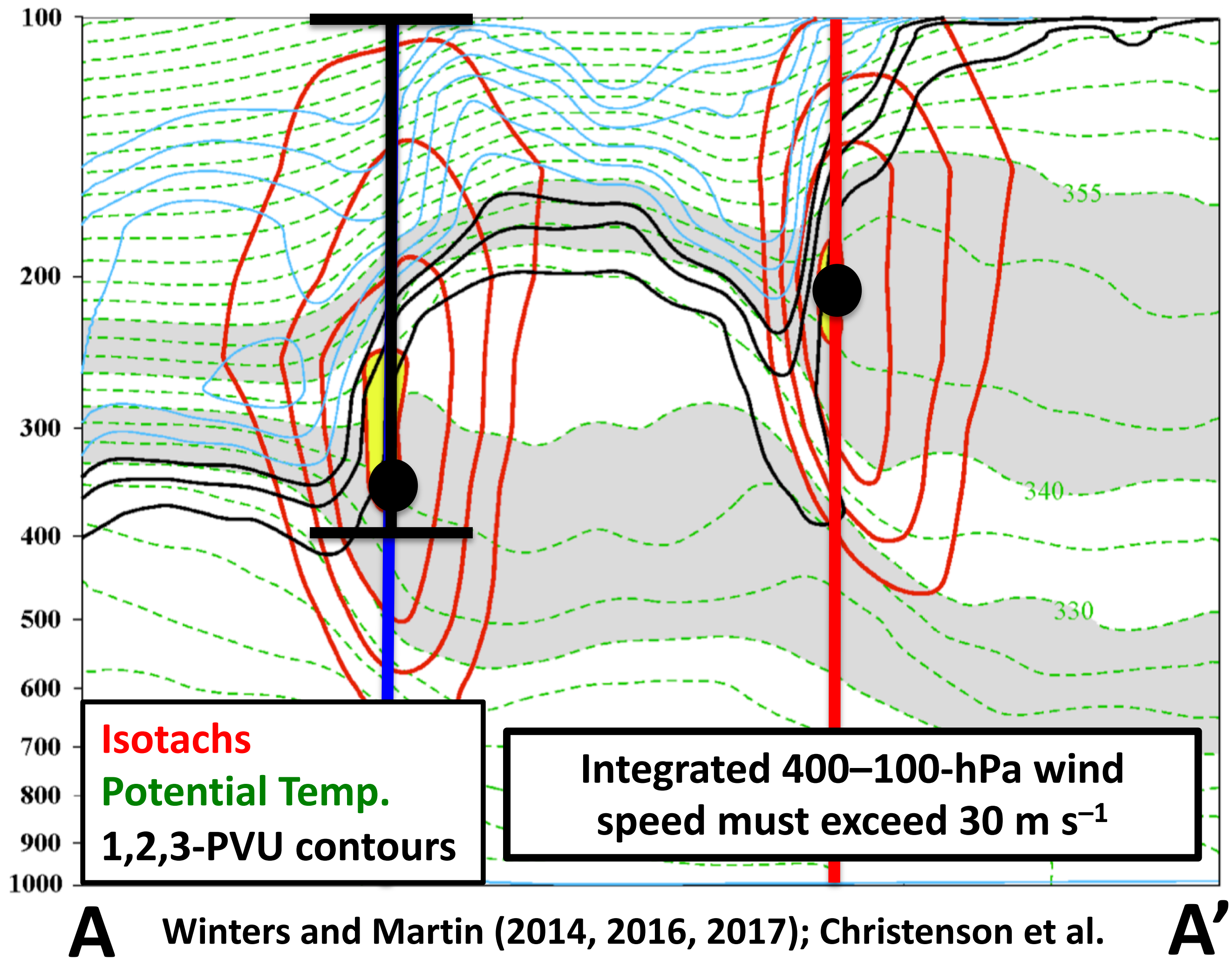

Winters and Martin (2014, 2016, 2017); Christenson et al. (2017); Handlos and Martin (2016)

Jet Superposition Event Identification

0000 UTC 27 April 2010

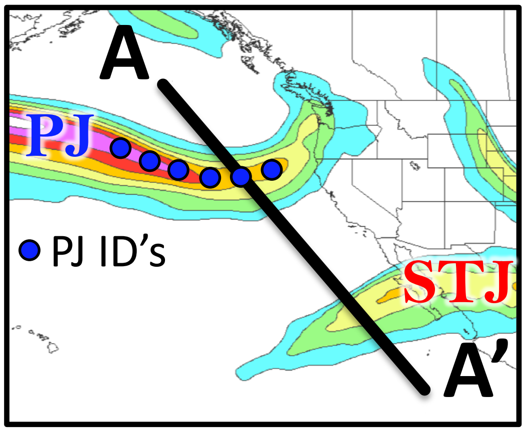

250-hPa wind speed

Isolated grid points over North America in the CFSR (Saha et al. 2014) characterized by polar and subtropical jets during Nov–Mar 1979–2010.

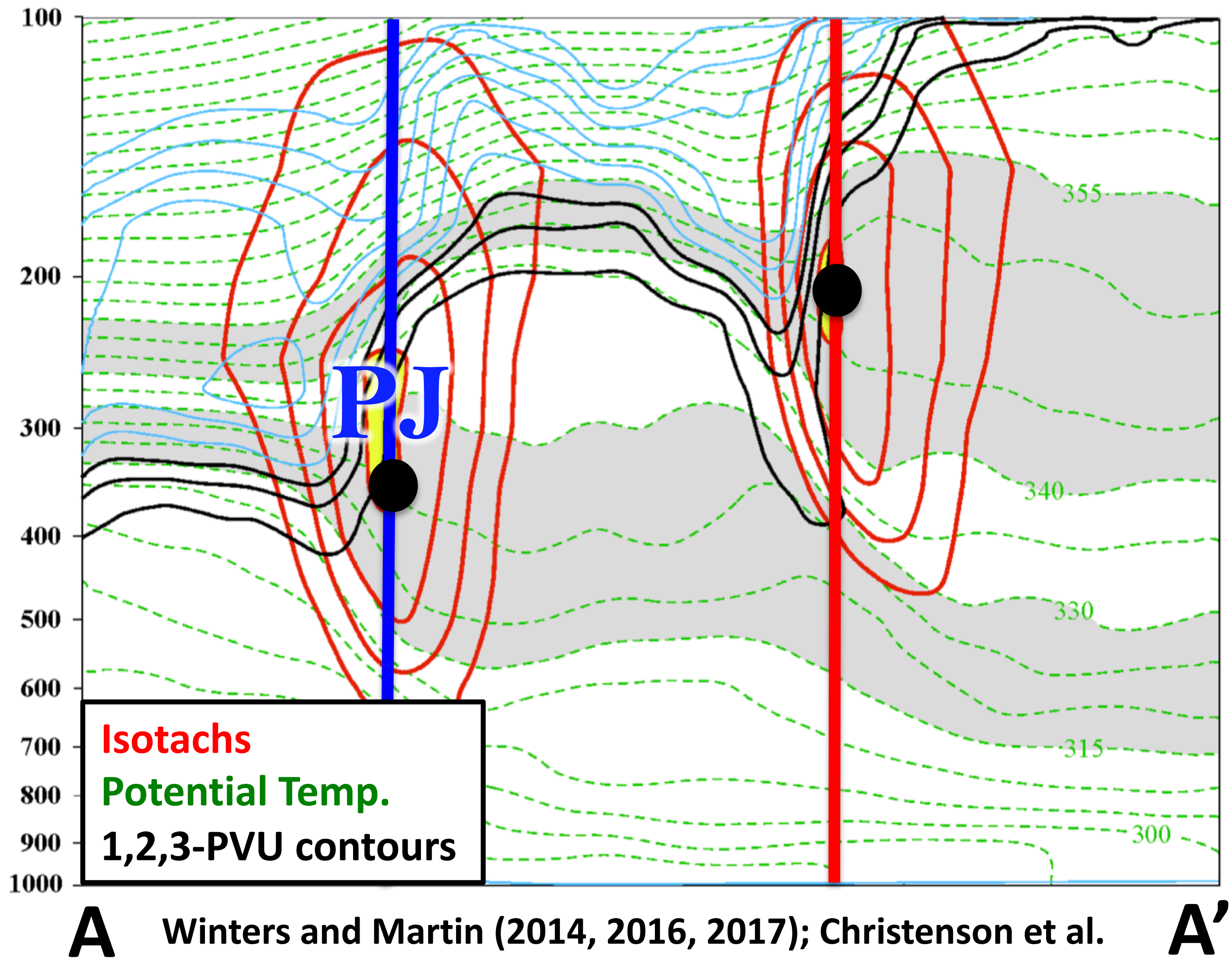

Winters and Martin (2014, 2016, 2017); Christenson et al. (2017); Handlos and Martin (2016)

Jet Superposition Event Identification

0000 UTC 27 April 2010

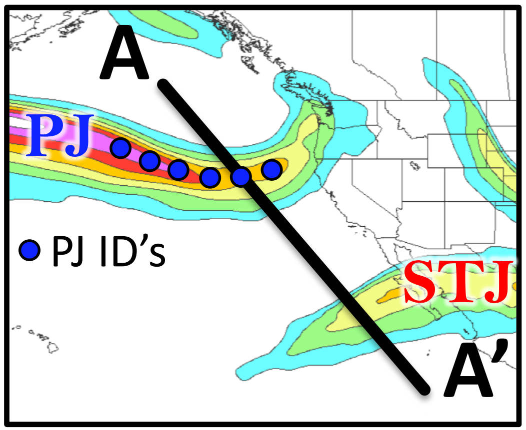

250-hPa wind speed

Isolated grid points over North America in the CFSR (Saha et al. 2014) characterized by polar and subtropical jets during Nov–Mar 1979–2010.

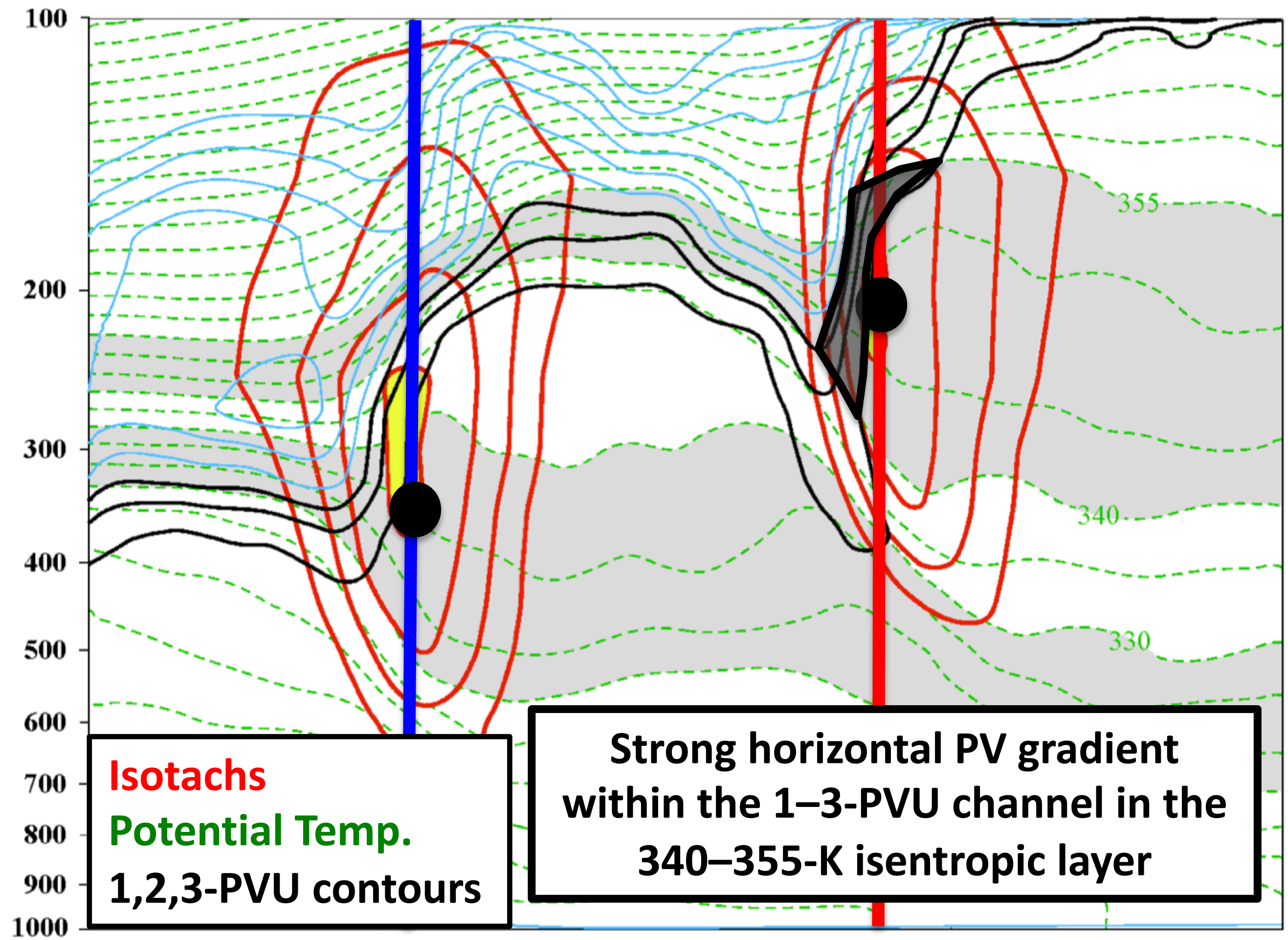

A A'

Winters and Martin (2014, 2016, 2017); Christenson et al. (2017); Handlos and Martin (2016)

Jet Superposition Event Identification

0000 UTC 27 April 2010

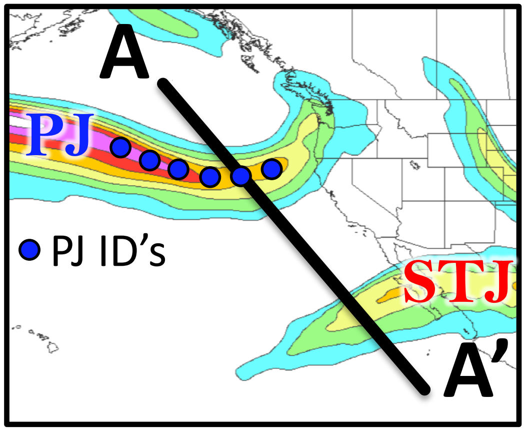

250-hPa wind speed

Isolated grid points over North America in the CFSR (Saha et al. 2014) characterized by polar and subtropical jets during Nov–Mar 1979–2010.

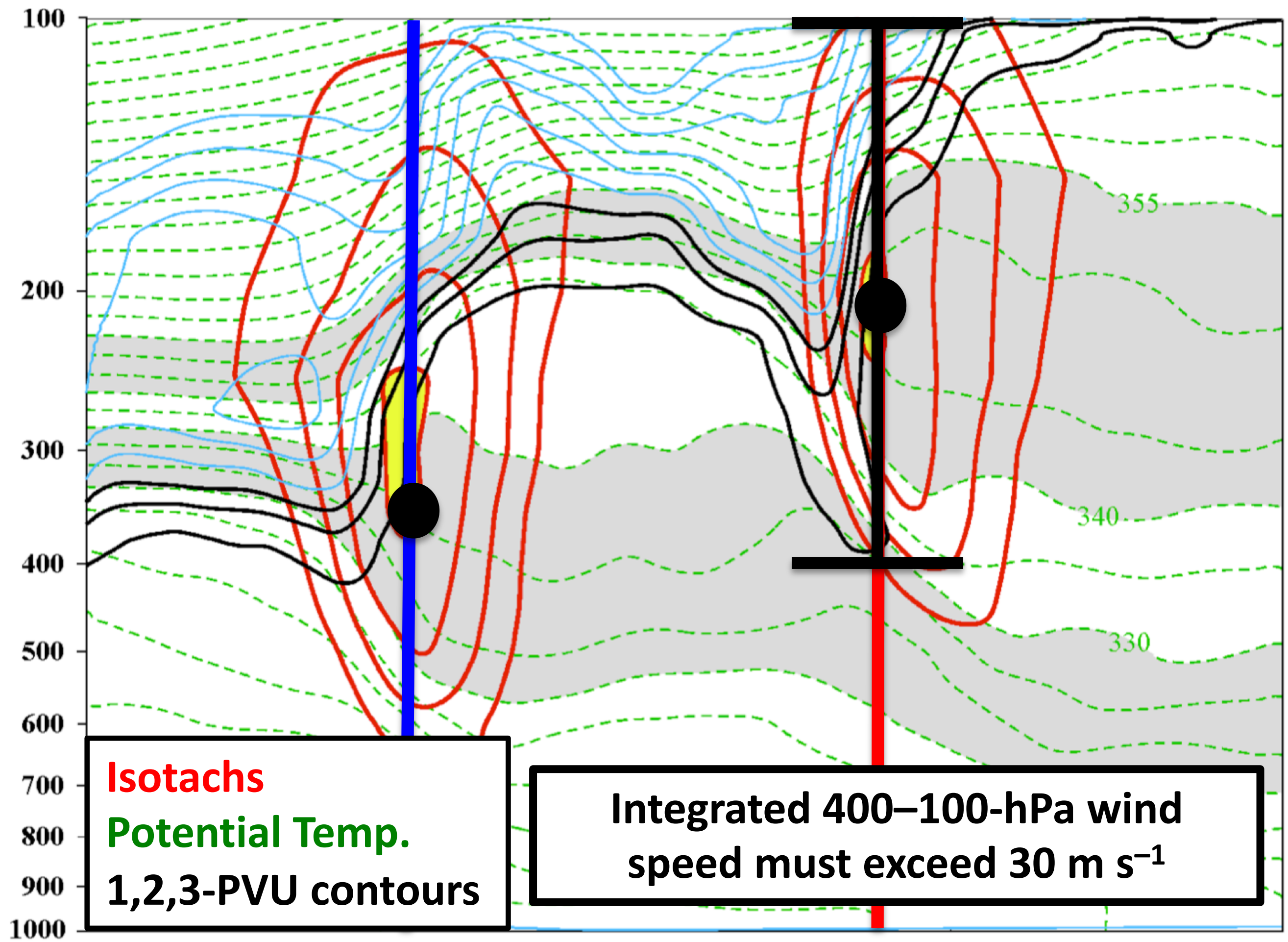

A Winters and Martin (2014, 2016, 2017); Christenson et al. (2017); Handlos and Martin (2016) **A'**

Jet Superposition Event Identification

0000 UTC 27 April 2010

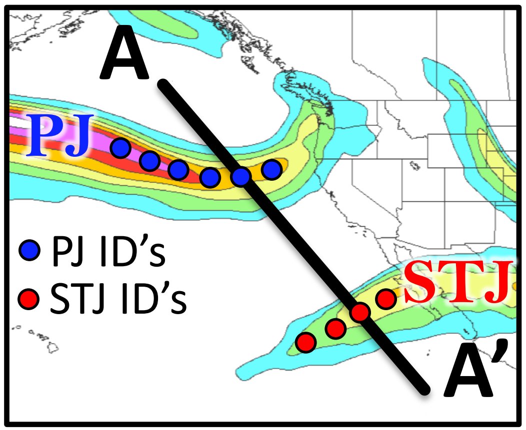

250-hPa wind speed

Isolated grid points over North America in the CFSR (Saha et al. 2014) characterized by polar and subtropical jets during Nov–Mar 1979–2010.

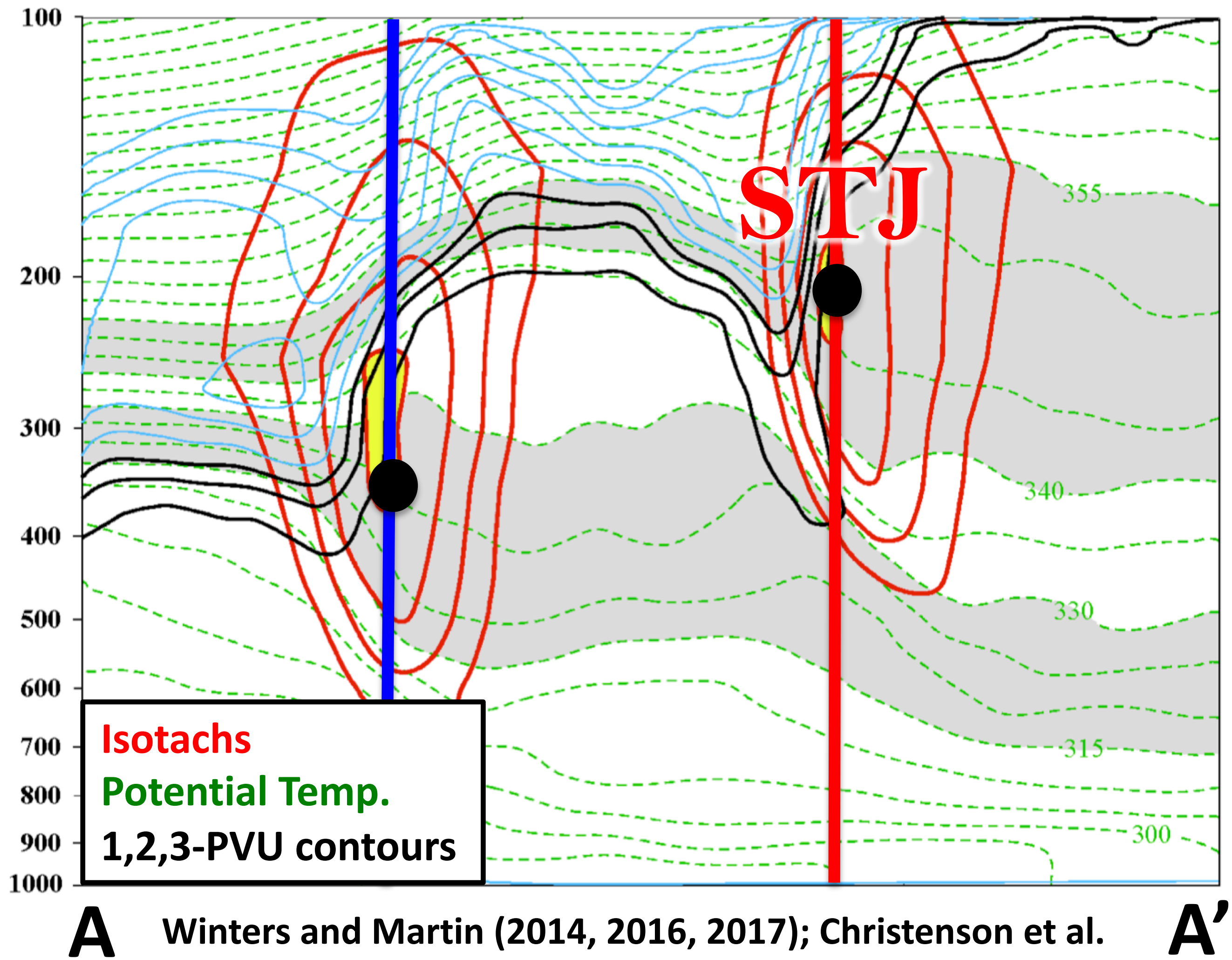

Winters and Martin (2014, 2016, 2017); Christenson et al. (2017); Handlos and Martin (2016)

Jet Superposition Event Identification

0000 UTC 24 October 2010

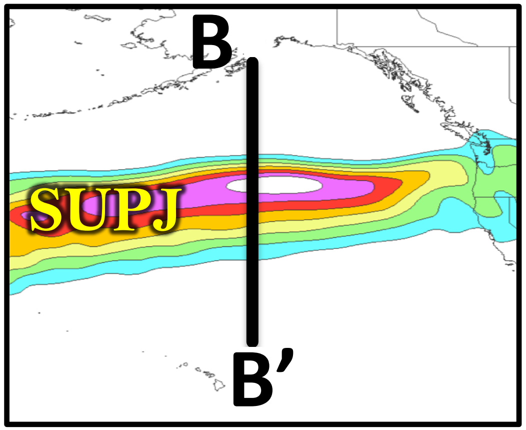

250-hPa wind speed

Isolated grid points over North America in the CFSR (Saha et al. 2014) characterized by a jet superposition during Nov–Mar 1979–2010.

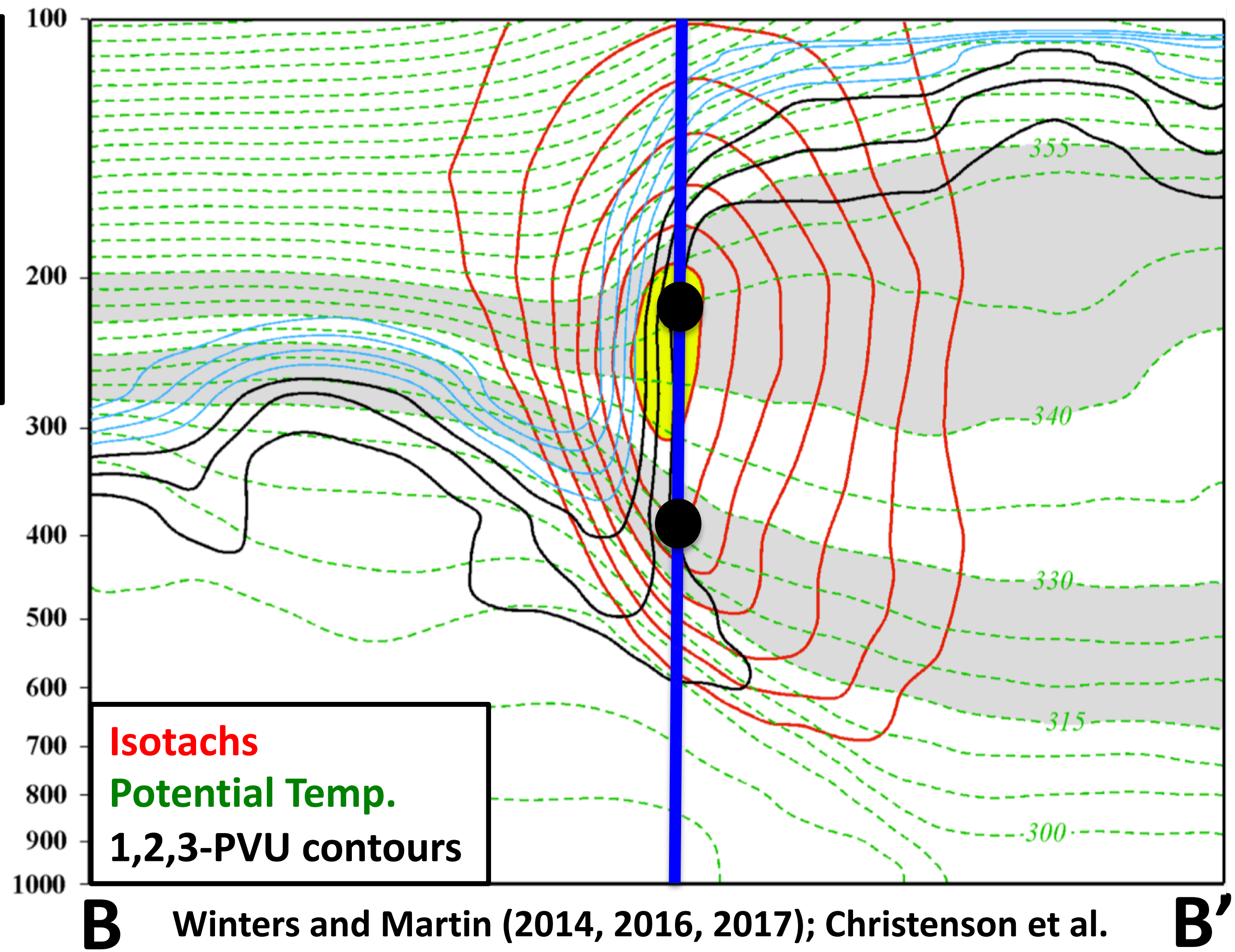

Winters and Martin (2014, 2016, 2017); Christenson et al. (2017); Handlos and Martin (2016)

Jet Superposition Event Identification

0000 UTC 24 October 2010

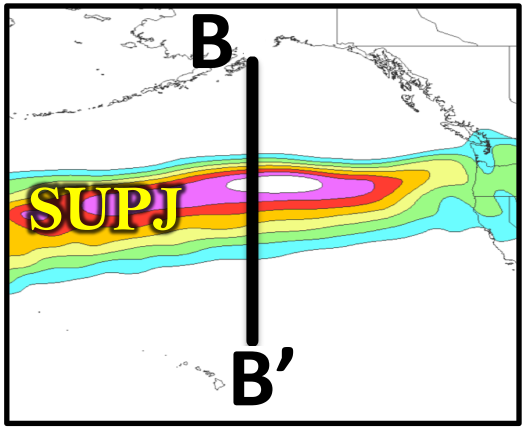

250-hPa wind speed

Isolated grid points over North America in the CFSR (Saha et al. 2014) characterized by a jet superposition during Nov–Mar 1979–2010.

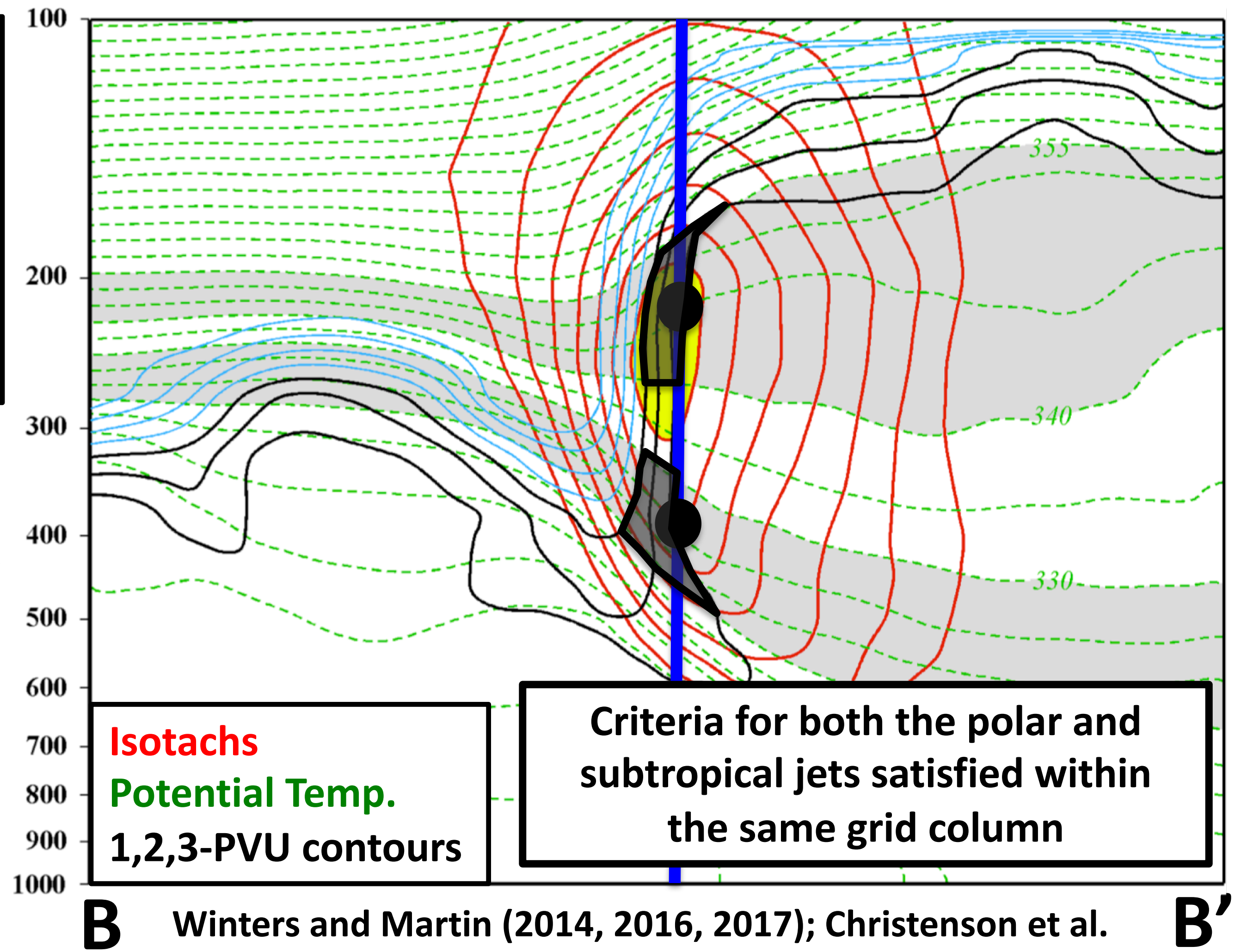

Winters and Martin (2014, 2016, 2017); Christenson et al. (2017); Handlos and Martin (2016)

Jet Superposition Event Identification

0000 UTC 24 October 2010

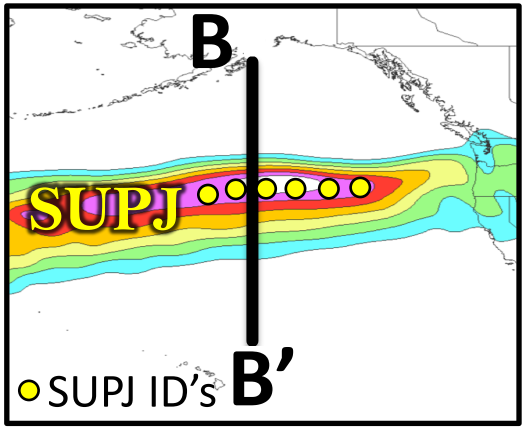

250-hPa wind speed

Isolated grid points over North America in the CFSR (Saha et al. 2014) characterized by a jet superposition during Nov–Mar 1979–2010.

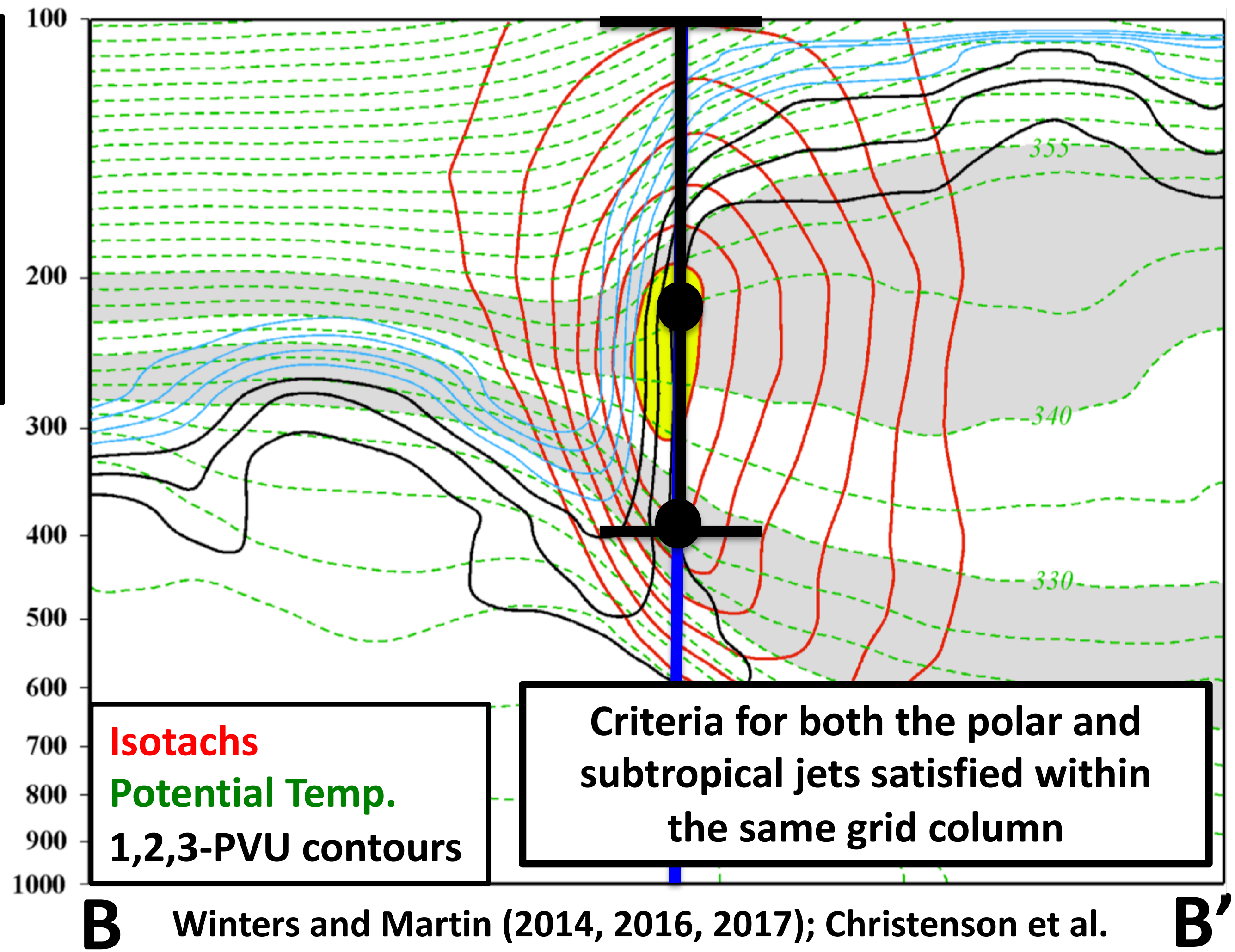

Winters and Martin (2014, 2016, 2017); Christenson et al. (2017); Handlos and Martin (2016)

Background

Christenson et al. (2017)

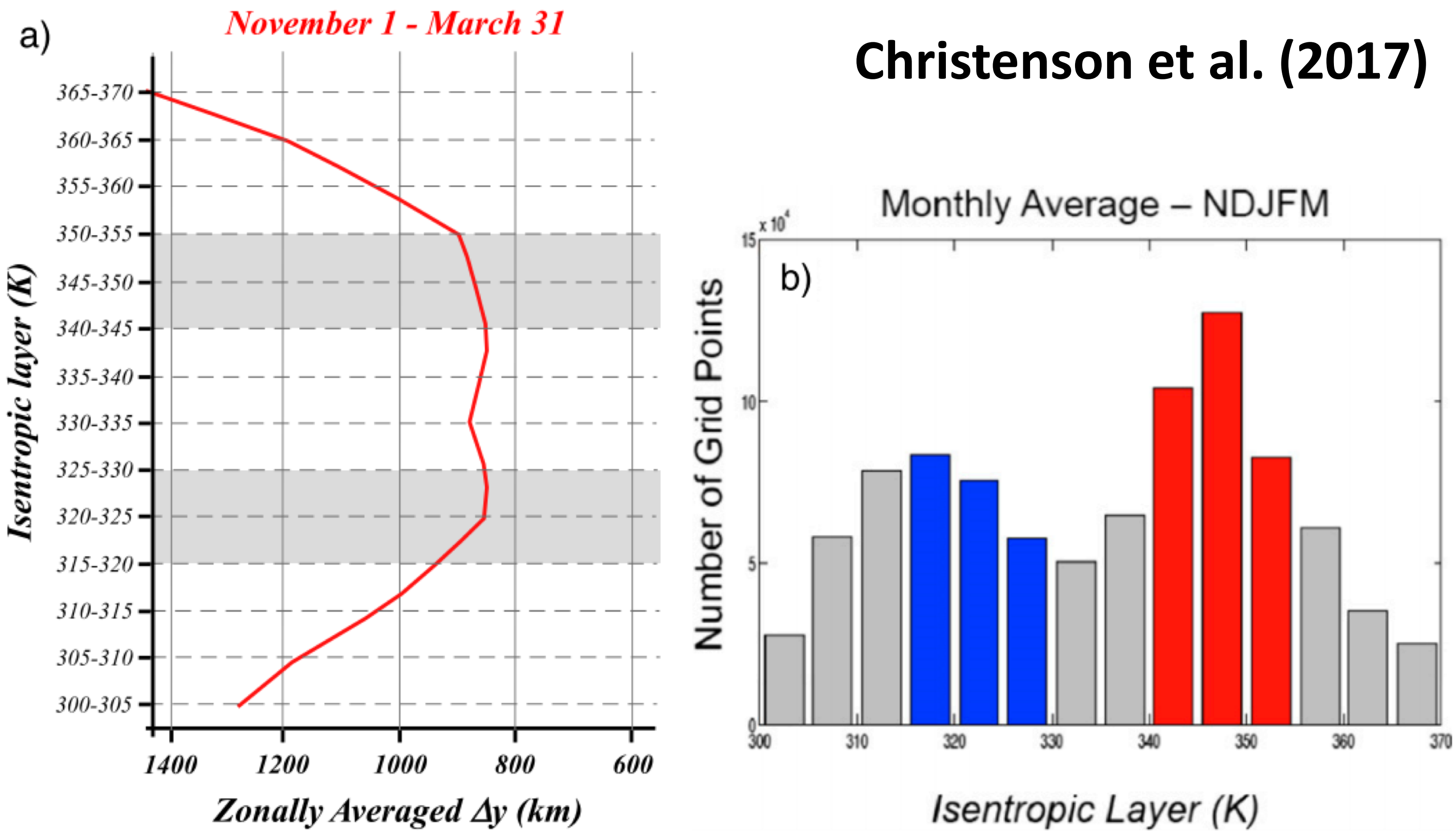

FIG. 2. (a) Cold season average of zonally averaged Δy (km) for 5-K isentropic layers ranging from 300–305 to 365–370 K. The 315–330- and 340–355-K layers are highlighted in light gray shading. (b) The average frequency of occurrence of grid points with a maximum wind speed value within the 5-K isentropic layers along the abscissa per cold season. The 315–330- and 340–355-K layers are shaded in blue and red, respectively.

Jet Superposition Event Identification

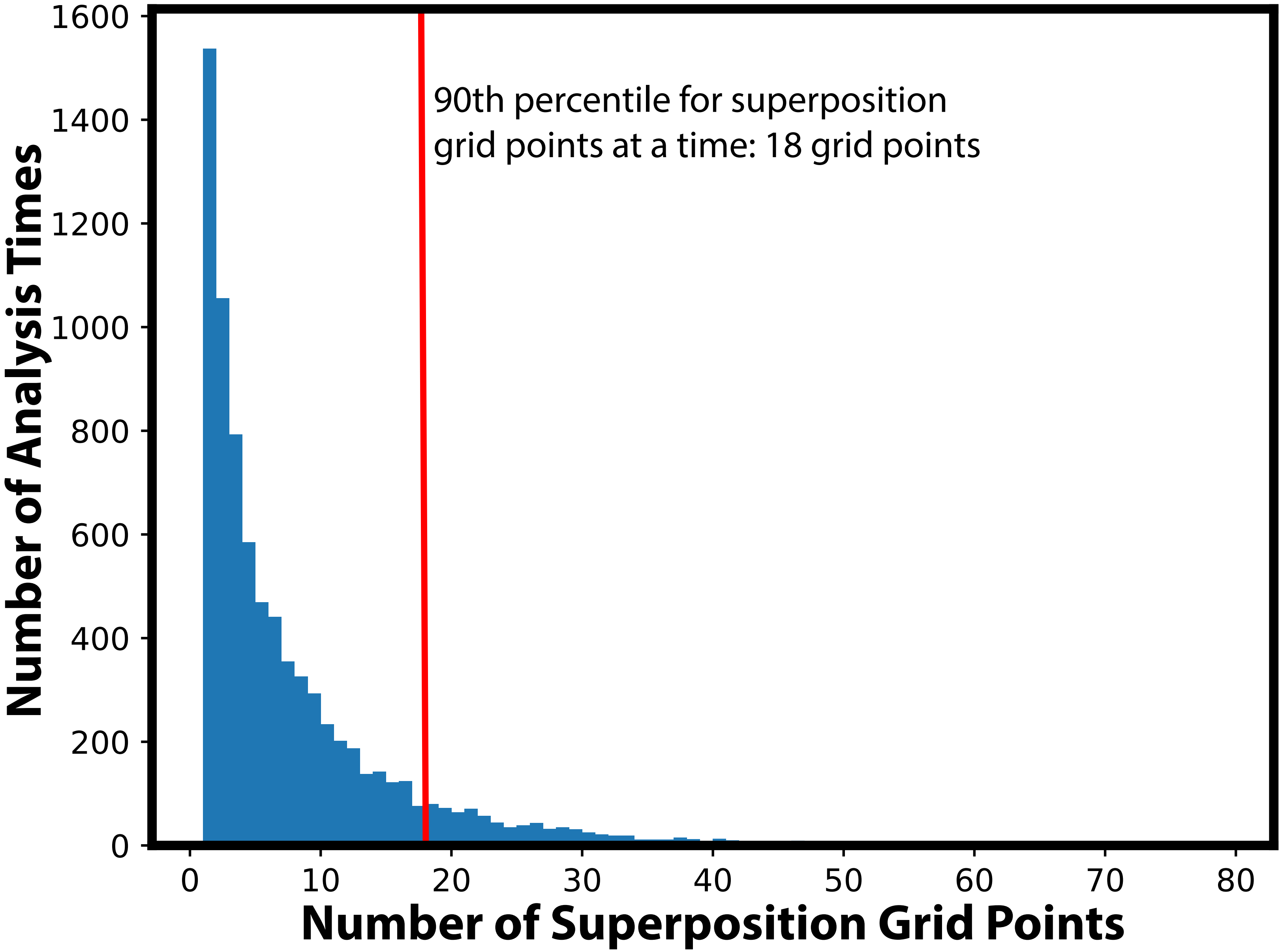

Jet Superposition Event Identification

Calculated the centroid of each jet superposition based on all valid grid points at a particular analysis time.

To calculate the centroid, there must exist a group of 18 superposition grid points, of which no superposition grid point is >1000 km away from another superposition grid point.

Sample Jet Superposition Centroid Calculation